Processing and Characterization of Micro-scale and Nanscale Silver Paste for Power Semiconductor Device Attachment

by

Zhiye Zhang

Dissertation submitted to the Faculty of the Virginia Polytechnic Institute and State University in partial fulfillment of the requirements for the degree of
DOCTOR OF PHILOSOPHY
in
ELECTRICAL ENGINEERING

Prof. Guo-Quan. Lu, Chair
Prof. Daan. van Wyk
Prof. Louis Guido
Prof. Rickey M. Davis
Prof. Yilu Liu

September 2005

Key words: Power packaging, die-attach, low-temperature sintering, nanoscale silver paste, high-temperature application

Processing and Characterization of Micro-scale and Nanscale Silver Paste for Power Semiconductor Devices Attachment

Zhiye Zhang

Advisor: Dr. Guo-Quan Lu

Electrical and Computer Engineering Department &

Center for power Electronics System

Virginia Polytechnic Institute and State University

Abstract

Die attachment is one of the most important processes in the packaging of power semiconductor devices. The current die-attach materials/techniques, including conductive adhesives and reflowed solders, can not meet the advance of power conversation application. Silver paste sintering has been widely used in microelectronics and been demonstrated the superior properties. The high processing temperature, however, prevents its application of interconnecting power semiconductor devices. This research focuses processing and characterization of micron-scale and nanoscale silver paste for power semiconductor devices attachment.

Lowering the processing temperature is the essential to implement sintering silver paste for power semiconductor devices attachment. Two low-temperature sintering techniques – pressure-assisted sintering micro-scale silver paste and sintering nanoscale silver paste without external pressure – were developed. With the large external pressure, the sintering temperature of micro-scale silver paste can be significantly lowered. The experimental results show that by using external pressure (>40MPa), the commercial micro-scale silver paste can be sintered to have eighty percent relative density at 240^{o}C, which is compatible with the temperature of solder reflowing. The measured properties including electrical conductivity, thermal conductivity, interfacial thermal resistance, and

the shear strength of sintered silver joints, are significantly better than those of the reflowed solder layer. Given only twenty percent of small pores in the submicron range, the reliability of the silver joints is also better than that of the solder joints under the thermal cycled environment. The large external pressure, however, makes this technique difficult to automatically implement and also has a potential to damage the brittle power semiconductor devices.

Reducing silver particles in the paste from micro-size to nanoscale can increases the sintering driving force and thus lowers the sintering temperature. Several approaches were developed to address sintering challenges of nanoscale silver particles, such as particles aggregation and/or agglomeration, and non-densification diffusion at low temperature. These approaches are : nanoscale silver slurry, instead of dry silver powder, is used to keep silver particles stable and prevent their aggregation. Ultrasonic vibration, instead of conventional ball milling, is applied to disperse nanoscale silver particles in the paste from to avoid from agglomerating. Selected organics in the paste are applied to delay the onset of mass-diffusion and prevent non-densification diffusion at low temperature. The measured results show that with heat-treatment at 300oC within one hour, the sintered nanoscale silver has significantly improved electrical and thermal properties than reflowed solders. The shear strength of sintered silver interconnection is compatible with that of solder.

The low-temperature sinterable nanoscale silver paste was applied to attach the bare Silicon carbide (SiC) schottky barrier diode (SBD) for high temperature application. Limited burn-out path for organics in the silver layer challenges the sintering die-attach. This difficulty was lessened by reducing organics ratio in the silver paste. The effects of die-size and heating rate on sintering die-attach were also investigated. The single chip packaging of SiC SBD was fabricated by sintering die-attach and wire-bonding. The tested results demonstrate that the sintering nanoscale silver paste can be applied as a viable die-attach solution for high-temperature application.

ACKNOWLEDGMENTS

Dr. Guo-Quan Lu, my advisor and mentor, provides me enormous support and encouragement throughout the course of this work and all the difficulties I encountered. His valuable guidance on the research process made this work possible. Far more than that, your patience, diligence, selflessness, and brilliancy mentally and physically encourage me enjoy the beauty of science not only in my Ph.D period, but also the whole life. The experience working with you is an enjoyable time period which I will cherish for ever.

I also want to express my gratitude to Dr J.D. van Wyk and Dr. Rick Davis for providing a number of key insights during the research process. Thanks are also due to Dr. Louis Guido and Dr. Yilu Liu for serving on the committee.

I am grateful to all my research group fellows: Dr. Jess Calata, Guofeng Ba, Dr. Sihua Wen, Kelly Stinson-Bagby, Guangying Lei, Xingdan Li and Mo Wu. I owe sincere thanks to packaging lab-mates: Dr Chen Rengang, Dr. Zhao Lingyin, Dr. Zhenxian Liang, Dr. Johan Strydom, Pieter Wolmarans, and Dr. Seung-Yo Lee. Especially thanks to lab managers Dan Huff and Bob Martin, for their great friendship and help.

I wish to thank all my colleagues and friends in CPES including the staffs and technitians. Thanks for all the help you gave to me during this work.

I also give my special thanks to my friend Wang Yi: without her help and encourage, this work will be more challenge.

None of this would have been possible without the constant support of my family: my father Zhongqing Zhang, my mother Wenfeng Tang, and my lovely sister Liangliang Zhang.

The research was sponsored by the National Science Foundation. This work made use of ERC Shared Facilities supported by the National Science Foundation under Award Number EEC-9731677.

Zhiye Zhang
September 2005
Blacksburg, Virginia

Table of Contents

List of Figures

List of Tables

Chapter 1 Introduction

1.1 Significance of power semiconductor devices attachment

Power semiconductor devices in single-chip package, shown in Figure 1.1 (a) or multi-chip power modules, shown in Figure 1.1 (b) are attached to substrate by a die-attach layer.

Figure 1.2 schematically shows a side view of the attachment of a single- chip package. The thickness of the die-attach layer has only tens of microns, but its quality, essentially affects the performance and reliability of the attached power semiconductor device while operating in the field. Die-attach layer in the power device packaging itself is an electrical connection, such as the drain interconnection of power MOSFETs (metal-oxide semiconductor field-effect transistors) or cathode of power diode. So, the electrical properties of die-attach layer directly affect electrical performance of power semiconductor devices such as turn-on resistance of power MOSFET (Rdson). As a comparison, all the electrical terminals of integrated circuit (IC) devices are usually on the top side and the die-attach layer only mechanically joins the bottom side of the device onto the substrate. More importantly, the die-attach layer supplies the majority heat dissipation path between the device and the packaging. Compared with those interconnections on the top-side of power semiconductor devices, such as wire-bonding or ball-grid-array (BGA), die-attach layer has much less thermal impedance. This is due to a large area and a thin thickness of the die-attach layer. With a constant power loss generated by power semiconductor devices, the temperature difference between junction and substrate is almost determined by the thermal properties of die-attach layer. Because the power rating of packaged devices is actually thermo-related, thermal properties of the die-attach layer become crucial to the power rating of packaged devices. The reliability of semiconductor devices are also highly related with the die-attach layer. A significant thermomechanical stress may occur during the cycled operation of semiconductor devices due to the mismatch of the coefficients of thermal expansion (CTE) between devices and

substrate. The die-attach layer sandwiched between the devices and substrate not only needs to withstand cycled stress, but also to cushion thermo-mechanical stress to ensure proper operation of the devices. The mechanical properties of die-attach layer essentially affect the reliability of the power devices.

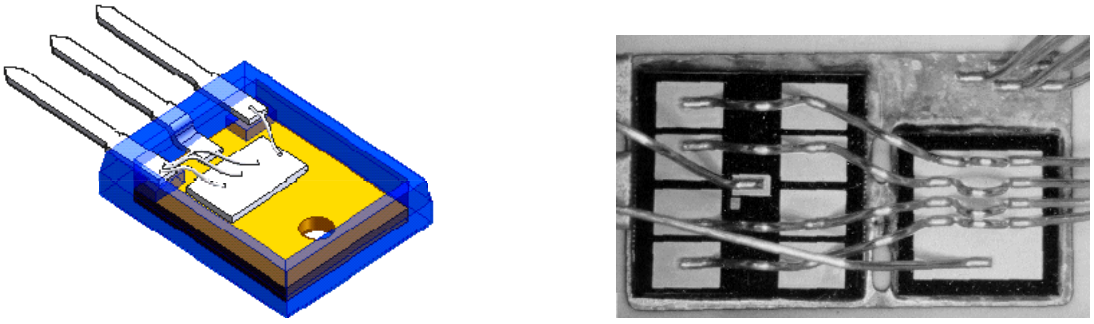

Figure 1.1 (a) individual packaged power device (TO-247), (b) multi-chip power module.

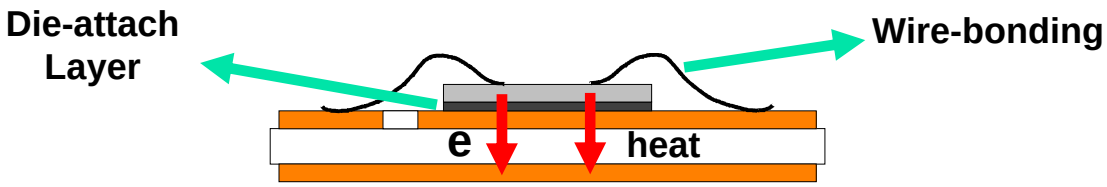

Figure 1.2. Schematic of single chip die-attachment.

Emerging applications for power conversion systems require power semiconductor devices to handle an increasingly higher level of power. At the same time, packaging and devices are progressively becoming smaller so that more efficient heat dissipation is required to cope with the increased power density. Furthermore, power electronics

modules and/or systems are expected to work at harsher environment, such as extremely high temperature with significantly-improved reliability for future applications. All these challenge the current die-attach materials and techniques. Consequently, exploring alternative die-attach materials and techniques is very critical in the power semiconductor devices packaging.

A good alternative die-attachment should have the following properties:

- high thermal conductance and low coefficient of thermal expansion (CTE) to minimize thermo-mechanical stresses;
- high electrical conductance to handle large current;
- high temperature stability;
- high mechanical strength and resistance to fatigue failure;
- environment friendly;
- reasonable materials cost;
- compatible processing achieved using existing die-attach instruments with little modification.

1.2 Current die-attach materials/techniques

1.2.1. Conductive adhesives

Polymer adhesives are widely used to attach integrated circuit devices due to the low processing temperature and simple processing procedure. Polymer adhesives consist of thermosetting polymers, which means that they remain solid once cured even if subjected further to high temperatures. On the other hand, 'thermoplastic' materials have the ability to reflow at a high enough temperature, even if curing has previously occurred. Most thermosetting polymers are bad electrical and thermal conductor and some of them are the candidates for isolators. A large percentage of metal fillers, usually higher than 80%, are added into these adhesives to improve the thermal and/or electrical conductivities. Silver flakes and/or particles are usually selected as metal fillers because silver has the highest thermal and electrical conductivity of all the metals.

Polymer adhesives initially contain solvents that allow easy dispensation and are cured at elevated temperature with the help of catalysts. According to the conduction direction, it can be divided into two sub-categories: isotropic conductive adhesive (ICA) and anisotropic conductive adhesive (ACA) [1]. The Figure 1.3 shows that the metal powder and flakes imbedded in the polymer matrix and form the conduction path. Due to the random arraying of silver particles and flakes, the conductivity of the isotropic conductive adhesive (ICA) is the same from any direction. Figure 1.4 shows joints formatted by anisotropic conductive adhesive (ACA). The silver particles in the polymer matrix only forms Z-axis interconnection under the press, so only one direction is electrical conductive.

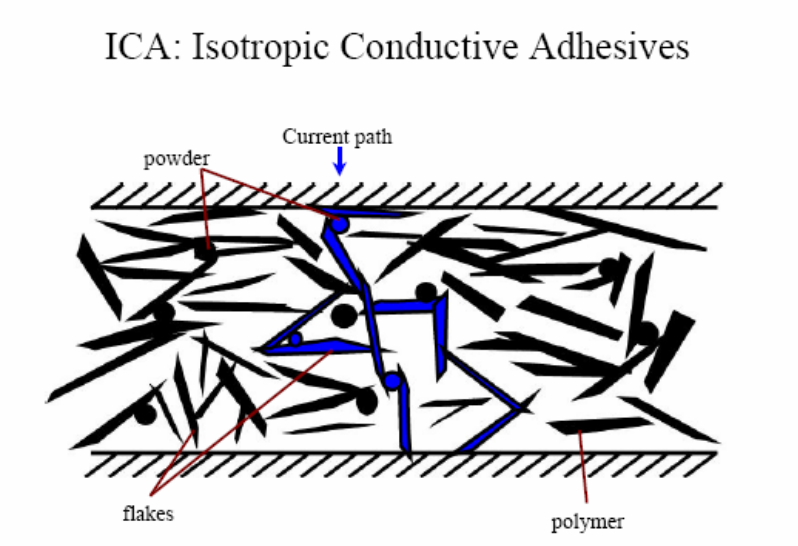

Figure 1.3 Schematic of the formation of isotropic conductive adhesives.

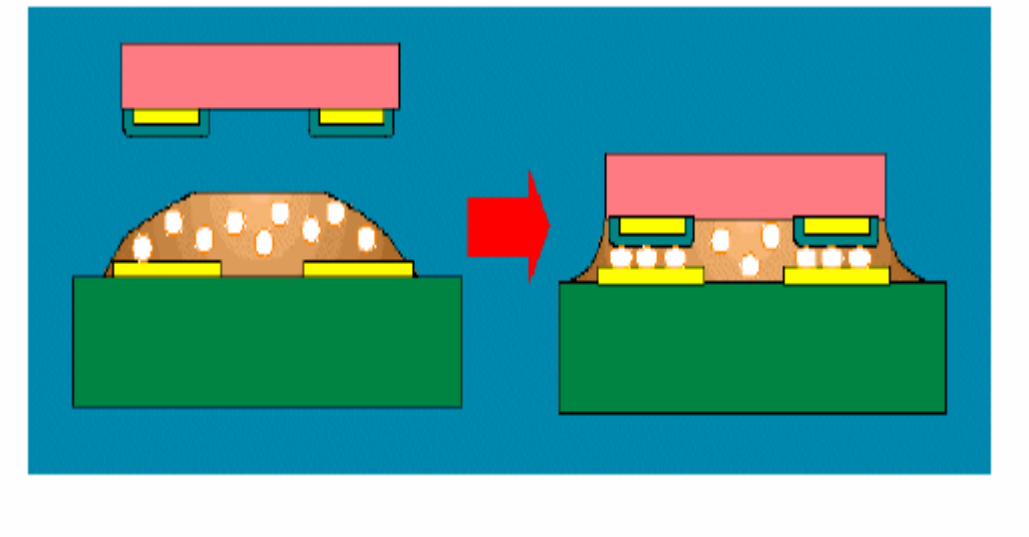

Figure 1.4 Joints formation of anisotropic conductive adhesive.

1.2.2. Reflowed solders

Solders usually consist of two or more metals, within which there are one or more phases. The melting temperature of solders is usually much lower than the melting temperature of its constituted elements. With the temperature higher than its melting temperature, the solder melts to liquid and wets the surfaces need to be bonded; after cooling down, the solder joints can be formed. Compared with conductive adhesives, solders usually have better electrical and thermal properties and thus are widely used to attach power semiconductor devices.

According to the composition of the solder, it can be divided into lead-contained solder and lead-free solder. Lead-contained solder is the widest used solder in industry practice and right now there are about 150 tons/year of high Pb-solder used in die-attach. The large amount of lead usage raises very serious environmental issues. Consequently, the legislation is continuing to restrict the use of Pb. The latest guideline of the European Community from April 2001 effectively bans Pb from many electronic applications until 2006 [2, 3]. The Japanese Environmental Agency (JEA) has also proposed that lead-containing scrap must be disposed of in sealed landfills to prevent lead leaching. Since

1992, different bills have been introduced at the U.S. Congress to ban lead from a wide variety of applications, which include solders [4].

Green electronics have been a tendency in the 21st century and driven the industry to research and develop lead free solders [5]. Lead-free solders such as tin-silver-copper, tin-copper and gold-tin solders have been commercialized to replace lead-tin solder. But there is no research that indicates the lead-free solders has a significantly better performance than the lead-contained solders. [6]

According to the melting point of solders, it can be divided into eutectic solder and non-eutectic solder. A eutectic alloy is an alloy with the lowest melting point possible for the metals combined in the alloy. The Pb-Sn eutectic alloy is the most common-used solder in semiconductor packaging. Figure 1.5 is the phase diagram of Pb-Sn. When the ratio of lead to tin is 61.9:38.1, the melting temperature of the alloy is the 183^{o}C, the lowest temperature during all the Pb-Sn alloys. In the phase diagram we can see the eutectic solder is the only lead-tin composition which has no such temperature zone in which liquid and solid phases can co-exist. Once the temperature is over 183^{o}C, all the solid solder turns to the liquid phase. This single melting point makes the eutectic solder easily for reflow processing. There are two phases in this eutectic solder, called α-phase and β-phase respectively shown in Figure 1.6. In the α phase, there is 19% tin element and the rest of 81% is lead; on the other hand, β phase has 97.5% tin, and only 2.5 % of tin. The α-phase is also called the lead-rich phase due to high lead contents and β-phase is called the tin-rich phase. In the eutectic lead-tin solder, there is 45% α phase and 55% β-phase. The two phases in the eutectic alloys may detrimentally affect the performance and reliability of solder joints such as dendritic and coarsening effects [7].

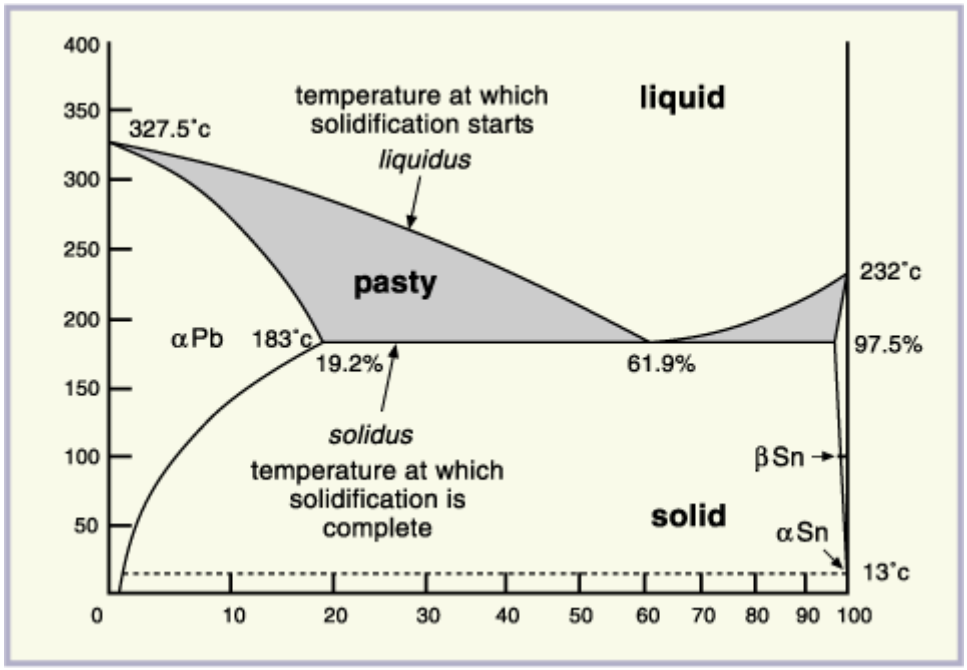

Figure 1.5 The phase diagram of Pb-Sn alloy.

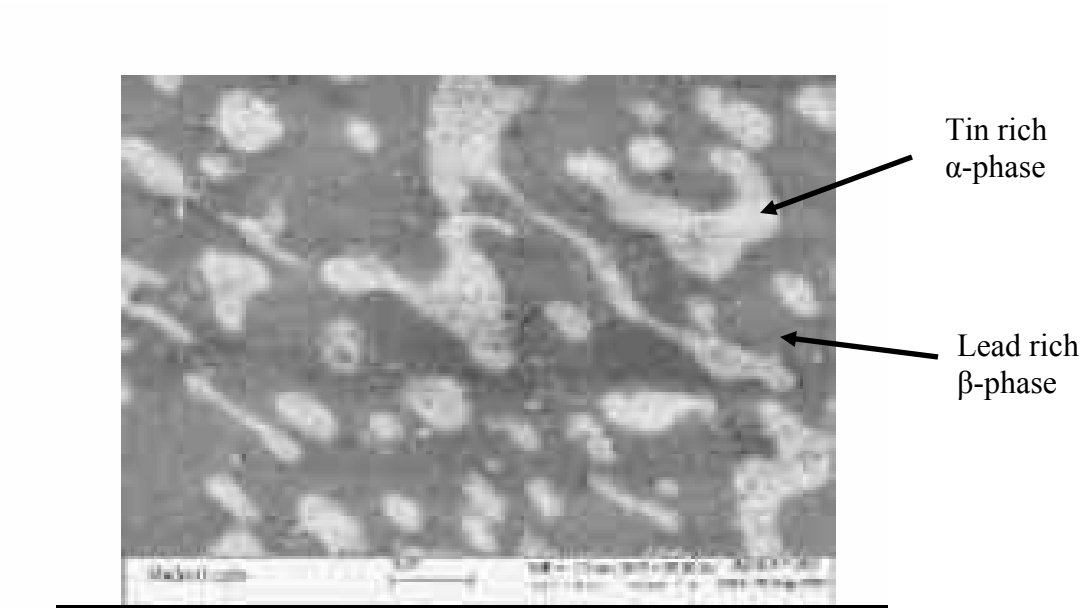

Figure 1.6. Microstructure of lead-tin (37%) eutectic solder: α phase 45%, β-phase 55%.

1.3 Motivation for developing low-temperature sintering silver die-attach

1.3.1. Issues of current die-attach techniques/materials

Attaching power semiconductor devices onto metallized substrates is one of the most critical processing steps in the manufacture of electronic power modules. [8] This connection has to have low electrical resistance to minimize the voltage drop and heat dissipation at the joint. The thermal resistance of the joint has to be small to prevent excessively heating the chip. The die-attach layer has to have sufficient mechanical strength to withstand the mechanical stresses arising from the operation condition. Finally, the joint has to be stable at elevated temperature to guarantee the reliability in harsh environment.

Conductive adhesives are extensively investigated as a non-lead die-attach solution in microelectronic packaging [9, 10]. Compared with lead-tin solder, they are more environmentally friendly, offer higher resolution capability (no chipping swimming problem) [11], have much lower processing temperature and less processing steps. Conductive adhesives, however, usually have lower electrical and thermal properties. Because polymer matrix usually has poor thermal and electrical conductivities, the majority of electrical and thermal conduction is achieved by the filled metal particles and/or flakes. Under a low processing temperature, these metal particles and/or flakes do not fuse together and thus only have point contacts with each other (shown in Figure 1.3 and Figure 1.4). The small contact area of metal particles and/or flakes causes conductive adhesives to have low thermal and electrical conductivity. Furthermore, conductive adhesives also suffer detrimental performance at elevated temperature and/or humidity because polymers usually can not be kept stable at these conditions. High electrical conductivity, high thermal conductivity and high-temperature stability are required for the power semiconductor devices attachment, so conductive adhesives are not widely used is power device die-attach for industry practice.

Reflowed solder usually has better thermal and electrical properties than those of conductive adhesives. This is because the solder melts and fuses together at the reflow temperature. But solders still belong to metal composites that have poor electrical and thermal conductivities. Further more, to form joints, processing temperature has to be higher than the melting temperature of solders. This is a disadvantage because it means that the operation temperature of solders has to be lower than the processing temperature due to the simple fact that the joint strength of the solder will be lost during the liquid phase. Since the solder reflow process involves the melting and solidification of solder particles in a flux mixture, voids are often unavoidable. This is because of entrapped gas evolving from the flux components and poor wetting of the surface by the solder.

Figure 1.7 shows the voids evolution during the cycled load [12]. The heat generated from the power device can not flow through the voids which increases the local temperature around voids (heat spots). The heat spots accelerate the growth of voids, further increasing the temperature and finally inducing the failure of attachments [13, 14]. Thermomechanical stress caused by the mismatch of coefficient of thermal expansion (CTE) during cycling load is another important reason for the growth of voids [15]. The initial voids accompanied with growth, have a detrimental effect on the thermal performance and reliability of the die-attached layers. The reflow processing also involves solid-liquid phase transition and the existing liquid phase may induce the chip swimming and ruin the accuracy of the attachment of die.

The use of lead-containing solders also raises a serious environmental and public health concern [4]. The reasons are (a) lead and its compounds are ranked as one of the top 10 hazardous materials and (b) lead is the number one environmental threat to children. Many major electronics companies, national laboratories, universities, research organizations, and solder vendors worldwide responded by initialing research programs to eliminate lead from solders [16-21]. Finally, SiC and other wide-band gap semiconductors, such as GaN and diamond, are capable of operating at high temperatures. Recent studies on SiC devices have shown [22-24] promising results on their switching characteristics and their ability to function at elevated temperatures up to 350ºC. This will result in a much lower demand on cooling and enable power system

working in much harsher environment. However, interconnecting these devices into a power electronics circuit still presents a challenge. Only some of the high-gold-content solders can potentially work at temperatures over 300°C but their melting points are still substantially lower than silver. The high gold content makes these alloys very expensive and difficult to process because of the higher reflow temperatures. In addition, their hardness and brittleness make them prone to transfer large thermomechanical stresses to the power devices rather than relax them [25]. Consequently, to improve the performance and reliability of the power devices, it is important to explore alternative die-attach materials and processes that can provide significantly improved performance and reliability metrics over the current solder-reflow practice.

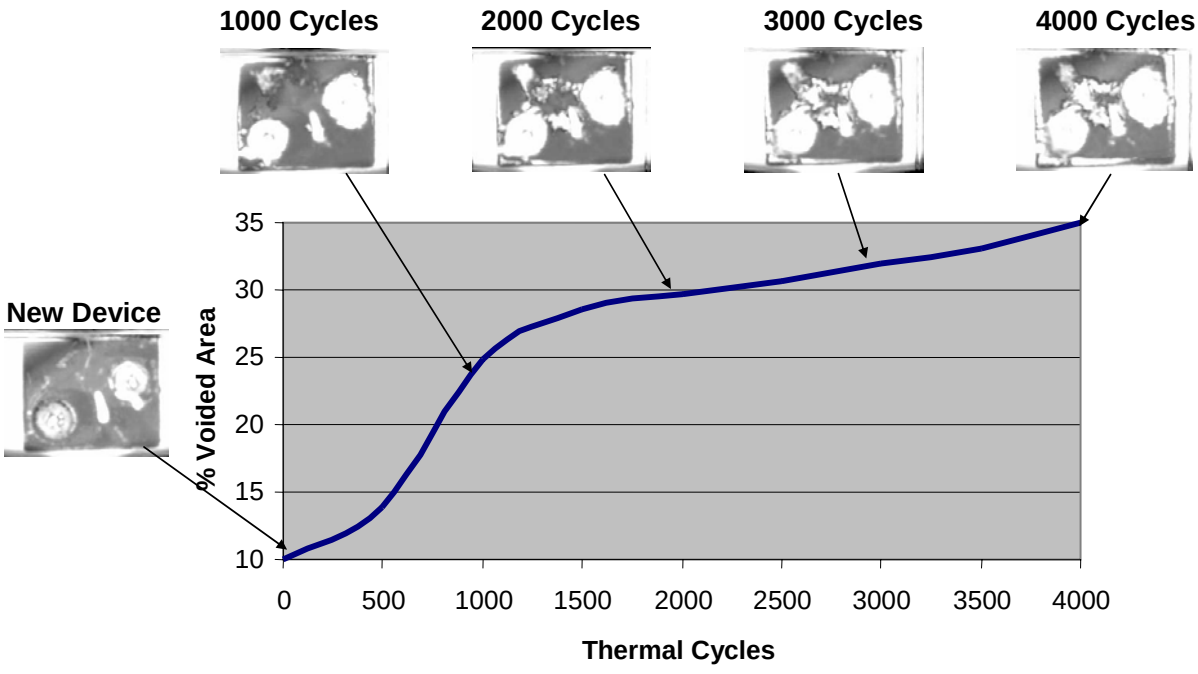

Figure 1.7 Solder voids evolution during thermal cycling.

Figure 1.8 compares the properties such as melting/curing temperature, electrical conductivity, thermal conductivity and tensile strength of conductive polymers, metal-filled epoxy, reflowed solders and noble metals. Compared with conductive polymers, metal-filled epoxy and reflowed solders, noble metal elements such as silver, gold and platinum have significantly improved electrical conductivity, thermal conductivity and mechanical property. They also have a much higher melting temperature (>900^{o}C). Such a high melting temperature can enable them to function at higher temperatures which solders can not withstand. The high melting temperature, however, is also the biggest technical challenge when using noble metal elements as interconnection material. The reflow technique can not be applied to interconnect devices using noble metal because no devices can bear such a high temperature. An alternative interconnection forming approach – sintering – has to be applied because it can form joints under a temperature below the melting temperature of noble metals.

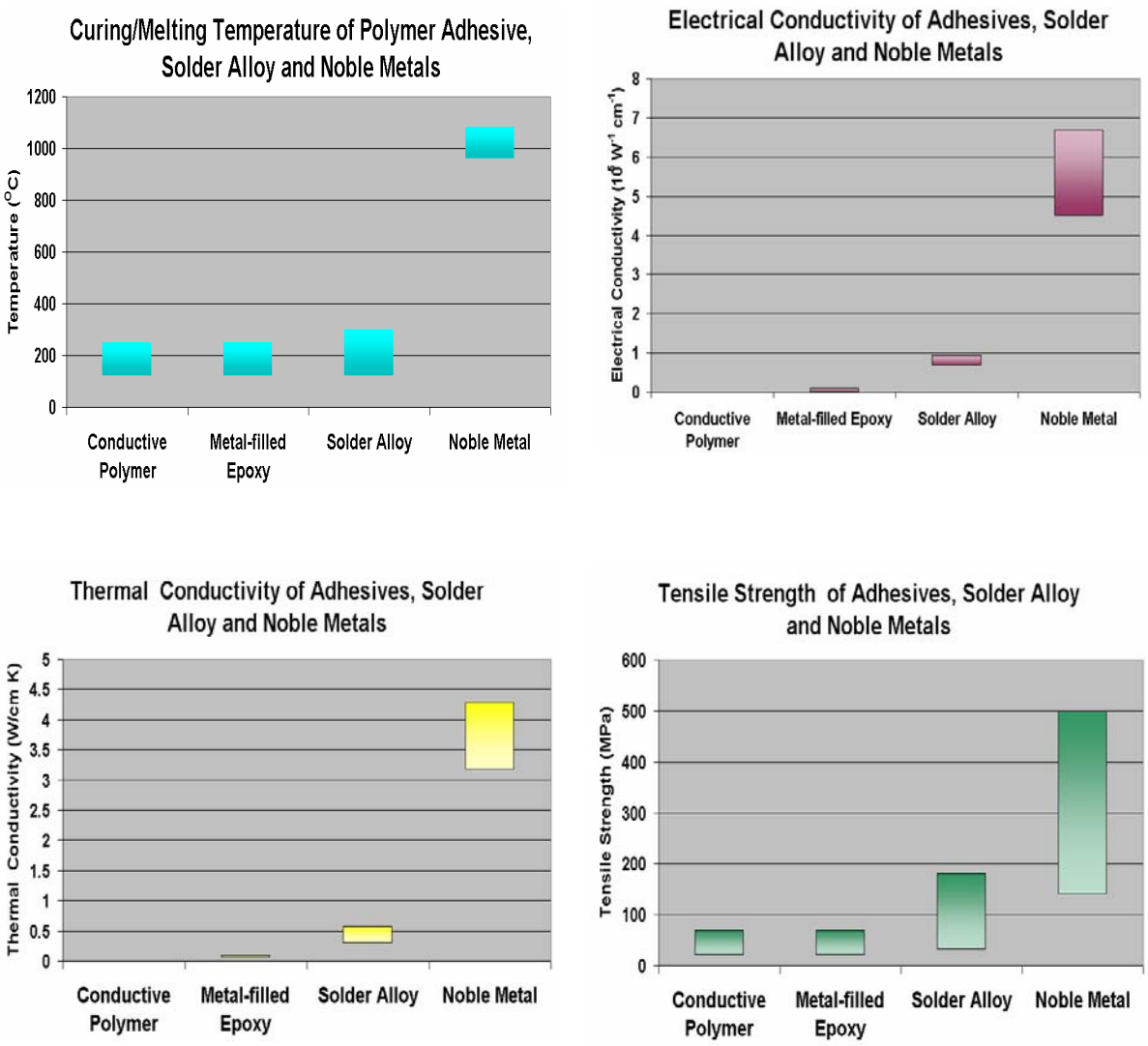

Figure 1.8 Properties of conductive adhesives, reflowed solders and noble metals.

1.3.2. Advantages for low-temperature sintering silver die-attach

Silver has the best electrical conductivity and the second best thermal conductivity in the world. Diamond has the best thermal conductivity (2000 w/ (m*T)), which is almost five times higher than that of silver; but, it is also an electrical insulator. The die-attach layer for power semiconductor devices itself is an electrical terminal, so diamond can not be a candidate, not to mention that diamond is also much more expensive than silver. Gold and platinum ware not consider as candidates because of their worse electrical and thermal properties, and much higher price than those of silver. Just the raw materials, gold is about 60 times higher, and platinum is 120 times higher than silver [26]. Copper is even cheaper than silver, but copper can be easily oxidized at evaluated temperature at air. Silver has the high-temperature stability (melting point: 961^{o}C) and very good mechanical properties. Unlike lead-contained solders, silver is environmentally friendly and has even been verified to kill bacteria in certain conditions [27]. Unlike most solders which have two or more elements with different phases, silver is a single element with only one phase. With single phase system, silver usually shows better mechanical property and reliability.

The sintering joints are formed by atomic diffusion and the processing temperature can be significantly lower than the melting temperature. Thus, the silver joints can be formed at relatively low temperature, but work at high temperature. Unlike solder reflow processing which has solid to liquid phase transition, sintering is an atomic diffusion processing: the bonding is accomplished by silver atomic diffusion and particles consolidation. Without liquid phase occurring in the solid state sintering, chip swimming during the die-attach can be avoided and thus the accuracy of die-placement can be improved. Table 1.1 lists the properties of commonly used solders and those of pure silver. It clearly shows the pure silver has a higher melting temperature, thermal and electrical conductivity and tensile strength than those of solders.

Table 1.1 Properties comparison of solders and pure silver.

Materials	MT (^oC)	Density (g/cm^3)	E-cond $(ohm*cm*10^5)$-1	T-cond (W/cm^oC)	CTE (um/m^oC)	Ten-str (PSI)
Sn63Pb37	183	8.4	11.9	0.50	25.0	6200
Pb60In40	205	8.5	5.2	0.19	26.0	5000
Pb88Sn10Ag2	267	10.8	8.5	0.27	29.1	3260
Au80Sn20	280	14.5	6.9	0.57	15.9	40000
Au88Ge12	356	14.7		0.44	13.4	26825
Au96.76Si3.24	363	15.4		0.27	12.3	36975
Pure Silver	961	10.5	66.7	4.19	19.3	20300

MT (melting temperature), E-cond (electrical conductivity), T-cond (thermal conductivity), CTE (coefficient of thermal expansion) Ten-str (tensile strength)

Due to the unique characteristics of silver and the sintering processing, sintering silver die-attach has the following advantages:

- high electrical and thermal conductivity;
- does not have much of a fatigue problem as in solder due to dendritic microstructure and/or large voids;
- is an atomic diffusion process without liquid phase during the intermediate stage and thus the chipping swimming problem can be eliminated;
- has a high melting points and a high-temperature stability suitable for high-temperature application;
- is environmentally friendly.

1.4 Objectives and outlines of this thesis

This research work focuses on processing and characterization of micro-scale and nanoscale silver paste for power semiconductor devices attachment. The thesis is organized as follows:

Chapter 1 introduces the significance of die-attach in power semiconductor packaging and the advantages of low-temperature sintering nanoscale silver paste as an alternative die-attach technique. It also outlines the objectives and structure of this dissertation.

Chapter 2 presents a literature review to gain a better understanding of this research work. In this chapter, solid state sintering theory is reviewed; the challenge to implement silver paste sintering die-attach – high processing temperature - is introduced. Based on that, two low-temperature sintering strategies - pressure-assisted sintering and reducing silver particles to nanoscale – are presented. Sintering difficulties of nanoscale materials such as aggregation, agglomeration and non-densification diffusion are also introduced.

Chapter 3 develops a pressure-assisted low-temperature sintering micro-size silver paste technique for power device attachment. The processing parameters such as temperature, pressure and time are evaluated. The study shows that by using large external pressure (>=40MPa), the commercial micro-size silver paste can be sintered to have 80% relative density at as low as 240^{o}C within a few minutes. The measured properties including electrical conductivity, thermal conductivity, interfacial thermal resistance, and shear strength of sintered silver layer, are also significantly better than those of the reflowed solder layer. Given only 20% pores in the submicron range, the reliability of silver joint is better than that of the solder joint under the thermal cycled environment. The large external pressure, however, makes this technique difficult to automatically implement and also has a potential to damage the power devices.

Chapter 4 develops a low-temperature sintering nanoscale silver paste technique without additional pressure. Several approaches were developed to address sintering challenges of nanoscale silver, such as particles aggregation and/or agglomeration and non-densification surface diffusion. Nanosale silver slurry, instead of dry silver powder, is used to keep silver particles stable and prevent silver particles aggregation. Ultrasonic vibration, instead of conventional ball milling, is applied to disperse nanoscale silver particles in the paste form to prevent agglomeration. Selected organics in the paste are applied to delay the onset of mass-diffusion and prevent non-densification diffusion at low-temperature. When the organics burn-out at relative higher temperature, the abrupt

densification caused by grain boundary diffusion and lattice diffusion can be realized. The properties of sintered nanoscale silver paste such as electrical conductivity, thermal conductivity and shear strength are characterized. The measured results show that with heat-treatment at 300^{o}C and less than one hour, the sintered nanoscale silver has significantly improved electrical and thermal properties than reflowed solders. The shear strength is compatible with solder joints.

Chapter 5 presents an application of sintering nanoscale silver paste technique: attaching SiC device for high-temperature application. Limited burn-out path for organics in the silver layer challenges the sintering die-attach. This difficulty was lessened by reducing organics ratio in the silver paste. The effects of die-size and heating rate on sintering die-attach were also investigated. The single chip packaging of SiC schottky barrier diode (SBD) was fabricated by sintering die-attach and wire-bonding. The tested results demonstrate that the sintering nanoscale silver paste can be applied as a viable die-attach solution for high-temperature application.

Chapter 6 is the summary of dissertation and gives the future of work for this research. Two low-temperature sintering techniques – pressure-assisted sintering micron-size silver paste and sintering nanoscale silver paste without external pressure – are developed as alternative die-attach solution for power semiconductor devices. Both techniques can enable high-temperature applications due to high melting temperature of silver. The pressure-assisted sintering die-attach has the difficulty for automatic manufacturing and can also potentially damage the devices, although it has the superior performance and reliability than those of solders. By eliminating the external pressure, the sintering nanoscale silver paste die-attach is demonstrated as a promising die-attach solution, especially at high-temperature. The sintering challenges of nanoscale silver paste are investigated and various approaches are developed to overcome these challenges. Due to the limited burn-out path of organics in the silver paste, this technique is still difficult to attach very-large dies. And also, silver migration always needs to be paid more attention when silver is used for electronic applications. Future research work needs to be conduct to study these issues. The sintered silver has broader applications besides attaching power semiconductor devices. Low-temperature sintering nanoscale

silver paste has the potential to be applied as a top-side interconnection technique for power semiconductor devices, conductive trace on various substrate and attachment for optical devices such as laser die. Further research work needs investigate the feasibility of these applications.

1.5 Original contributions

This thesis offers the following original contributions:

I. Proposed a novel interconnection technique - low-temperature sintering nanoscale silver paste – to attach power semiconductor devices with improved high-temperature stability and performance. This technique can interconnect the semiconductor devices and the substrate to form a joint at low temperature and enable high-temperature applications.

II. Develop a low-temperature sinterable nanoscale silver paste by overcome sintering challenges such as agglomeration, aggregation and non-densification diffusion.

III. Demonstrated this sintering technique to attach a SiC device for high-temperature application .

Chapter 2 Literature survey

2.1 Solid-state sintering

2.1.1. Sintering Vs. soldering

Sintering is a heating process that causes particles to bond together, resulting in significant strengthening and improved thermal, electrical and mechanical properties.[28] It commonly refers to processes involved in the heat treatment of powder compacts where mass-diffusion transport is appreciable. During the sintering processing, the applied pressure can accelerate mass transformation thus shortening the sintering time, improving the sintering microstructure, and etc[28]. The sintered materials usually have significantly improved thermal, electrical and mechanical properties than the initial powder system because of much denser microstructure. Sintering of powder compacts is an important process in the manufacture of conventional and advanced ceramic and metallic materials with various applications including rocket nozzles, ultrasonic transducers, automobile engines, dental implants, and semiconductor packaging. There is no phase transition during the sintering processing, and thus the bonding is achieved only by solid-state diffusion. Sintering offers an opportunity to form a bonding below the melting temperature of interconnecting materials. Welding technique is actually a sintering processing: the bonding is formed by atomic diffusion with the assistance of temperature (below melting temperature) and pressure.

Soldering is the process of joining two metals by using a solder alloy and melting the solders. In essential, the processing temperature of solders has to be higher than the melting point of solders. To lower the processing temperature (reflow temperature), the metal alloys with low melting points are usually choose as soldering materials, such as lead-tin alloy. Figure 2.1 shows the major difference between sintering and soldering: there is a intermediate stage - liquid phase – during the solder reflow; and the solder joints are formed by liquid-phase solidification. [23]

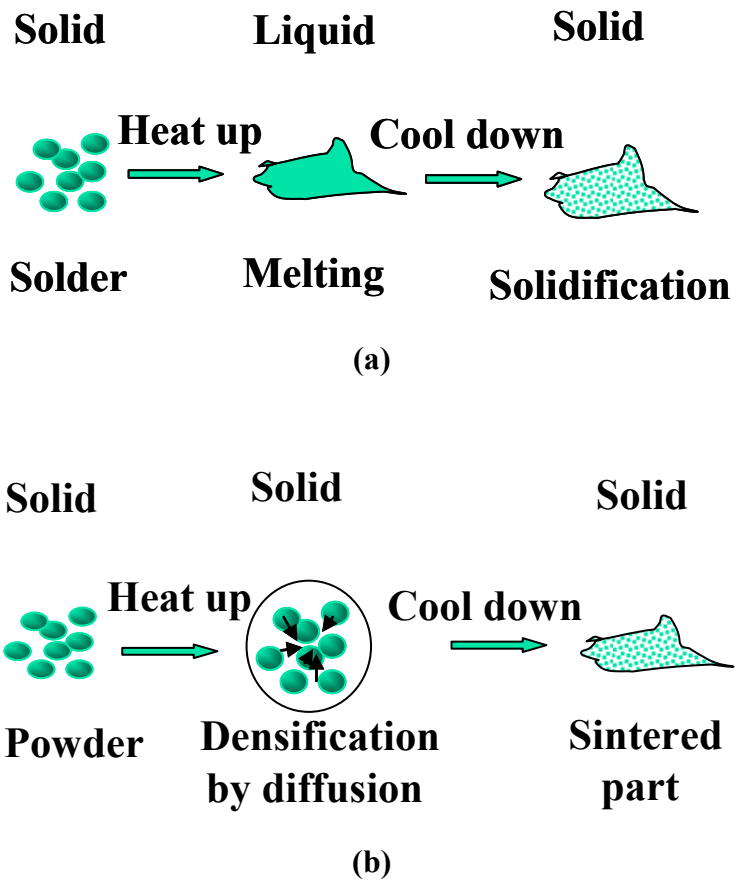

Figure 2.1. (a) Solder processing: solid-liquid phase transition; (b) sintering processing: atomic diffusion.

2.1.2. Sintering mechanisms

Solid state sintering is a process involved in the heat treatment of powder compacts at elevated temperatures where mass-diffusion transport is appreciable. During the sintering process, mass flows from regions of higher chemical potential to regions of lower chemical potential (thermodynamics), and how it flows is determined by the transport mechanism (kinetics). From the thermodynamic point of view, sintering is an irreversible process in which a free energy decrease is brought about by a decrease in surface area. In the solid-state sintering, the driving force for sintering is the excess

surface energy of a powder compact a sintering phenomena result in the reduction in the total interfacial energy. There are two important driving forces which lead to material transport. The first one is the chemical potential gradient. The difference between the chemical potential of an atom under a curved surface of principle radii of curvature r1 and r2 and and r2 (μ) and a flat surface (μ_o) is given by

$$\Delta\mu = \mu - \mu_o = \gamma\Omega\left[\frac{1}{r_1} + \frac{1}{r_2}\right] \quad \textbf{Equation 2. 1}$$

where Ω is the atomic volume and γ is the surface energy per unit area, r_1 and r_2 are positive if the surface is convex, and negative if it is concave. Thus, the atoms move from the convex to the concave regions to decrease the potential gradient. The vacancies, therefore, diffuse from the contact area between the solid particles and sink at the dislocations or grain boundaries.

The second driving force for mass transport is the stress generated at the contacts between particles. Figure 2.2 schematically shows the two-sphere model of sintering [29], one of the simplest model for sintering. Figure 2.3 shows the scanning electronic microscopy image of sintered two-sphere particles Considering the geometry of the contacts in Figure 2.2, it can be shown that the outer edge of the contact is subjected to a tensile stress, σ , given by

$$\sigma = \gamma\left[\frac{1}{\rho} - \frac{1}{x}\right] \qquad \textbf{Equation 2. 2}$$

where γ is the surface tension. If this stress is greater than the yield stress of the material, the mass will transport through microscopic viscous or plastic flow. If external pressure is applied, this mass transport will be very significant. Because the pressure applied to the external surface of a green compact is transmitted to the component's

interior through what is initially the much smaller effective surface of the contacting particles, the local contact pressure, or "effective pressure", drives localized particle deformation by yield and creep, and causes progressive densification. However, as densification proceeds, the contact area increases and the additional driving force for densification rapidly decreases. This results in apparent "geometrical hardening" of the compacts which are sintered with the assistance of pressure.

Although these microscopic mass transport mechanisms can be modeled, in the real sintering of a powder compact, only the shrinkage of the whole powder compact can be observed. Thus, from a macroscopic point of view, the driving force for sintering can be regarded as a "sintering pressure", which combines the effects of chemical potential gradient, stress, ect. and represents the overall driving force. Raj analyzed the sintering pressure from thermodynamic point of view. One simple expression for the sintering pressure was derived as

$$P_o = (2\gamma_b / \Delta) + (2\gamma / r) \qquad \textbf{Equation 2. 3}$$

where γ_b is the grain boundary free energy, γ is the surface free energy, Δ is the grain size and r is the radius of curvature of the pore surface. If an external pressure is applied, the sintering pressure can be approximated as:

$$P_o = (2\gamma_b / \Delta) + (2\gamma / r) + \sigma_{eff} \qquad \textbf{Equation 2. 4}$$

σ_{eff} is the effective pressure caused by external pressure. During the initial sintering stage, the σ_{eff} can be several orders than the external pressure because the compact particle only have point contact. In the sintering of polycrystalline materials, such as noble metals, an increase in density is usually accompanied by an increase of grain size, implying that the sintering pressure may become small at high densities.

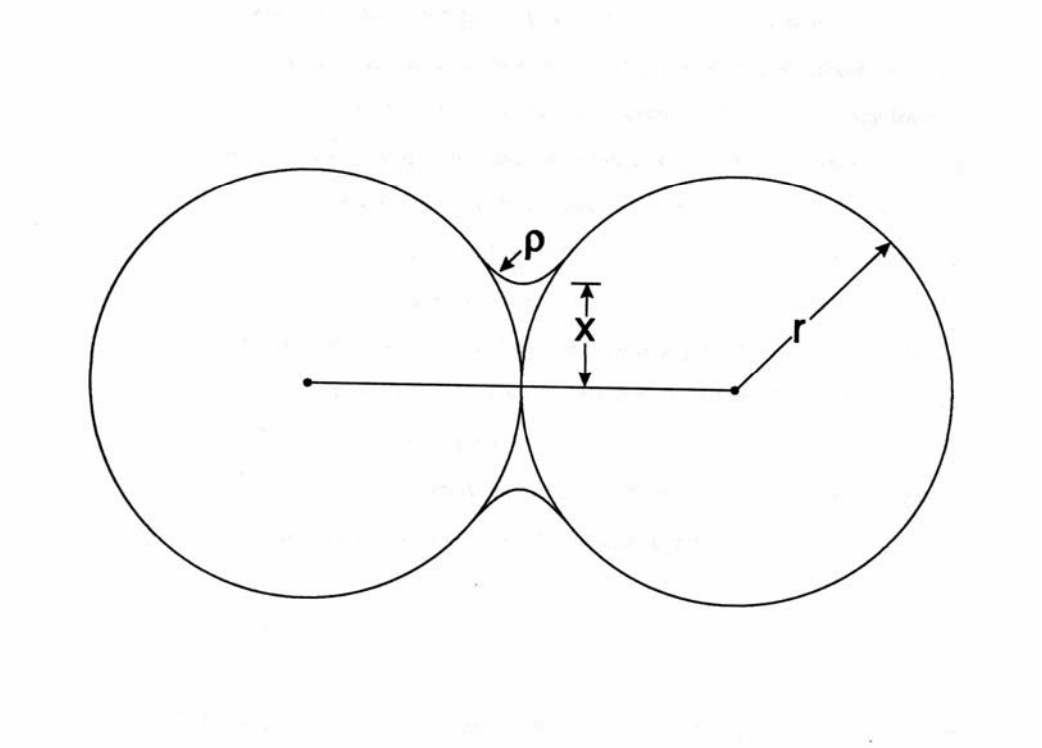

Figure 2.2. Schematic of two-sphere model.

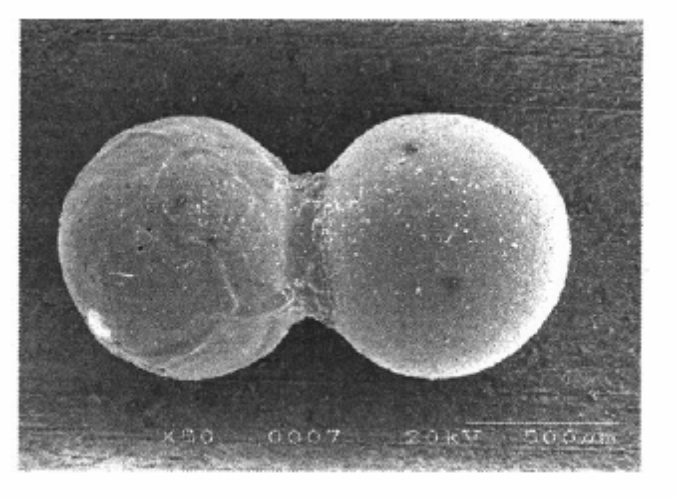

Figure 2.3 SEM photographs, left-Cu, right-Ni (Heating rate_300K per hour, sintering temperature: 1313K, isothermal sintering time: 600min).

From the kinetics point of view, mass transportation rate is activated by temperature and all the transport mechanisms are accelerated by elevated temperature. Simplified, the sintering/densification rate of compact powder can be approximated as:

Densification Rate = [Driving Force]*[Mobility] **Equation 2. 5**

And mobility is determined by mass transportation mechanism, which is thermal activated.

2.2 Challenges of sintering silver die-attach: high processing temperature

Due to the superior properties, sintered silver has already been widely used in microelectronic packaging such as conductive trace in ceramic substrate, electrode in monolithic inductor and capacitor, and etc. Figure 2.4 shows one hybrid circuit including Al_2O_3 substrate, conductive trace and electronic components such as capacities and inductors. The conductive trace is formed by sintering commercial silver paste with micron-size particle size. The electrodes in monolithic inductors and capacitors are also the sintered silver by low temperature co-fired ceramic (LTCC) technique [30, 31]. The fabrication processing is simple and mature: commercial silver pastes are screen-printed or stencil-printed onto the green tape of ceramics and co-sintered at high-temperature (>750^{o}C) [32].

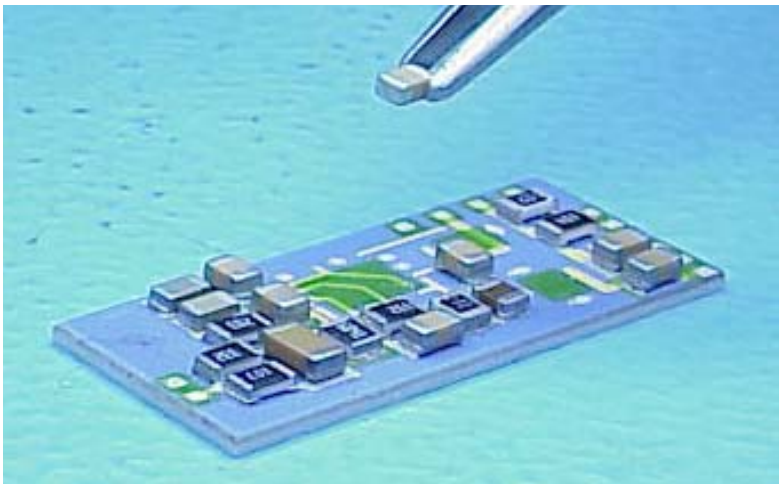

Figure 2.4. Applications of sintered silver paste: conductive trace in hybrid substrate and electrode in monolithic devices.

The challenge to implement silver sintering technique for die-attach is the high-processing temperature. The physical properties of a certain material are determined by its microstructure. To achieve dense microstructure, which has the desire properties such as good thermal and electrical conductivities with certain amount of sintering time, a high densification rate has to been attained. Equation 2.5 shows that the densification rate is controlled by driving force and mobility. Mobility is thermal activities, and thus the densification rate can be much faster at elevated temperature. Figure 2.5 shows the commercialized micron-size silver powders can not be sintered at a temperature at 300^{o}C. With low sintering temperature, the silver can not form the dense structure and thus can not have the desired properties. In order to attain high density, a high-temperature, usually higher than 750^{o}C, has to be applied to sinter micron-size silver paste. Such a high temperature will destroy semiconductor devices, substrates and any other interconnection materials. This is the reason why silver sintering is not applied to attach semiconductor devices for current industry practice.

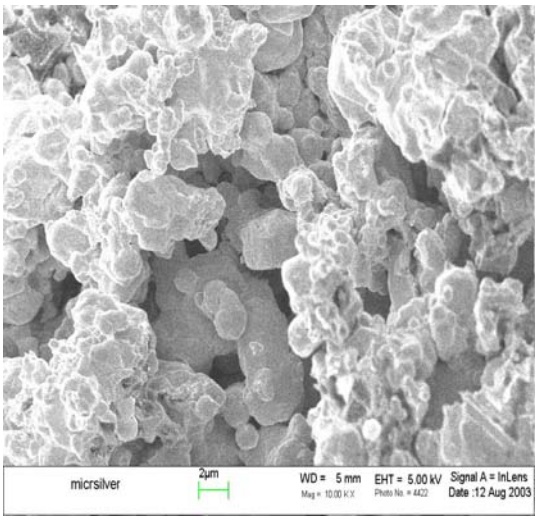

Figure 2.5. SEM observation of micron-size silver paste sintered at 300^{o}C.

2.3 Low-temperature sintering strategy I: pressure-assisted sintering

Equation 2.5 shows that the densification rate is only relative to mobility which is thermal activited; also the sintering driving force. In order to desnify silver compacts at a relative low temperature, the sintering driving force has to be increased since the thermal activated mobility is low. Equation 2.4 indicates that the application of external pressure can lower the sintering temperature since it can increase the sintering driving force. Several research works have already conducted to low-temperature sinter micro-size silver paste with the assitance of external pressure: Schwarzbauer, et al., developed a "diffusion welding joint technique"[33-35] for improved power device performance. Klaka and Sitting proposed that this technique will reduce thermo-mechanical stress [36]. Scheuermann, et al., reported the use of pressure to lower the sintering temperature of silver powder compacts for attaching power semiconductor devices in building power electronics modules, and demonstrated the achievement of significant improvements in performance and reliability in these power modules over the solder attached modules [33]. In chapter 3, the author also reports on the study of the pressure-assisted low-temperature sintering of silver pastes as a feasible die-attach alternative process to solder

reflow. The research works show that the measured properties of sintered silver joints are significantly better than those of solder joints. The large external pressure, however, makes the automatic manufacutre difficult to implement and also has the potential to break the brittle semiconductor devices.

2.4 Low-temperature sintering strategy II: reducing particle size to nanoscale

2.4.1. Nanoscale powder sintering challenge: agglomeration, aggregation and coarsening

Nanoscale material refers to the material with the particle size 1nm to 100nm. Compared with conventional micron-size powder, nanoscale powder has significantly larger surface energy. The driving force for sintering is the excess surface energy of a powder compact, and all sintering phenomena result in the reduction in the total interfacial energy. Thus, reducing the silver particle size from the micrometer to the nanoscale range can theoretically lower the sintering temperature. The sintering, however, is a processing which depends on mass transportation by atomic diffusion. The densification rate is not only determined by how easy the atoms can diffuse (driving force), but also by how the atoms diffusion (diffusion mechanisms). Agglomeration, aggregation and non-densification diffusion can ruin the sinterability of nanoscale materials.

The agglomeration and aggregation easily occur during nanoscale material due to the fine particle size of nanoscale powders. Figure 2.6 shows the difference between agglomeration and aggregation. Agglomerate is a mass of interconnected particles bonded together by weak forces (e.g Van der Waals (VDW) forces and/or electrostatic force). The agglomerated particles can be redispersed by external energy such as milling or ultrasonic vibration. Aggregate is a mass of interconnected particles bonded together by solid necks of significant strength such as chemical bonds [37]. The aggregation can barely be redispersed by external energy because of the strong bonding.

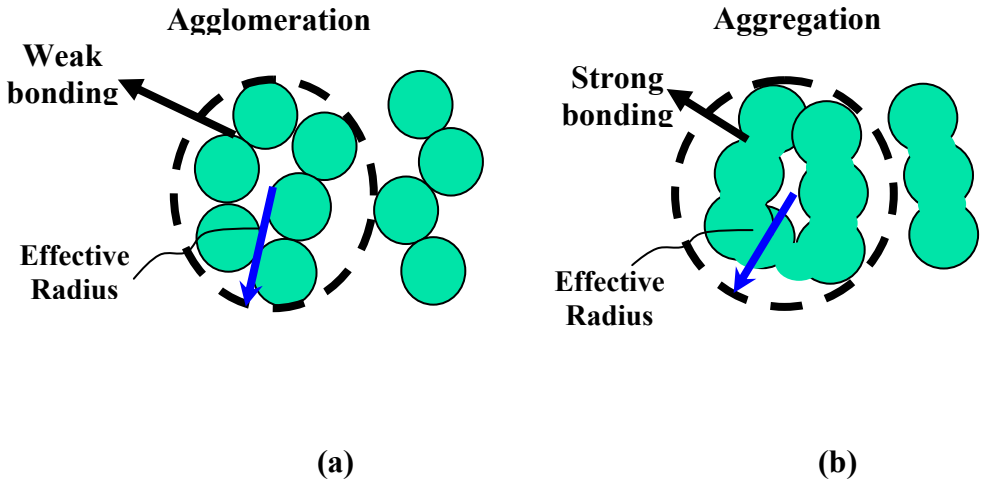

Figure 2.6 Schematics of agglomeration (a) and aggregation (b).

Both agglomeration and aggregation detrimentally result in the inhomogeneous distribution of particles and thus the large voids can be formed and initial density powder compacts before sintering can be significantly lower [38]. The lower initial density ruined the sinterability. The effective radius instead of the real radius of particle, are usually used to characterize the degenerated sinterability of agglomerated/aggregated particles. Figure 2.6 shows that the effective radius can be much larger than those of particles. When the effective radius reaches the micron size, the advantages of nanoscale particles are lost. Agglomeration can be eliminated by redisperstion with the assistance of external energy since they bond together by weak force. However, once aggregation forms, it can not be redispersed by the following processing, and thus, aggregation should be avoided from the powder preparation.

Another challenge for nanoscale material sintering is the non-densification diffusion at low-temperature. When a powder compact is sintered, necks form between the powder particles (mass transportation), and the compact may increase the density or just result in grain growth, particles rounding and etc; in other words, mass transportation is not a must to densify the compact. Densification is not only determined by how easily the mass transportation occurs, it also is determined by what kind of mass transport

mechanism occurs. It is generally agreed that there are six distinguished mechanisms contribute to the neck growth and to densification. Most of these mechanisms that involve the diffusive transport of matter to the growing neck; and Figure 2.7 shows these diffusion paths. Table 2.1 shows the sources and sinks of matter for each of these six mechanisms. All these transports of matter can cause neck growing and thus consume the sintering driving force; but only three of them can densify the powder compacts.

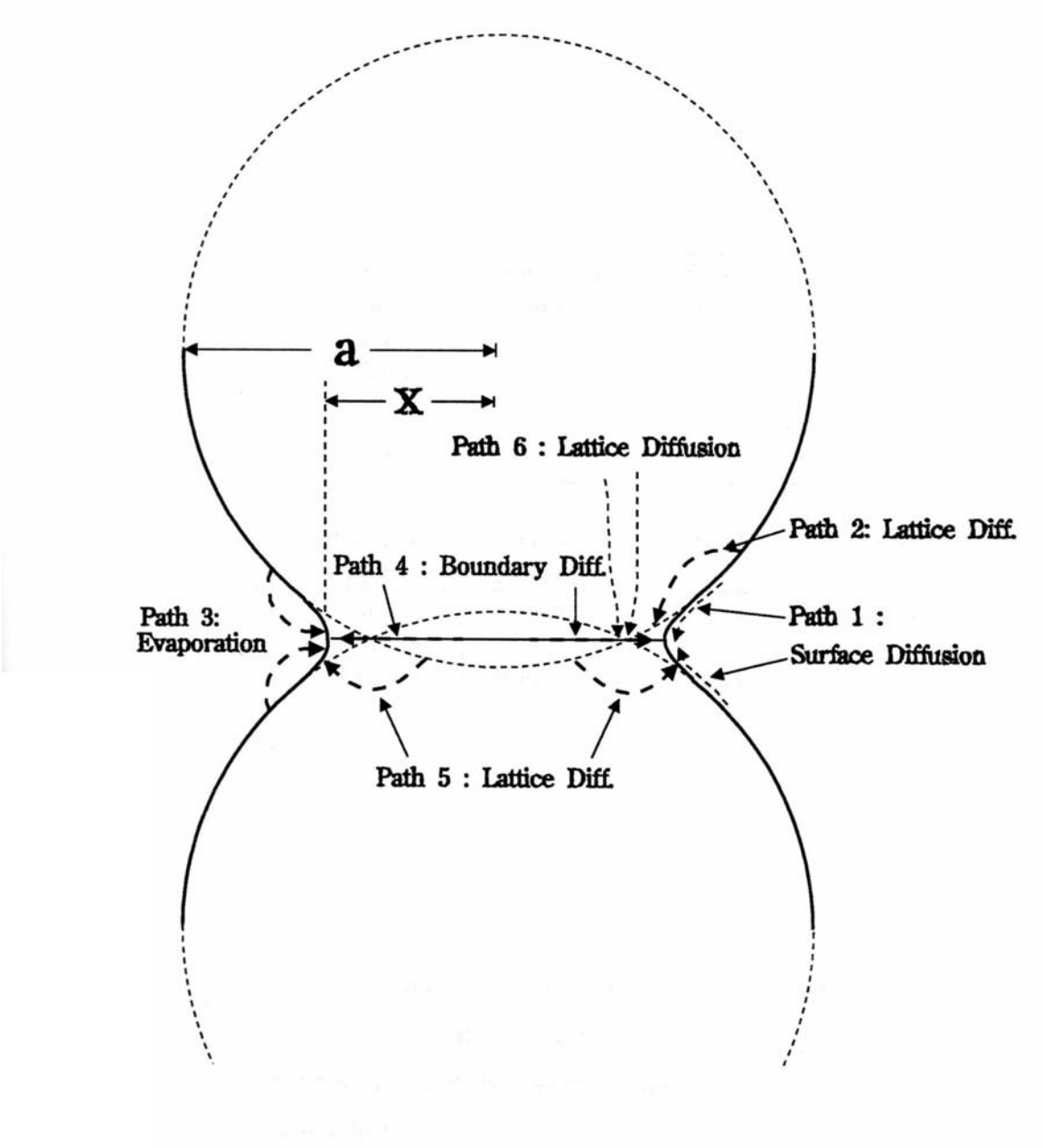

Figure 2.7 Six paths for matter transport. Only paths 4,5 and 6 causes densification.

Table 2.1 The transport paths, sources and sinks of matter and whether densification occurs or not during sintering.

Mechanism Number	Transport Path	Source of Atoms	Sink of Atoms	Densification ???
1	Surface Diffusion	Surface	Neck	No
2	Lattice Diffusion	Surface	Neck	No
3	Vapor Diffusion	Surface	Neck	No
4	Boundary Diffusion	Grain Boundary	Neck	Yes
5	Lattice Diffusion	Grain Boundary	Neck	Yes
6	Lattice Diffusion	Disclocations	Neck	Yes

There are several dominated mass transfer mechanisms operative in the sintering of noble metal compacts. [39] (see Figure 2.8). At low temperatures, it is controlled by surface diffusion and results in neck formation between particles (strong bonding) and/or significant grain growth, but little actual densification. At higher temperatures, either grain boundary diffusion or lattice diffusion, dominates the sintering process and leads to densification. If a non-densifying mechanism, such as surface diffusion, is allowed to proceed, it will consume the driving force needed for densification, making it difficult to achieve high density later in the sintering process. Nanoscale materials are particularly susceptible to this problem because they have very high surface area to volume ratio. The high surface area to volume ratio enhances the surface diffusion rate at very low temperature. The non-densifying diffusion may rounds the particles, enlarge the particle size (coarsening) and/or even aggregate particles. Figure 2.8 also shows the schematic of change in the densification rate with temperature. According to rapid rate sintering theory, the low-temperature regime should correspond to poor or no densification

(surface diffusion), and high-temperature regime should correspond to much more efficient densification (via grain boundary or lattice diffusion). So, the final density (desired properties) of sintered nanoscale materials is not only determined by initial particle size and sintering temperature, but also the heating rate.

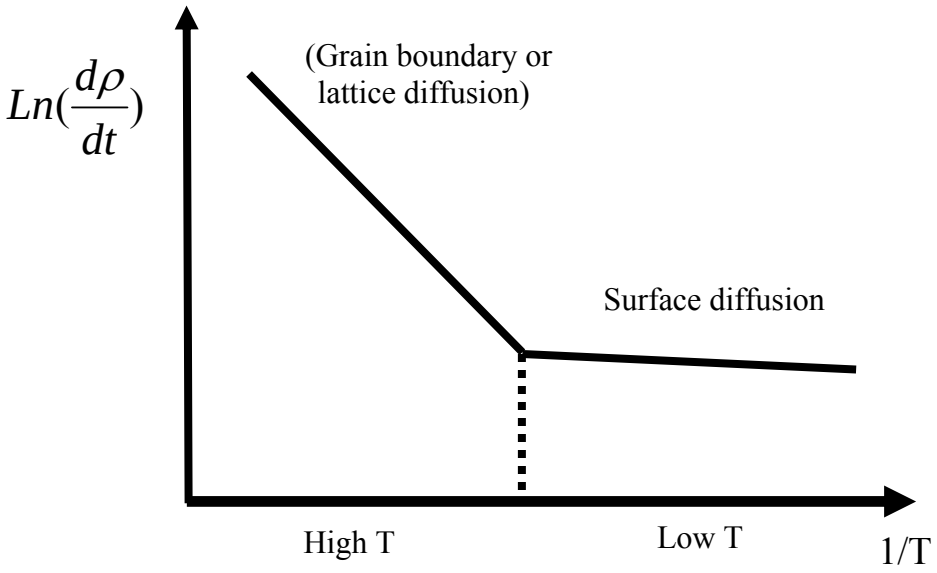

Figure 2.8 Schematic of change in densification rate with temperature; according to rapid rate sintering theory, the two regimes should correspond to poor or no densification (surface diffusion) at low temperature and much more efficient densification (via grain boundary or lattice diffusion) at high temperature.

2.4.2. Current sintering strategy to overcome non-densification diffusion– fast heating rate

An approach to avoid non-densification diffusion is to use a fast heating rate to bypass the low-temperature regime quickly. With this approach, the surface diffusion has no sufficient time to occur and the non-densification diffusion can be avoided at low-temperature. At high-temperature, the densification diffusion such as grain boundary diffusion and/or lattice diffusion have already dominated and can densify the powders.

Several advanced sintering techniques have been developed to improve the heating rate, such as microwave sintering, plasma activated sintering, laser sintering, field-activated sintering technique (FAST), etc [40-43] . An extremely high heating rate (4900^{o}C/min) realized by microwave sintering suppresses grain growth and enhances densification rates by up to 4 orders of magnitude compared to slower conventional heating [44]. Figure 2.9 shows lead zirconate titanate (LZT) sintered at 1150°C for 2 hours in air: (a) with the heating rate 0.5°C/minute; (b) with the heating rate 100°C/minute. The sintered lead zirconate titanate with fast heating rate has much denser microstructure than the one with a slow heating rate. Table 2.2 shows the microwave sintering nanoscale copper with particle size 52nm at 868^{o}C with a different heating rate. By using a fast heating rate (microwave sintering 5 minutes), 83% relative density can be obtained; the conventional sintering (furnace sintering 120 minutes) can only achieve 76 % density [45]. All these evidences show that the fast heating rate can enhance the densification and prevent particles coarsening. The enhanced heating rate, however, may induce significant thermal shock. This is a drawback for microelectronic packaging, because it is one of the major failure mechanisms in electronic packages [46, 47]. Also, the facilities to realize fast heating rate are much complicated and expensive than baking oven (for conductive adhesives) and/or reflow furnace (for solders), both of which are widely used in electronic industry. Figure 2.10 shows the schematic and facility to realize field-activated sintering technique (FAST). Due to these reasons, a fast heating rate is not practicable for sintering die-attach application.

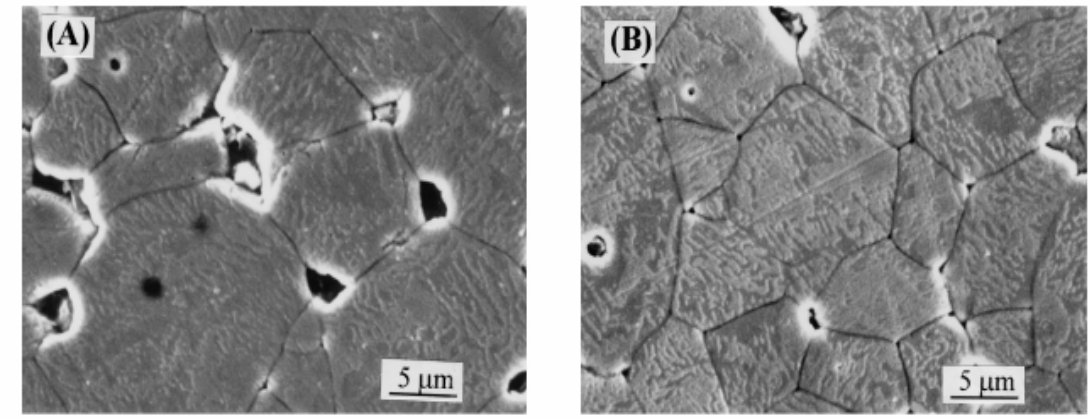

(a) **(b)**

Figure 2.9 The SEM micrographs of PZT (LEAD ZIRCONATE TITANATE) sintered at 1150°C for 2 h in air: (a) with the heating rate 0.5°C/minute; (b) with the heating rate 100°C/minute.

Table 2.2 Microwave sintering nanoscale copper with particle size 52nm at 868^{o}C.

Sintering	time	Sintered density	Crystallite
Conventional	120 min	76%	296 nm
Microwave	5 min	83%	71 nm

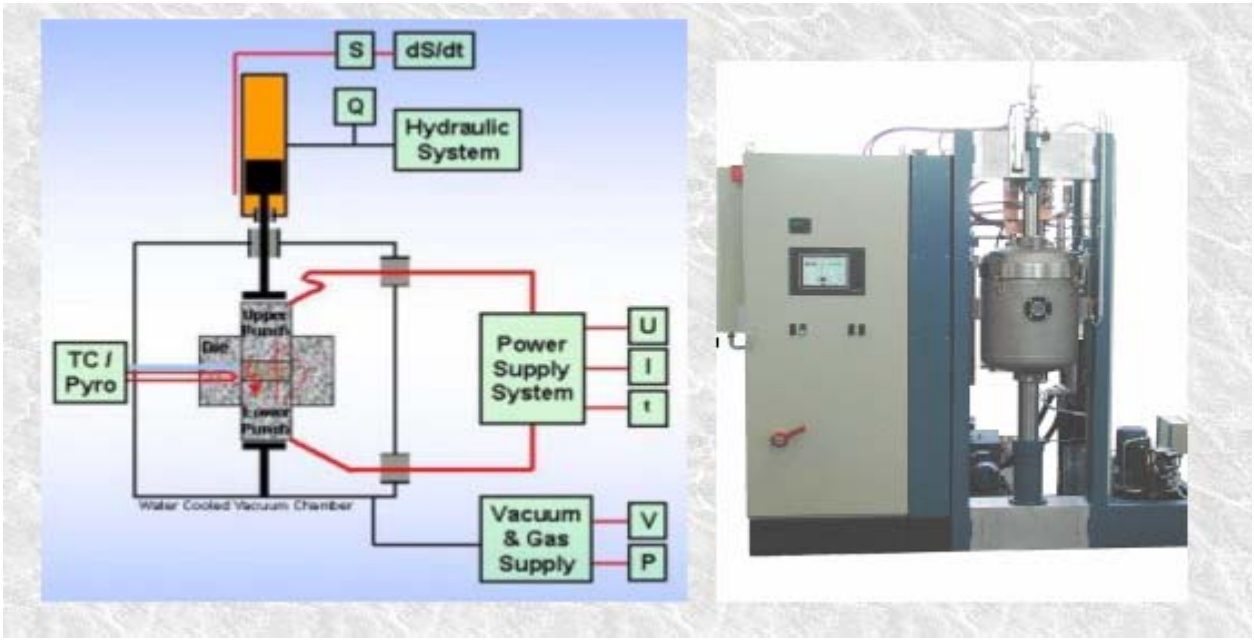

Figure 2.10 The schematic and facility to realize FAST sintering.

Chapter 3 Pressure-assisted low-temperature sintering of micro-scale silver paste for die-attach

Sintered silver has demonstrated superior properties in microelectronic packaging and many other applications. The potential advantages such as high temperature stability, high electrical and thermal conductivity, good mechanical properties and etc make it a promising candidate for die-attach application. The high processing temperature, however, is the biggest challenge. The essential way to implement sintering technique for die-attach application is to lower the sintering temperature. With a lower processing temperature, the mobility, which is thermally activated, keeps low, and the sintering driving force has to be boosted to compensate the low mobility (Equation 2.5). Equation 2.1 to Equation 2.4 show that one possibility to increase the driving force is to apply external pressure. In this chapter, pressure-assisted low-temperature sintering of silver paste is presented to be a viable alternative to solder reflow as a die-attachment solution.

To prevent damaging the semiconductor power devices, a quasi-hydrostatic pressure is used to lower the sintering temperature. The effect of processing parameters such as temperature, pressure and sintering time are investigated. Characterization of the silver-attached samples shows that the external pressure can significantly lower the sintering temperature. With the assistance of a large external pressure (larger than 40 MPa), the micron-size silver paste can be sintered at a temperature as low as 240^{o}C for a few minutes. The measured results show a significant improvement in electrical conductivity, thermal conductivity and mechanical strength of the joints. Given that silver deforms with little accumulation of inelastic strains, and given the absence of large voids in the attachment layer, the joint is more resistant to fatigue failure than solder attached joints. This alternative process is also suitable for high temperature packages due to the high melting temperature of silver. The large external pressure, however, makes the automation difficulty and also is a potential to damage the device.

3.1 Experimental procedure

3.1.1. Pressure-assisted sintering die-attach procedure

The pressure-assisted low-temperature sintering process consists of four major steps. Figure 3. 1 schematically shows these steps: (1) substrate metalization with a silver film by electroplating or vapor deposition; (2) silver paste screen/stencil printing; (3) pre-heat; and (4) pressure-assisted sintering in a quasi-hydrostatic press. Direct bond copper (DBC) ceramic substrate was selected as substrate to attach the semiconductor devices due to its superior properties such as low coefficient thermal expansion (CTE), high thermal conductivity, etc. A thin silver layer was electroplated on the substrate with the thickness 5 to 20 micron. If copper is the terminal surface of the substrate, then a thin layer of nickel was plated before the silver deposition in order to improve the adhesion between silver and the substrate. Two kinds of commercial silver pastes were purchased from Heraeus with product number C8772 and C1075. From the product datasheet, we know that paste C8772 is a low-temperature sinterable paste and can be sintered at a temperate as low as 500^{o}C. Paste C1075 is a common-purpose silver paste with a suggested sintering temperature 850^{o}C. Besides silver particles, the pastes also have organic contents such as binder, thinner, and etc. The morphology and purity of the silver particles in the paste were examined using Scanning Electron Microscopy (SEM) and Energy Dispersive Spectrometer (EDS). The chosen silver paste was stencil-printed on the substrate to a thickness of 40 to 100 microns, and trapped air pockets within the films were subsequently removed by a vacuum pump. The printed silver layers were pre-heated at temperatures below 300^{o}C for a few hours to remove much of the organic components, solvents and binders, in the paste. The pre-heat conditions were determined by studying the paste binder burnout process using Thermal Gravitational Analysis (TGA) and examining the heat-treated microstructure using Scanning Electron Microscopy (SEM). Finally, the pre-heated silver was pressurized and sintered at a temperature similar to that for solder-reflow. The pressure-assisted sintering was realized by a hot-pressure laminating machine. Semiconductor materials usually have a very high yielded stress, and a 40 MPa pressure with homogenous distribution theoretically will not

damage the devices. Unfortunately, semiconductor materials also belong to brittle materials, just like some ceramic materials. Given a low fracture toughness, for instance single crystal silicon with fracture tough 0.8 MPa*m $^{1/2}$, the semiconductor materials present a catastrophic fracture failure, which leads to the failure resistance of brittle materials several orders lower than the theoretical value. Any local stress concentration will permanently damage the device. Directly applying mechanical force on the semiconductor die will unavoidably cause stress concentration and destroy the device. To avoid cracking the semiconductor devices due to stress-concentration spots, a fixture filled with soft silicone rubbers was designed and fabricated for carrying out pressure-assisted sintering. Figure 3. 2 schematically shows how the quasi-hydrostatic pressure was achieved by this fixture. Due to the flexibility of the silicone rubber, the stress concentration can be avoided. Figure 3. 3 shows the facilities to achieve pressure-assisted sintering. Figure 3. 3 (a) is a laminating machine, which can supply both elevated temperature and mechanical force for pressure-assisted sintering. The laminating machine itself has a temperature controller, but the temperature overshoot can only be controlled within 10% percent. An additional temperature controller shown in Figure 3. 3 (a) was also built to precisely control the temperature. With this temperature controller, the temperature overshoot can be controlled within 1%. To ensure a stable temperature signal, the top and bottom plates have a deep hole respectively. The J type thermal couples were place into these holes to sample the temperature signals. To reduce the temperature gradient, both plates are controlled at the same temperature. There is a temperature difference between plates and die-attach samples. Temperature calibration was conducted by measuring the temperature difference and the difference was compensated to control the temperature of the die-attach samples at desire temperatures. Figure 3. 3 (b) is the fixture filled with silicone rubber, which is used to realize quasi-hydrostatic pressure.

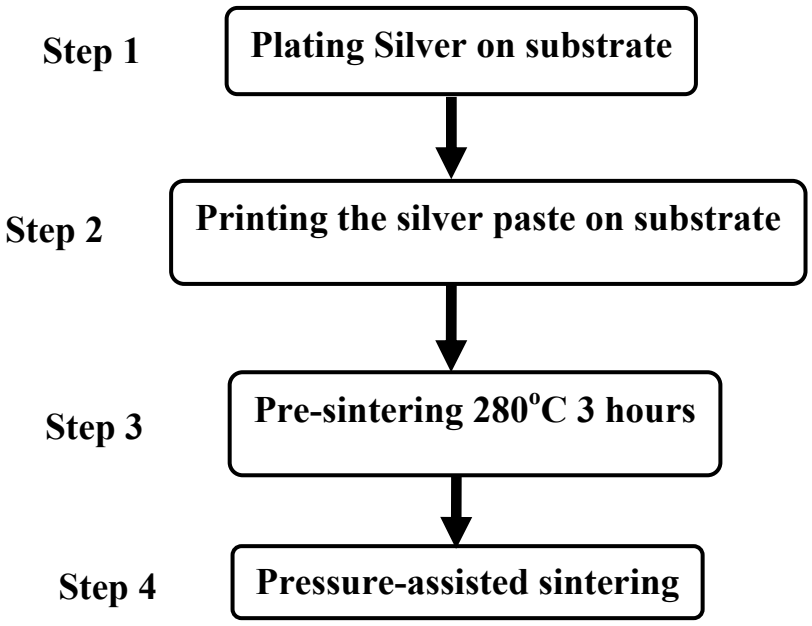

Figure 3. 1. Pressure-assisted sintering die-attach procedure.

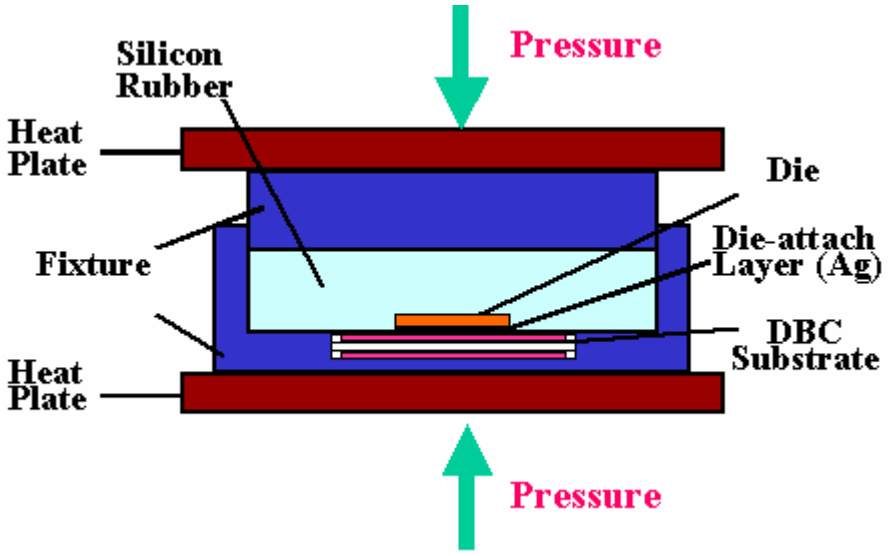

Figure 3. 2 Scheme of a fixture used for sintering under quasi-hydrostatic conditions.

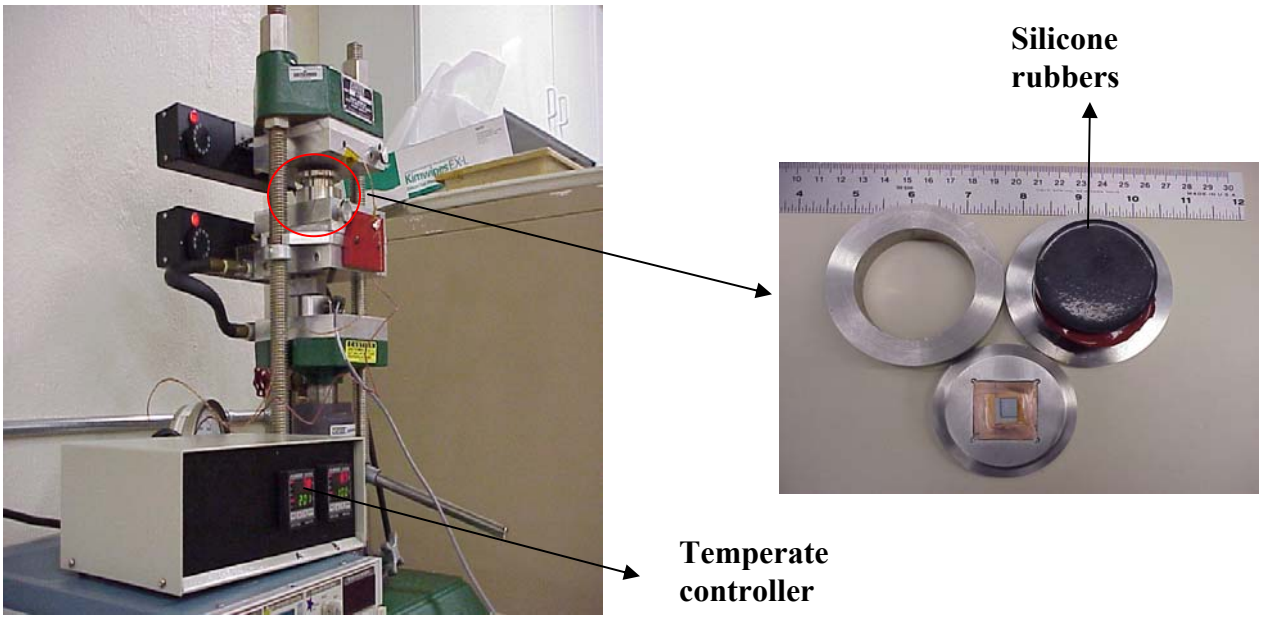

(a) (b)

Figure 3. 3. Facilities for achieving pressure-assisted sintering: (a) laminated machine and (b) fixture filled with silicone rubbers.

During the pressure-assisted sintering, there are three processing parameters – temperature, pressure and time. To symmetrically study how these processing conditions affect the sintering, a partial three-level factorial experiment was conduct. The experimental parameters selection is shown in Table 3.1. Owing to the amount of work and time required to perform a full factorial experiment, only a fraction of the experiments was done. To reduce the number of tests, two of the variables were fixed when investigating the effect of one variable. The fixed values for the variables are 240^{o}C, 40 MPa and 5 minutes when one variable is being changed.

Table 3.1 Experimental parameters selection to investigate the effect of processing parameters to the pressure-assisted sintering.

	10MPa			20MPa			40MPa		
Time / Temp	2 min	5 min	10 min	2 min	5 min	10 min	2 min	5 min	10 min
170°C								Yes	
240°C		Yes			Yes		Yes	Yes	Yes
300°C								Yes	

3.1.2. Properties characterization of sintered silver joints

To investigate the properties of pressure-assisted low-temperature sintered silver layers, the ratio of porosity (relative density), mechanical strength, electrical and thermal conductivity of the layers were measured and compared with those of the solder reflowed layers. Since it is difficult to determine the relative density of sintered films, we prepared bulk silver samples using a die and plunger with half inch diameter. The silver paste was put into the die and pre-heated to 300°C for 3 hours. After that the pressure-assisted sintering was realized by pressing the plunger during the heating process. The prepared samples are with the thickness 1.5 to 2 mm. The densities of the sintered bulk samples were determined by the Archimedes' method. This principle states that every solid body immersed in a fluid loses weight by an amount equal to that of the fluid it displaces. The density of a solid is determined with the aid of a liquid whose density ρ_o is known (DI water). The weight of solid in air (A) can directly be measured by a balance (OHAUS, Explorer). The weight of solid in auxiliary liquid (B) can be measured by the same

balance with the assistance of densification determination kit (Ohaus 470007) shown in Figure 3. 4. The density of solid (ρ_1) can be calculated by

$$\rho_1 = \frac{A}{A-B} * \rho_o \qquad \textbf{Equation 3. 1}$$

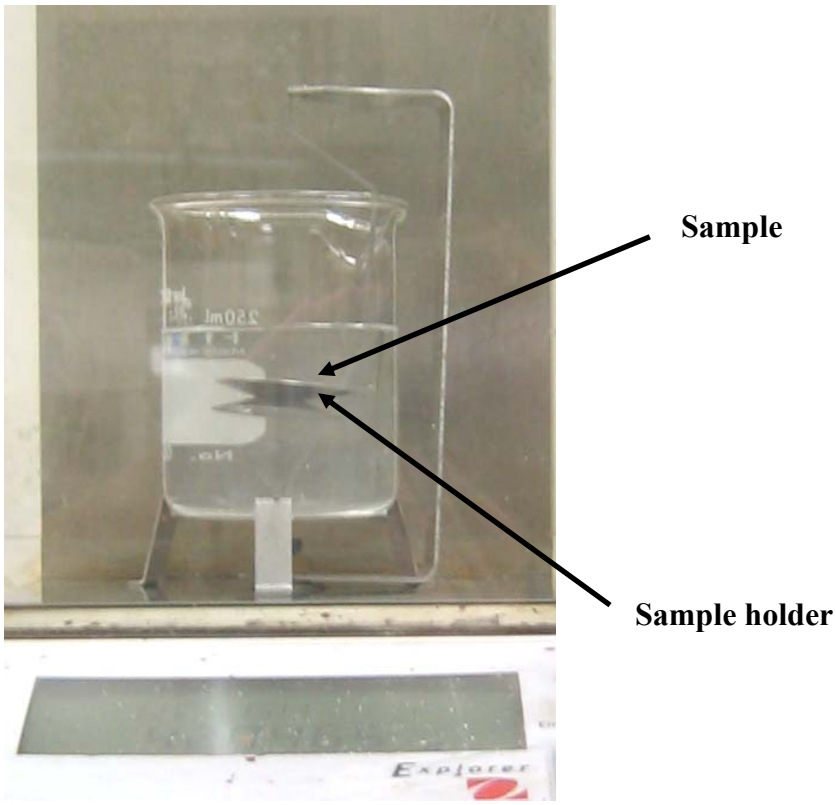

Figure 3. 4 Archimedes' method to measure density.

Of the samples that were attached to substrates through the sintered silver films, the mechanical strength of the joints was measured using an Instron 5566 Universal Testing Machine. In order to measure the resistivity of the sintered silver joints, silver prints formed like the resistor pattern were prepared by screen-printing and sintered under pressure, and their resistances were measured with a digital multi-meter. Figure 3. 5 shows the printed pattern for resistivity measurement of sintered silver paste. The cross-

sectional area of the resistor line in the pattern was measured using a Dek-Tak3 profilometer. The average of three measurements was used to determine the cross-sectional area. The resistivity of the silver trace is calculated by:

$$\rho = \frac{R^* A_{average}}{L} \qquad \textbf{Equation 3. 2}$$

where ρ is resistivity; R is the resistance; $A_{average}$ is the average cross-sectional area; and L is the total length of the line.

Figure 3. 5. The silver resistor pattern used for resistance measurement.

Thermal resistance can be measured by a steady-state method using equation:

$$R_t = Q/(T_t - T_b) \qquad \textbf{Equation 3. 3}$$

where, R_t is the thermal resistance of measured materials, T_t is the top surface temperature of the measured materials, and T_b is the bottom surface temperature of the

measured materials. The main drawback of this method is the need to know exact amount of heat flow into the measured specimen and the temperature difference between top and bottom surfaces of the specimen, which are also difficult to measure. In my dissertation, the laser flash-light method thermal is applied to measure the conductivity of the sintered bulk silver samples. The thermal conductivity was determined by measuring its thermal diffusivity, specific heat, and density. The thermal diffusivity was obtained using Parker's flash-light method [9]. The laser flash technique is schematically shown in Figure 3. 6. This technique is based on the measurement of the thermal transient of the specimen's backside surface when a pulsed laser illuminates the front. With this arrangement, it is possible to avoid interferences between the thermal sensor and the heat source [48]. If the specimen is a homogenous material without thermal interfacial resistance, we can derive thermal diffusivity by the well-known Parker equation [49]:

$$a = \left(0.139 * D^2\right) \Big/ t_{1/2} \qquad \textbf{Equation 3. 4}$$

where a is the thermal diffusivity, D is the thickness of the sample and $t_{1/2}$ is the half-temperature rise-time of the specimen's backside. The specific heat is measured using differential scanning calorimetry (DSC). A Netzsch Model 404 differential scanning calorimeter (DSC) is used to measure specific heats and a known mass sapphire is applied as a standard. The density of samples is measured by Archimedes method. The thermal conductivity can be derived:

$$\kappa = \alpha * c * \rho \qquad \textbf{Equation 3. 5}$$

where κ is the thermal conductivity, α is the thermal diffusivity, c is specific heat and ρ is the density.

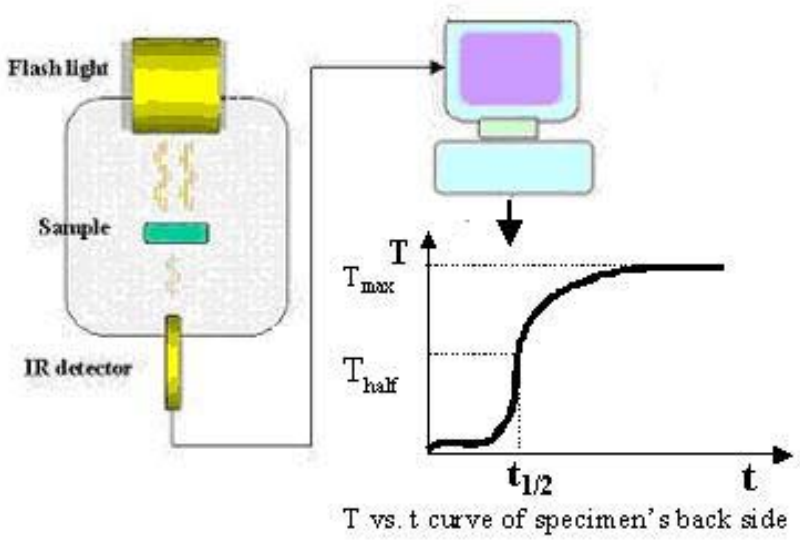

Figure 3. 6 Schematic for measuring thermal diffusivity by the laser flash technique.

By conventional stead-state method, the interfacial thermal resistance is even more difficult to measure because the interface is too thin to measure the exact temperature difference across it. To measure and investigate the thermal properties of the die-attach layer, the laser flash technique, which was used to obtain the interfacial thermal resistances of the silver/copper and solder/copper that is usually present in the attached structures. This transient method does not need to know the exact amount of heat, and thus it is possible to avoid interferences between the thermal sensor and the heat source. It requires samples of small size and simple geometry and allows rapid data acquisition, which is another advantage compared with steady-state methods for measuring thermal diffusivity/conductivity.

Applying this method to measure the interfacial thermal resistance is more complex than thermal conductivity measurement. Figure 3. 7 schematically shows the method to measure the interfacial thermal resistance. Firstly, we assume the laser flash is an ideal heat pulse with homogenous heat distribution in the Y-Z plane and heat only flows from the front to back surface of the specimen. Then we can consider this as a one

dimensional heat transfer case. The differential equations for heat diffusion that must be solved are given in Equation 3.3 and Equation 3.4. Equation 3.5 and Equation 3.6 are the boundary condition, and Equation 3.7 is the initial condition.

$$a\frac{\partial^2 T_1(x,t)}{\partial x} = \partial\frac{T_1(x,t)}{\partial t} \qquad \textbf{Equation 3. 6}$$

$$a\frac{\partial^2 T_2(x,t)}{\partial x} = \partial\frac{T_2(x,t)}{\partial t} \qquad \textbf{Equation 3. 7}$$

$$-k\frac{\partial\ T_1(-l_1,t)}{\partial x} = q(t) \qquad \textbf{Equation 3. 8}$$

$$-k\frac{\partial\ T_1(0,t)}{\partial x} = -k\frac{\partial\ T_2(0,t)}{\partial x} = h(T_1(0,t) - T_2(0,t)) \qquad \textbf{Equation 3. 9}$$

$$T_1(x,0) = T_2(x,0) = 0 \qquad \textbf{Equation 3. 10}$$

where T is the temperature, t is the time, k is the thermal conductivity and q is the flash energy illuminating onto the specimen, h is the heat transfer coefficient, and thus $1/h$ is the thermal resistance per area caused by die-attach layer. H can be expressed as a function of $a1$, $p1$, c_1, D_1, a_2, p_2, c_2, D_2 and $t_{1/2}$, by solving the above differential equations, where a, p, c are thermal diffusivity, density and specific heat of materials 1 and 2. Obviously, the thermal resistance per area caused by the die-attach layer, $1/h$ can be calculated once we measure $t_{1/2}$ and know the materials' properties. Several $1/h$ with different thickness of the die-attach layer can be obtained and the intercept at zero thickness (R_i) represents the thermal interfacial impedance of the specimen. Hung Joo Lee [50] gave the solution of the heat transfer equation and numerical-analysis software was developed to calculate the heat transfer coefficient.

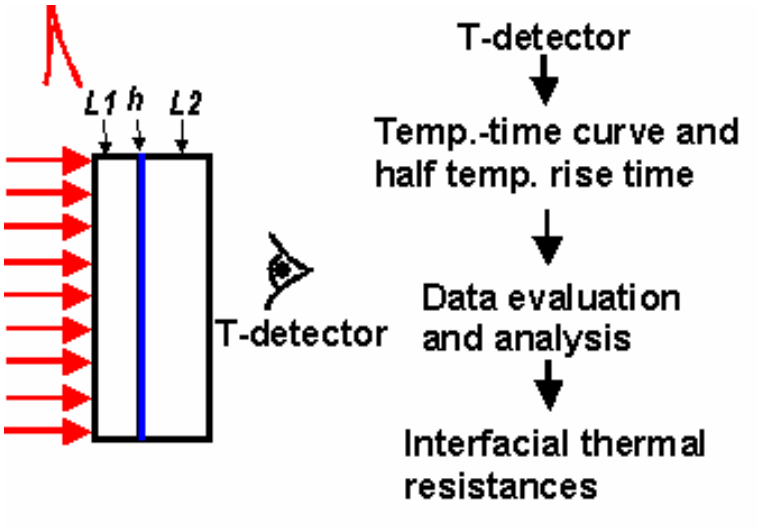

Figure 3. 7 Schematic for measuring interfacial thermal resistance in a bilayer structure with a thin attachment layer.

The samples for laser flash measurements were prepared by bonding copper discs with either Pb-Sn solder or silver. To fabricate the silver connected discs, the silver paste was sintered under an applied pressure using a set-up similar to that shown in Figure 3. 2 to investigate pressure assisted sintering of silver paste at low temperature. To ensure good bonding, the copper discs were plated with a thin layer of gold using an electroless gold bath since the silver paste does not contain flux and is unable to clean the copper surface. The sintering process was carried out in air at 240^{o}C under a 40 MPa external pressure for 5 minutes and allowed to cool in air. The solder-attached samples were fabricated by reflowing the sandwiched solder paste in a belt-type Sikama reflow oven following the typical heating profile for eutectic Pb-Sn solder reflow with a peak temperature of 210^{o}C. The copper discs in one set of samples were soldered bare while the discs in another set were plated with gold using the same procedure used for the discs in the sintered silver-attached samples. The thickness of the solder layer was controlled by varying the amount of solder paste and by embedding several high-lead solder balls in

the paste layer. Excess solder on the edges were polished off and the samples were cleaned with an aqueous flux cleaner.

Coating of the substrate with a noble metal like gold is commonly used to improve die-attach joint quality. To determine if the coating has an effect on the interfacial resistance, one set copper discs with different thicknesses were subjected to the laser flash technique before and after gold plating to obtain the half-temperature rise time. The discs were then bonded using reflowed solder (Pb-Sn) or sintered silver to form the specimens for thermal interfacial resistance measurement. The resulting structure is shown in Figure 3. 8 and except for the absence of a silicon device, is structurally similar to device die-attach structures. Three types of samples were fabricated: solder-attached bare copper discs, solder-attached gold-plated copper discs, and sintered silver-attached gold-coated copper discs. Half-temperature rise-times of the samples were measured using the laser flash apparatus, and the heat transfer coefficient contribution from the attachment layers were calculated using the numerical-analysis software available with the experimental apparatus.

Figure 3. 8 The samples prepared to measure the thermal interfacial resistance.

3.1.3. Reliability evaluation of sintered die-attachment

Destructive testing was done to determine the adhesive strength of the silver joint using a chisel to detach chips from the direct-bonded-copper (DBC) substrate. A Tenney Jr environmental chamber was used for the thermal cycling test. The JEDEC standard H (JESD22-A104-B) was selected as the testing condition and the temperature profile is shown in Figure 3. 9. The devices, supplied by IXYS (9 mm x 7 mm), were attached onto direct bond copper (DBC) substrates (25.4mm x 25.4 mm) using pressured-assisted sintering (240^{o}C, 40MPa and five minutes) or eutectic solder (Sn63Pb37) reflow. During testing, one thermal cycle time lasted about 84 minutes. Scanning acoustic microscopy (SAM) and scanning electronic microscopy (SEM) were used to monitor and determine the failure mechanism of the samples.

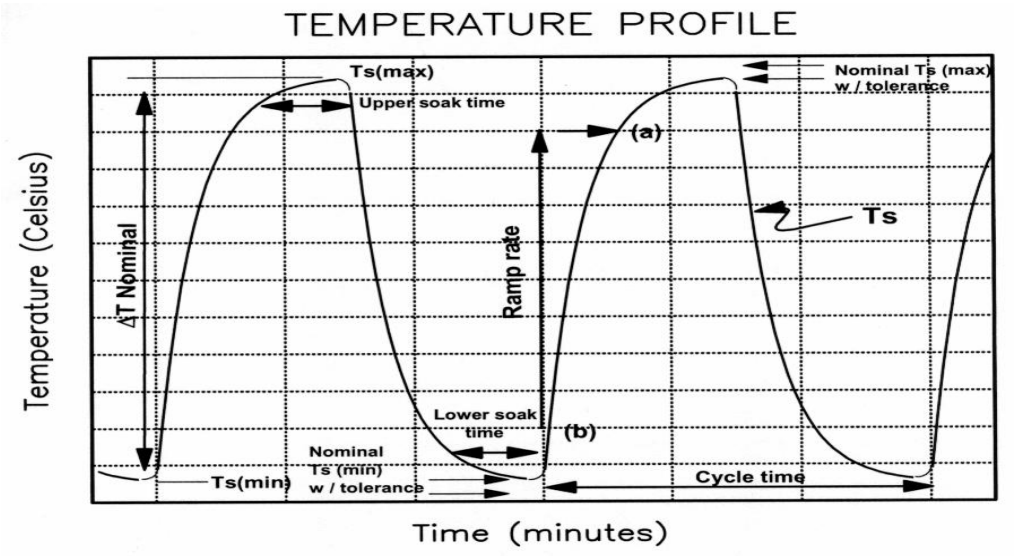

Figure 3. 9 Temperature cycling profile for reliability testing of the die-attach layers.

SAM is a non-destructive imaging technique, which can detect voids and defects under the devices using acoustic signal. When an ultrasonic wave is incident on an interface between two different materials, part of the wave is transmitted while the other part is reflected. The amplitude, time of flight and polarity of the reflected signal provide

crucial information about the voids. Reflection of an acoustic signal is governed by acoustic impedance of a material, which is the ratio of the acoustic pressure to the particle velocity per unit area; acoustic impedance is defined as the following,

$$Z = \rho.v \qquad \textbf{Equation 3. 11}$$

where, Z_i is the acoustic impedance, ρ is the density of the material, and v = velocity of sound in material. SAM microscope employs a focused transducer to generate and receive the ultrasound beneath the surface of the sample. The transducer is scanned across the sample in several passes for image generation. Scan time varies from seconds to minutes depending on the desired resolution and the area of scan. Ultrasonic waves are very sensitive to the density variations and thus can detect the voids underneath the attached devices. Usually, one SAM microscope has several transducers which can emit sonic with different frequency. Table 3.2 lists the resolution and penetration of transducers with different frequency. Selecting suitable transducers is based on the trade-off between resolution and penetration. Basically, high frequency acoustic gives us higher resolution, but less penetration. In my experiment, 75MHz transducer is chosen based on the penetration and resolution consideration.

Table 3.2 Resolution and Penetration of transducers with different frequency

Frequency (MHz)	Wavelength in Water (micrometer)	Resolution (surface) (micrometer)	Resolution in Material (micrometer)	Penetration (micrometer)
30	50	35	70-175	7000
50	30	20	40-100	5000
100	15	10	20-50	2000
500	3	2	4-10	400
1000	1.5	1	2-5	200

Scanning electronic microscopy (SEM) is a destructive method to study the microstructure of die-attach layer. The die-attached samples need to be sectioned and

polished for observation under SEM. First, the samples were mounted in a permanent, slow-cure, two-part epoxy. After that, attached samples were sectioned using a slow speed diamond saw using moderate pressure for cutting. To the begin with, the samples are grinded and polished. Finally, the samples were coated with ultra-thin gold (about 2 nm) before putting into the chamber of scanning electronic microscopy.

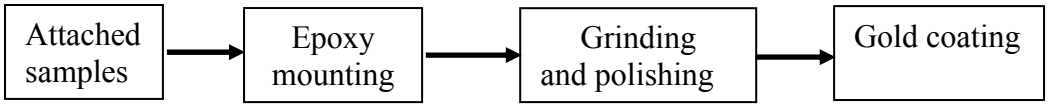

Figure 3. 10 Samples preparation for SEM observation.

3.2 Results and discussion

3.2.1. Characterization of micron-size silver paste

Two kinds of silver pastes, with the product number C1075 and C8772, are acquired from Heraeus. The particle size of both pastes ranges from 1 to 3 microns. Shown in Figure 3. 11 is the SEM and EDS results of the silver pastes pre-heated at 270^{o}C for 3 hours, indicating that the C1075 paste contains nearly pure silver particles, while the C8772 has about 20% lead. Figure 3. 12 shows the phase diagram of silver and lead. The phase diagram indicates that a liquid phase will coexist with a silver-rich solid phase when the temperature is 273^{o}C. A temperature higher than that temperature will increase the ratio of liquid phase to the silver rich solid phase. Until about 820^{o}C, the whole composition turns into liquid phase. The existing liquidized phase can lower the sintering temperature of silver because it increases the mobility of silver particles, and can also fills into the large voids between silver particles to increase the relative density. The additional 20% lead makes silver paste C8772 a pseudo low-temperature sinterable silver paste. The application of silver paste C8772 for die-attach has several drawbacks.

The additional lead potentially ruins the superior performance of pure silver. The low melting temperature (liquid phase starts to occur at a temperature as low as 273^{o}C) makes it impossible for high-temperature application. Also, the lead-contained silver raises serious health and environmental concerns. Due to the reasons listed above, the pure silver paste C1075 is used as sintering die-attach material.

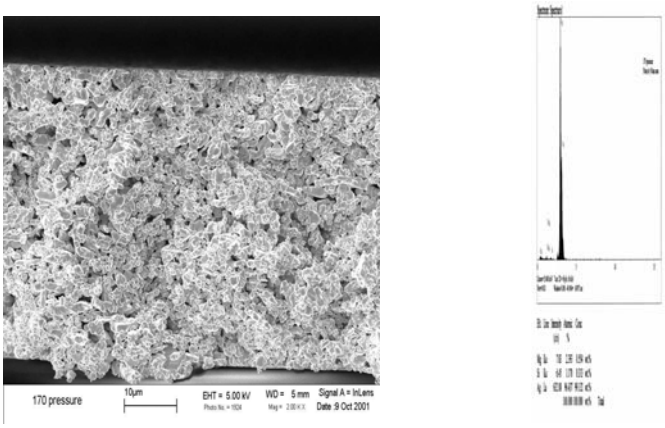

(a)

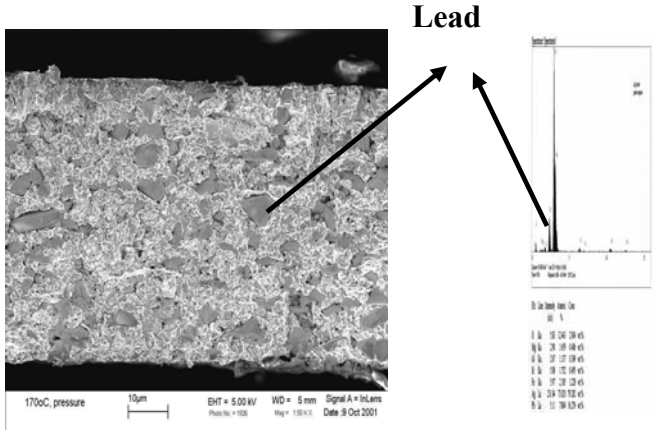

(b)

Figure 3. 11 Scanning Electron Microscopy (SEM) micrograph and Energy Dispersive Spectrometer of two silver pastes. (a) is C1075; (b) is C8772.

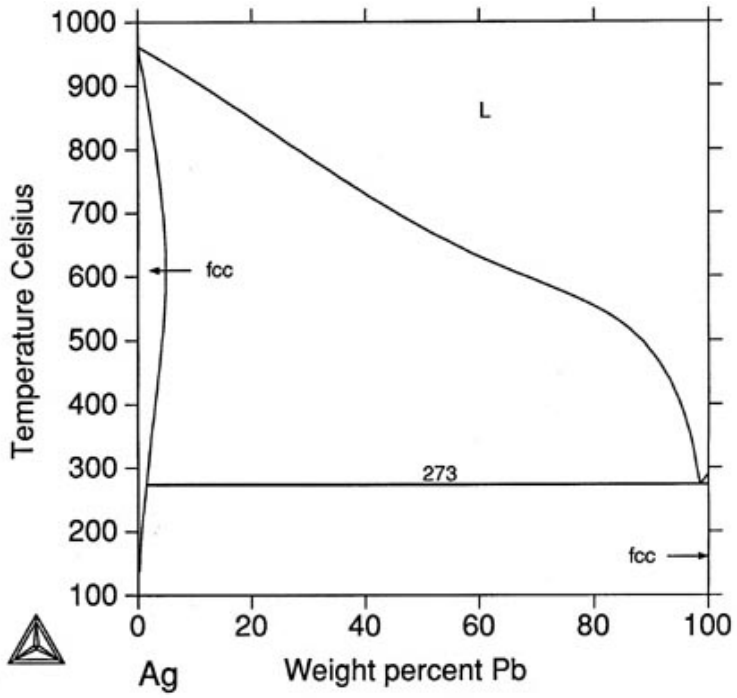

Figure 3. 12 Phase diagram of the Ag-Pb.

3.2.2. Pre-heat condition

Figure 3. 13 shows the weight loss curve of the C1075 paste as it is heated in a TGA chamber from room temperature. It is evident that upon heating, volatile solvents and decomposed binders were progressively driven out of the paste. Figure 3. 14 is a SEM micrograph of the silver paste after a binder burnout heat treatment at 300^{o}C for 10 minutes. Although necking was developed between the silver particles, there was no significant densification. The necking is a result of silver self-diffusion along the particle surface driven by the reduction of surface free energy. We believe that necking may hinder the deformation process under pressure, thus we selected a preheat treatment at 270^{o}C for 3 hours for binder burnout prior to sintering.

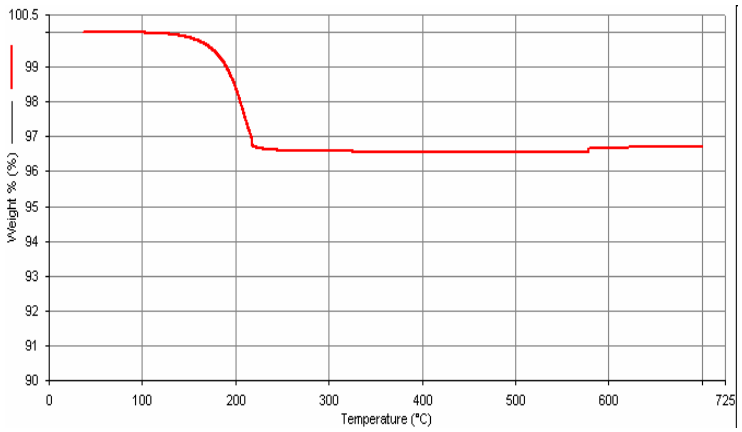

Figure 3. 13 Gravity Thermal Analysis (TGA) of weight loss inthe C1075 silver paste during binder burnout.

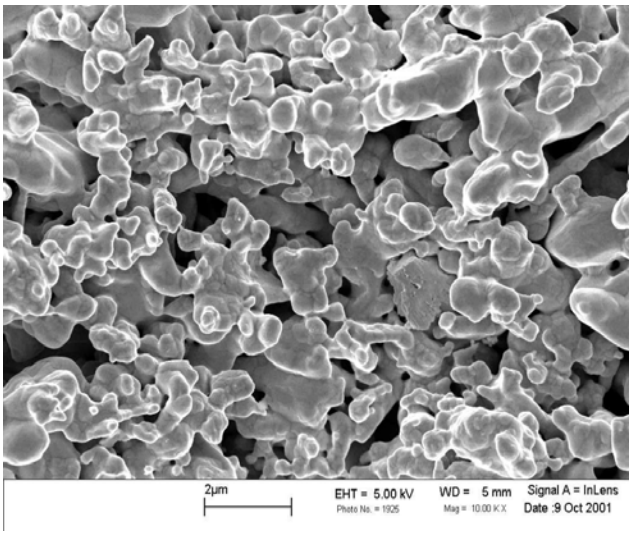

Figure 3. 14 SEM micrograph of C1075 silver paste heated at 300^{o}C for 10 minutes.

3.2.3. Properties of sintered silver joints

Figure 3. 15 shows the silver paste sintered at three different conditions: (a) at 250^{o}C without any pressure; (b) at 250^{o}C with an applied pressure of 10 MPa; and (c) at 800^{o}C without pressure. The SEM observations indicate that the applied pressure significantly assists the densification process even at a temperature as low as 250^{o}C. We believe that the pressure helps the densification process by (1) eliminating some fraction of pores through compression/deformation and (2) increasing the contact area between the silver particles, which therefore speeds up the free surface area reduction.

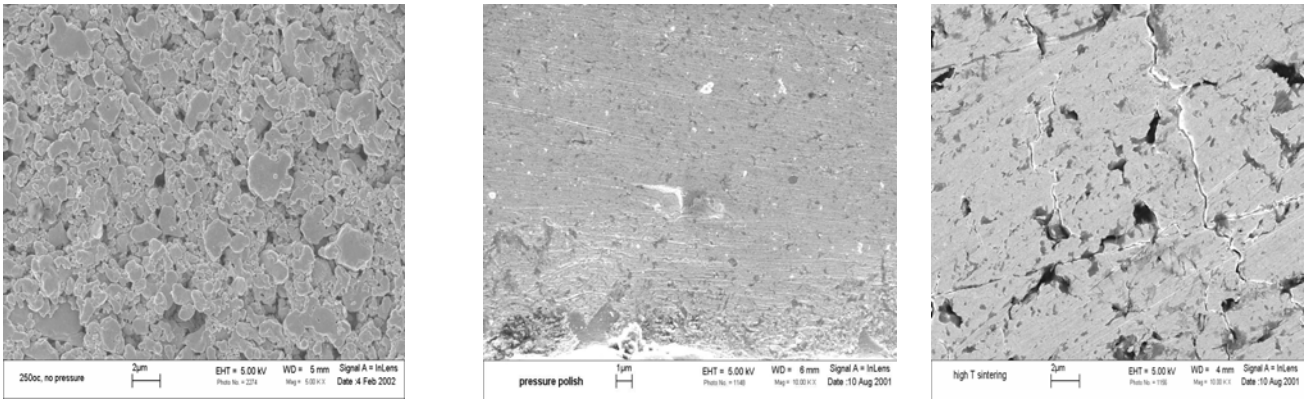

(a) (b) (c)

Figure 3. 15 SEM images of silver pastes treated (a) at 250^{o}C, (b) at 10MPa and 250^{o}C, and (c) at 800^{o}C no pressure.

Effects of sintering parameters

A partial three-level factorial experiment was applied to study the effects of processing parameters. In order to not damage die, 300^{o}C and 40MPa were selected as

maximum processing temperature and pressure. Maximum time - 10 minutes - was selected to be compatible with solder reflow process. Figure 3. 17 to Figure 3. 19 show the properties (electrical conductivity, thermal conductivity, and shear strength) of the sintered silver layer under different processing conditions. Increasing the temperature and pressure improved the electrical and thermal conductivity, and the shear strength. For instance, under identical conditions (40MPa, 5 minutes), the electrical conductivity increased almost 1.6 times, thermal conductivity almost 3.5 times and the shear strength almost five times, when the temperature was increased from 170^{o}C to 300^{o}C. Similarly, under the same temperature and time (240^{o}C and five minutes), the electrical conductivity increased almost 1.5 times, thermal conductivity almost 2.5 times and shear strength almost 3.3 times, when pressure was increased from 10MPa to 40MPa. Higher temperature and pressure can increase the sintering driving force, accelerate the silver atom diffusion and bonding, increase the sintered bulk density, and thus significantly improve the properties of sintered silver. Increasing the time beyond two minutes did not change the properties significantly. That means pressure-assisted sintering is relatively fast and is almost complete within the first two minutes even though the densifying mechanism is by atomic diffusion in the crystal.

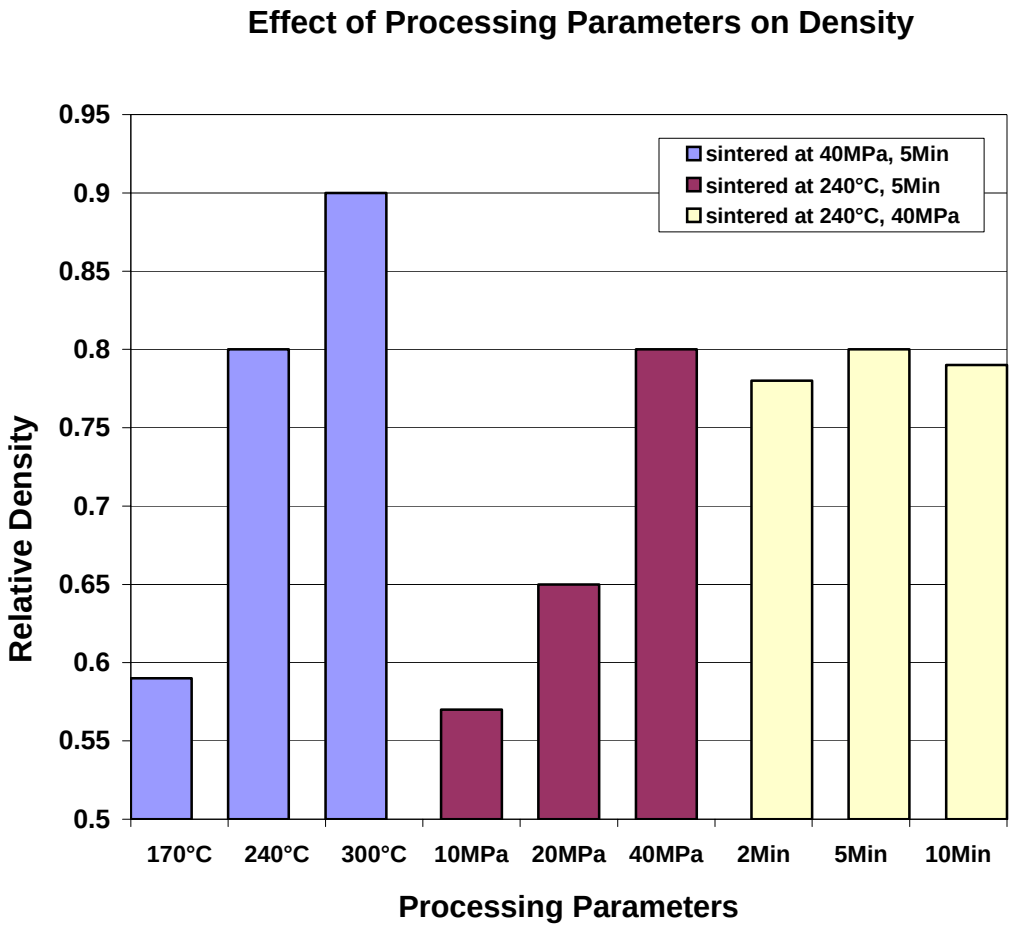

Figure 3. 16 Effect of processing variables on relative density of the sintered silver.

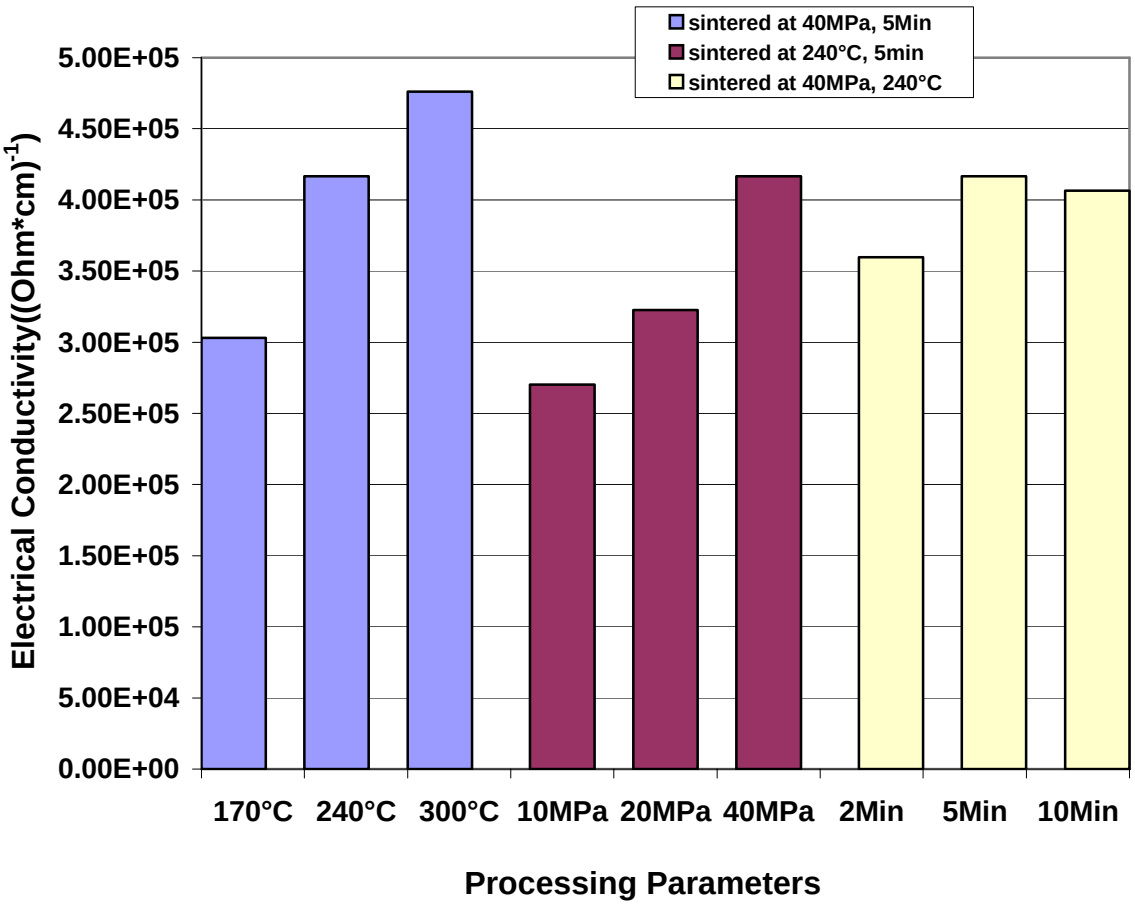

Figure 3. 17 Effect of processing variables on electrical conductivity of the sintered silver.

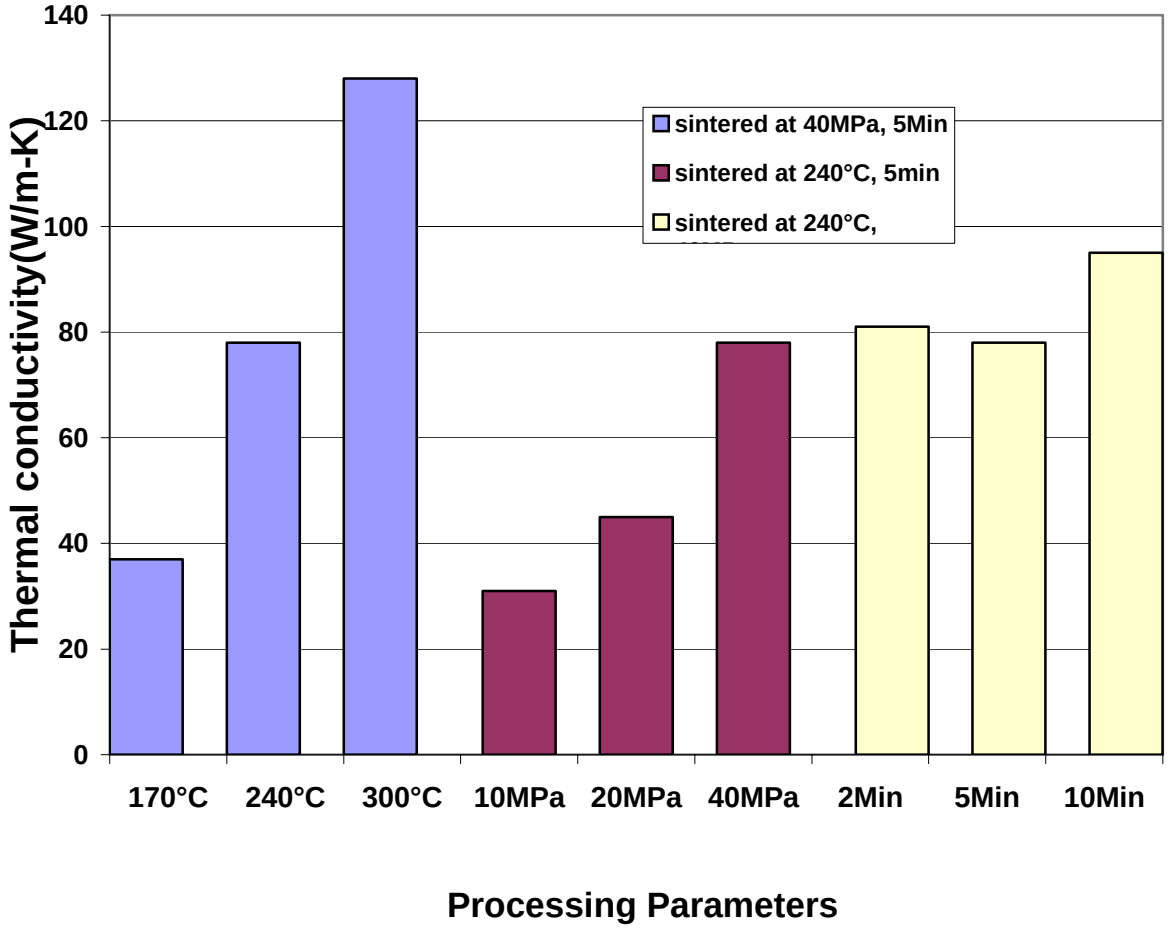

Figure 3. 18 Effect of processing variables on thermal conductivity of sintered silver.

240^{o}C

Figure 3. 19 Effect of processing variables on shear strength.

The sintering die-attach samples at 280°C, 40MPa and 5 minutes were compared with reflowed solder as following. The relative density of the pressure-assisted low-temperature sintered bulk silver sample was found to be about 80% by Archimedes method and confirmed from the SEM micrograph of its porous microstructure. Table 3.3 lists the properties of pressure-assisted low-temperature sintered silver films at this condition and joints along with those from eutectic solder (Sn63+Pb37) and some properties on pure silver. Measured results on the sintered films/joints- electrical and thermal conductivity and adhesion strength - are clearly better than those for soldered joints. The porous films also have lower electrical and thermal conductivity than those of pure silver. However, we believe that the porous microstructure can provide the compliancy necessary to relieve the thermo-mechanical stresses generated from mismatched coefficients of thermal expansion in the joined structure, thus leading to better reliability.

Table 3.3 Summary of properties measured on sintered silver and soldered joints.

	Sintered Silver Joint	**Solder Joint (Sn63Pb37)**	**Pure Silver**
Joining Temperature	**240°C**	**210°C**	
Pressure	**40MPa**	**No**	
Metalization	**Ag**	**Cu/Ag/Ni**	
Joint Shear Strength (MPa)	**50**	**20**	**140**
Electrical Resistivity (ohm-cm)	**2.4E-6**	***1.4 E-5 to 5E-5**	***1.5E-06**
Thermal Conductivity (w/m-K)	**80**	**43**	***428**

Data * from www.matweb.com [51]

Interfacial thermal properties

Figure 3. 20 shows the thermal resistance per unit area (1/h) caused by the die-attach layer. The results obtained from the soldered discs show an increasing trend in the thermal resistance with increasing die-attach thickness. This indicates that the thermal resistance is an additive value of the interfacial resistance and the thermal resistance of the solder die-attach material. The results from both gold-plated and non-plated discs show a linear trend. Linear extrapolation of the data to zero thickness will yield the interfacial resistivity. The gold-plated interface showed an improvement in the interfacial resistivity, which though small compared to the layer resistance, is nearly half (45%) that of the non-plated disc interface. At a 200 um solder-attach layer thickness, the interfacial thermal resistance accounts for 22.5% of the total thermal resistance when the discs are gold-coated as compared to 41.5% when the discs are not coated. The improvement is most likely the result of better wetting of the surface by the solder resulting in good contact and lesser incidence of large voids, a common occurrence in sandwiched reflowed solder.

The third set of data points are from the sintered die-attach samples (280^{o}C, 40MPa and 5 minutes) which were obtained from the sintered-silver attached discs. The thermal resistivity of silver (and hence sintered silver) is very small compared to that of solder so that the contribution of the silver layer to the total thermal resistance is likewise very small over the layer thickness range that was measured. The measured total thermal resistance is very small so that any change with thickness fell within the error of the instrument. For practical purposes, it can be assumed that the measurements represent the interfacial thermal resistivity of the silver-attached discs. This number is still lower than the best result from the solder-attached discs, that of the gold-plated discs. The lower thermal resistivity may be attributed to the extensive formation of a chemically bonded interface between the silver and gold and the absence of large voids that can hinder heat flow. This can be confirmed by SAM of sintered die-attach layer shown in Figure 3. 22 (c) and (d).

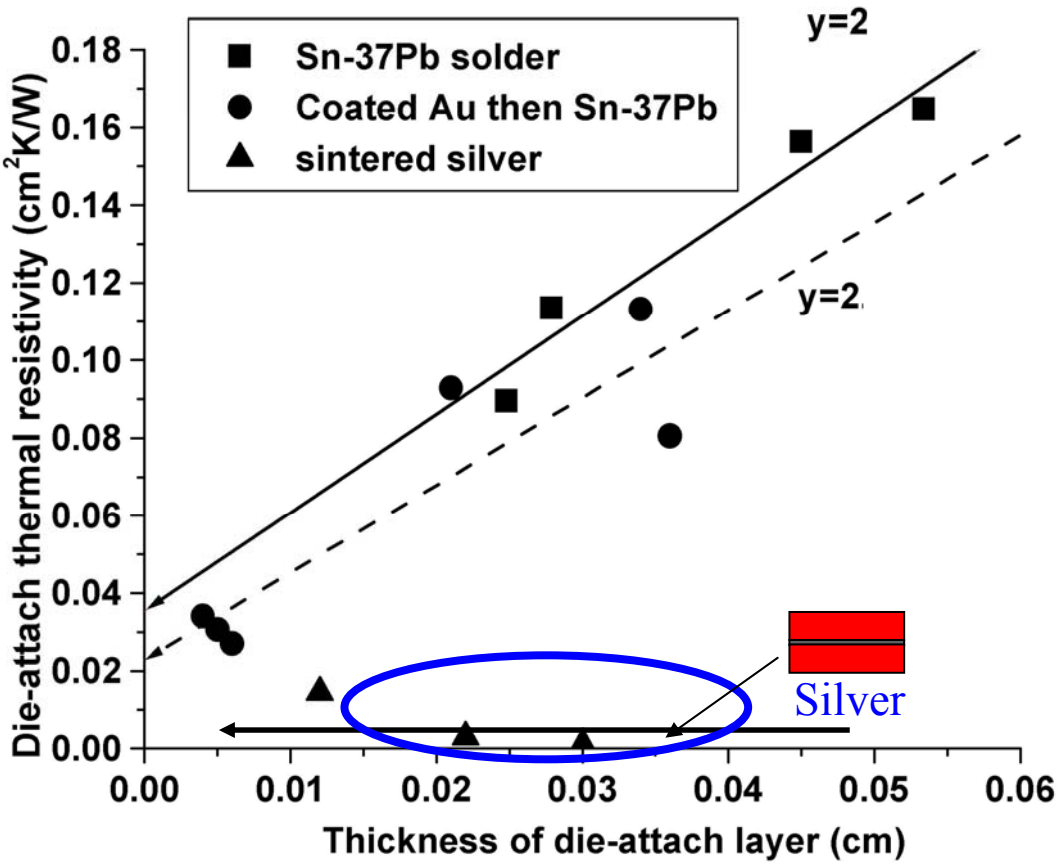

Figure 3. 20 Plots of the thermal resistance per area with thickness of die-attach layer.

Reliability testing

A simple and qualitative way to investigate the reliability of the bonding is to chisel the die from the substrate. The sintered die-attach samples (280^{o}C, 40MPa, and 5 minutes) were tested by this destructive way and shown in Figure 3. 21. It was observed that the sintered joint had good adhesion even after the silicon was detached.

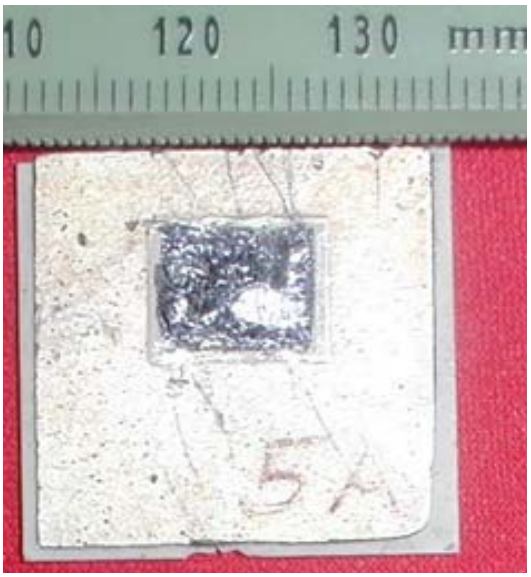

Figure 3. 21 Destructive adhesion test by chiseling the chip from the substrate.

Thermal cycling was performed on samples with solder and silver die-attach layers (280^{o}C, 40MPa and 5 minutes). The samples were alternately heated to 150^{o}C and cooled down to –55^{o}C. The samples were periodically removed for inspection and testing. The cycling test provided an excellent contrast between the two die-attach methods. Figure 3. 22 shows the SAM micrographs of the solder die-attach layer and the sintered layer underneath the silicon power devices before cycling and after 300 thermal cycles. The image of the solder layer shows the presence of initial large voids formed by entrapped gas from the flux in the solder paste. During the cycling process, these voids grow larger and new voids appear. Stress concentration at the edge of the device can induce edge cracking as seen in the upper left corner of Figure 3. 22 (b). The acoustic microscope shows the uniform and void-free microstructure of the sintered silver layer before and after cycling, because the acoustic microscope was unable to resolve the sub-micron pores remaining in the partially sintered film.

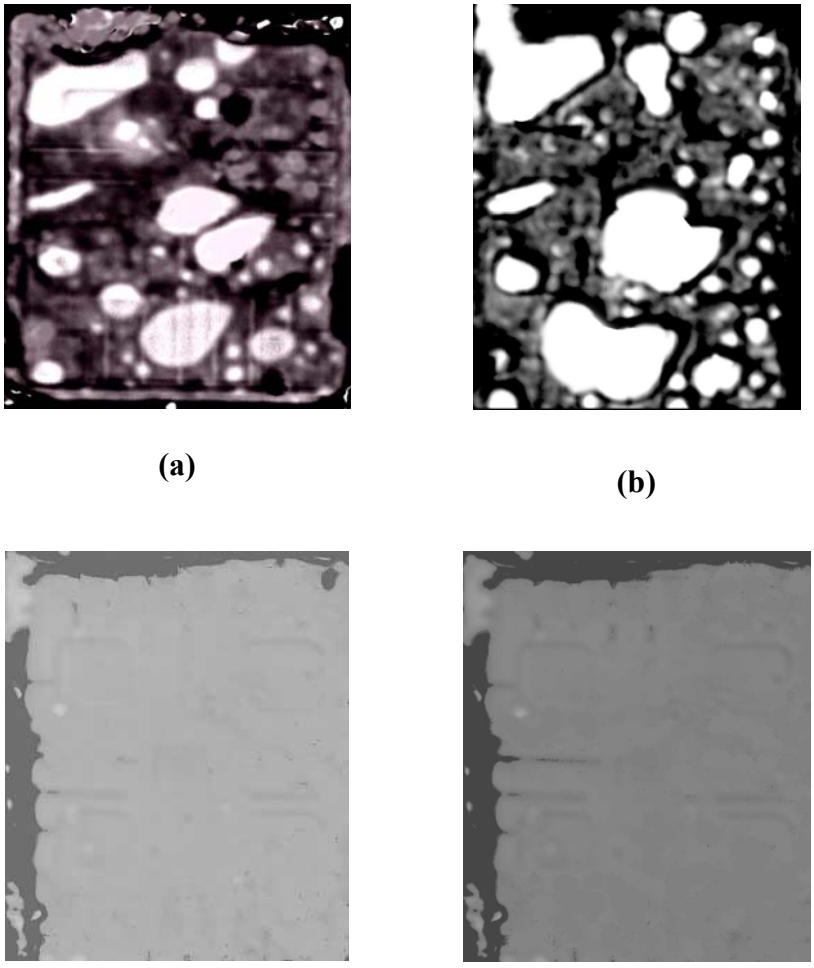

Figure 3. 22 SAM images of reflowed solder (a) before and (b) after 300 thermal cycles, and sintered silver (c) before and (d) after 300 thermal cycles.

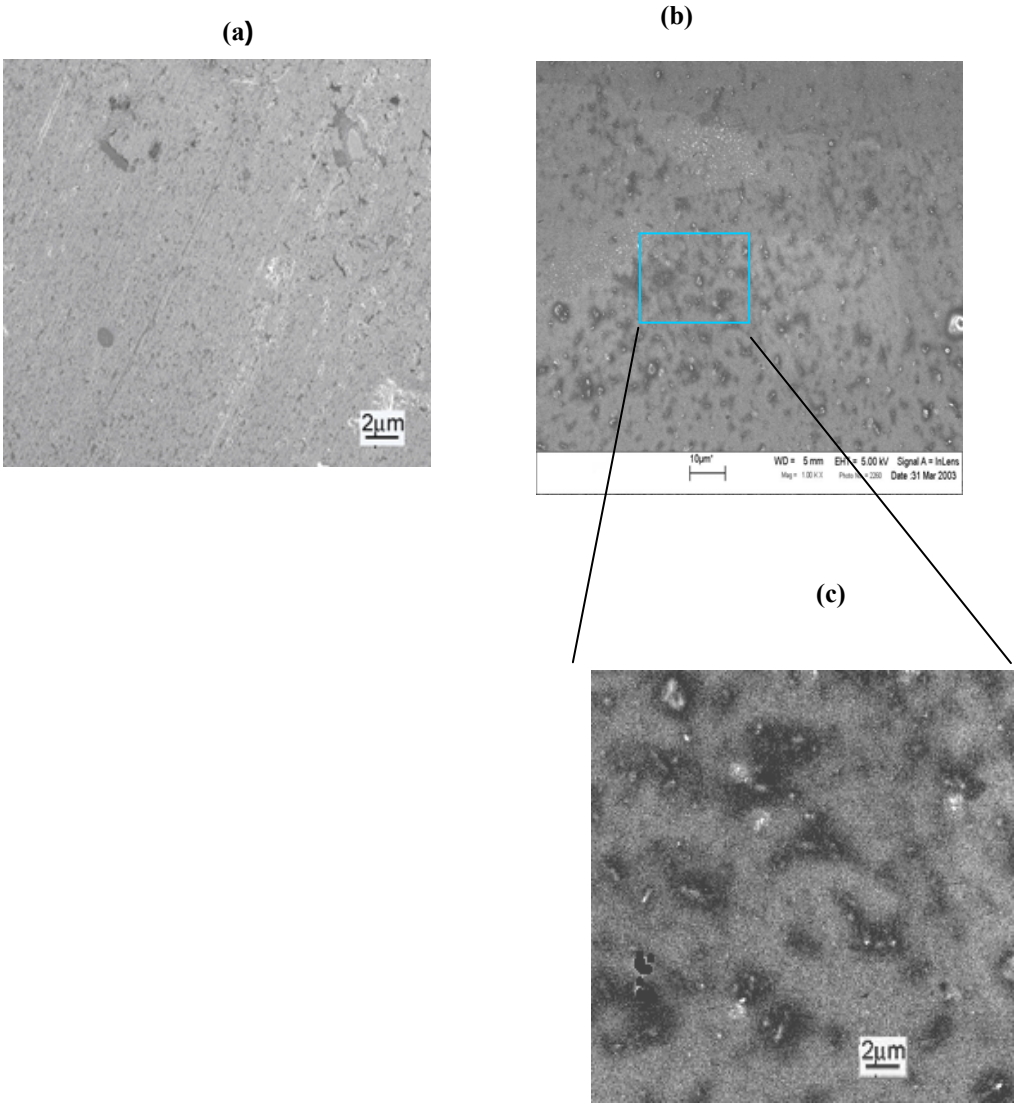

Figure 3. 23 Typical SEM images of sintered silver (a) before cycling, and after 300 thermal cycles (b) and (c).

Figure 3. 23 shows the SEM images of the silver die-attached layer before cycling and after 300 cycles. Micrometer size and smaller pores are visible in the sintered silver layers. These tiny pores can absorb the cracking energy created by CTE mismatch during the cycling process and grow larger. These initial pores and their growth are beneficial to the module's reliability.

3.3 Conclusion

A die-attach alternative to solder reflow, referred to as pressure-assisted low-temperature sintering, was demonstrated to be superior to solder reflow. Measurements of the electrical and thermal conductivity of silver paste, sintered at temperatures as low as 240 °C under a quasistatic pressure of 40 MPa, were found to be significantly better that those in a eutectic solder layer. The shear strength of the sintered silver joint is also found to be stronger than that of the soldered joint. The low-temperature sintered silver has a density of about 80%, which results in lower electrical and thermal conductivity than are obtained using pure silver. Because silver has a much higher melting temperature (960 ^{o}C) than solder (183 ^{o}C to 300 ^{o}C), this alternative die-attach process is also suitable for high-temperature packages. Since silver deforms with little accumulation of inelastic strains and contains no large voids, which are known to be detrimental to the reliability and thermal properties of the packaged devices, the sintered silver joint is more resistant to fatigue failure than a solder-attached junction. Furthermore, the uniform porous microstructure in the sintered layer may relieve the thermo-mechanical stresses that occur due to mismatched coefficients of thermal expansion, thus improving the joint reliability under thermal or power cycling. The thermal-cycling test shows the sintered silver joints have better reliability

This pressure-assisted sintering approach does have disadvantages. To reduce the cost and improve the die-position accurate, die-attach has been a highly automatic-manufacture processing for industry practice. The large quasistatic pressure, which is essential in lowering the sintering temperature, makes the automatic manufacture difficult to implement. Furthermore, the semiconductor materials are usually very brittle. If the

large external pressure is not implemented properly, it is also a potential to damage the device.

Chapter 4 Low-temperature sintering of nanoscale silver paste

Chapter 3 has demonstrates a pressure-assisted sintering die-attach approach. With the assistance of large external pressure, the micron-size silver paste can be sintered at the temperature as low as 240^{o}C. The measured properties and reliability of the sintered joints are better than those of reflowed solders. However, the large external pressure causes problems: 1) difficulty to auto-manufacture and 2) potentially damaging to devices. In this chapter, low-temperature sintering nanoscale silver paste will be presented as another alternative technique to attach semiconductor devices.

Besides application of large external pressure, reducing particle size to nanoscale is another approach to increase the sintering driving force. Thermodynamically, nanoscale materials have significantly larger driving force, which can compensate for the low mobility and drive the densification rate to a high level even at a low temperature. However, the fact that solid-state sintering depends on atomic diffusion leads to several challenges for low-temperature sintering: such as agglomeration, aggregation and non-densification diffusion. The agglomeration and aggregation in the initial powder systems result in the effective radius that is much larger than the real radius of particles and thus the low-temperature sinterability of nanoscale materials can be lost. The non-densification diffusion at relatively low-temperature consumes the driving force during the heat-treatment processing and contributes little densification. Unfortunately, agglomeration, aggregation and non-densification diffusion easily occur during nanoscale materials preparation, storage and processing due to the natural of nanoscale: extremely fine particle size and large surface energy.

In this chapter, the particle size effect of silver powders on sintering was first studied. The results show the possibility of lowering sintering temperature by reducing particle size if aggregation/agglomeration can be avoided.

After that, experiments are conduct to understand low-temperature sintering challenges of nanoscale silver paste and several approaches are developed and/or

suggested to overcome sintering problems: aggregation, agglomeration and non-densifying diffusion at initial stage of sintering.

The slurry form of silver with organic solvent and a little bit surfactant is applied to increase the stability and avoid the aggregation of dry silver powder. The observation of SEM shows the aggregation of nanoscale silver particles that can be avoided in the slurry form.

Ultrasonic vibration dispersion is developed to reduce particles agglomeration. Compared with the paste prepared by conventional ball-milling processing, the silver paste prepared with ultrasonic dispersion has a more uniform distribution and a much denser microstructure after sintering.

Controlling the burn-out temperature is developed to reduce non-densifying diffusion and thus realize abrupt sintering. By adding organics with proper burn-out temperature, the non-densifying surface diffusion can be retarded at a relatively low temperature; after organics burn out, densifying diffusions such as lattice and/or bulk diffusion can take over and an abrupt densification can be realized.

Eventually, the characteristics of sintering nanoscale silver paste were characterized. The measured electrical and thermal properties of sintered silver paste are significantly better than those of solder joints, and the die shear strength is compatible with solder joints.

4.1 Experimental procedure

4.1.1. Experiments to study size effect of silver particles on sintering

Three dry silver powders with different particle size (10 nm to 20 nm, 30 nm to 50 nm and 100nm) are obtained from Nanoamor. Transmission electron microscopy (TEM) is applied to investigate the particle size and distribution. Specific samples need to be prepared before observation of transmission electron microscopy. The sample preparation procedure is shown as follows: first, small amounts of these powders (about 0.1 gram) were put into the beakers with 50 ml deionizer (DI) water respectively. After that, ultrasonic vibration was applied to sufficiently disperse these powders in the DI

water for 20 minutes. After that, the colloid solution (DI water and silver powders) was dipped into a 200 mesh copper grid coated in carbon. After an adequate dry, a monolayer of dried out powders is formed on the grid. In the chamber of transmission electron microscopy (TEM) , an electron beam is focused on a monolayer of dried out powders on the gird. Electrons pass through the powder monolayer at a slower rate than through the plain carbon grid, and hence, a shadow is detected by the film when it is exposed for the purpose of taking a photograph. Transmission electron microscopy has a better resolution than the scanning electron microscopy (SEM) and thus is suitablly applied to observe samples with size a few to tens of nano meters.

To study the size effect of silver particles on the sintering, silver powders with different particle size were pressed into pellets and sintered at two different temperatures (250^{o}C and 300^{o}C) for ten minutes. Table 4.1 lists the conditions to prepare these samples. Silver powders are placed into a die with a diameter half inch and pressed by a laminated machine using 40 MPa pressure at room temperature. For each type of silver powder, four samples are prepared. Two of them are sintered at 250^{o}C and another two sintered at 300^{o}C. The green density (the initial density of silver powder after press) and the final density (the density of samples after sintering) are measured by Archimedes method. The fast heating rate is applied to eliminate coarsening effects and is realized by putting samples directly into the pre-heated furnace.

Table 4.1 Conditions to prepare samples to study size effect of particle on sintering.

Particle Size	Press Pressure	Sintering Temperature I	Sintering Temperature II
10 to 20nm	40MPa	250^{o}C	300^{o}C
30 to 50nm	40MPa	250^{o}C	300^{o}C
100nm	40MPa	250^{o}C	300^{o}C

To investigate the aggregation condition of nanoscale powders, the powders are mixed into the DI water and ultrasonic dispersed by four hours. After that, the colloid solution (DI water with silver powders) was filtered by a filter (MILLIPORE, Express™ PLUS). The go-through diameter of this filter is 220 nm.

Three of these powders are also prepared into the paste by the same dispersion approach – ultrasonic dispersion, which will be described in the next section. During the dispersion, the same dispersion time (4 hours) is applied and the same amount of organics (22 w%) is put into the powder systems. The silver to organics ratio listed in Table 4.2. The prepared pastes are sintered with sintering profile shown in Figure 4.1 respectively. The SEM was applied to investigate the microstructure of these sintered nanoscale silver pastes.

Table 4.2 Organics ratio and dispersion time to prepare nanoscale silver past

Nano Silver Powder (gram)	Surfactant (gram)	Binder (gram)	Thinner (gram)	Dispersion time
10	0.15	1.5	0.8	4 hours

Surfactant: fatty acid, binder: PRV 914, thinner: PRV 912

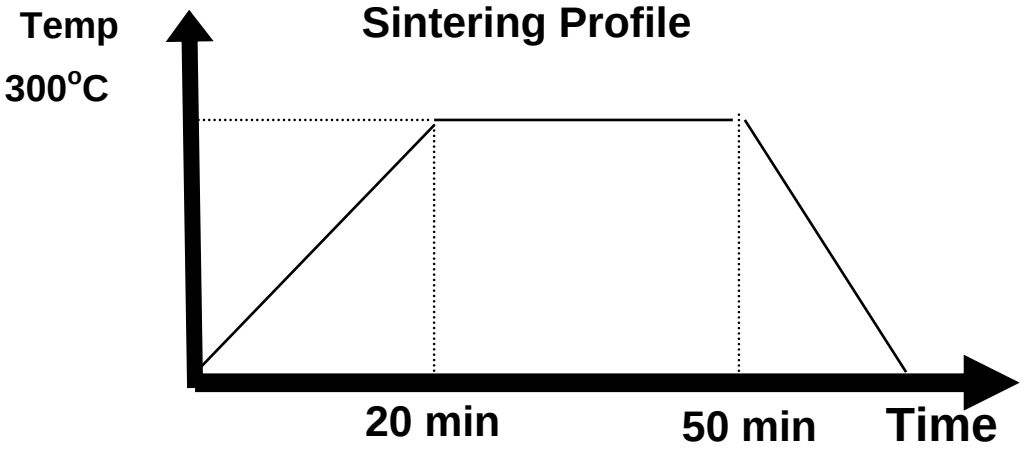

Figure 4.1 Sintering profile of nanoscale silver paste.

4.1.2. Experiments to develop dispersion method to prevent agglomeration of nanoscale silver paste

Silver paste consisted of silver powders and organic components. Figure 4.3 schematically shows the composition of the paste and the functionality of the organics. There are usually three different organics in the paste. Surfactant (dispersion) is a short carbon-chain organic, which attaches to the surface of silver particles and prevents silver particles agglomeration and/or aggregation. Figure 4.2 shows one commonly used surfactant – lauric acid. Lauric acid is one kind of fatty acid which has twelve carbons in its chain. It comprises two functional groups: polar function group and the hydrocarbon chain. The polar function group attaches onto the surface of particles by hydrogen bonding; the hydrocarbon chain prevents particles from agglomerating. Binder has a longer carbon chain and cross-links the silver particles together to prevent silver film cracking during the heat-treatment and/or handling. Thinner is applied to adjust the viscosity of the paste for different processing conditions such as screen and / or stencil printing. The thinner usually has the shortest carbon chain and the lowest viscosity during three organic components.

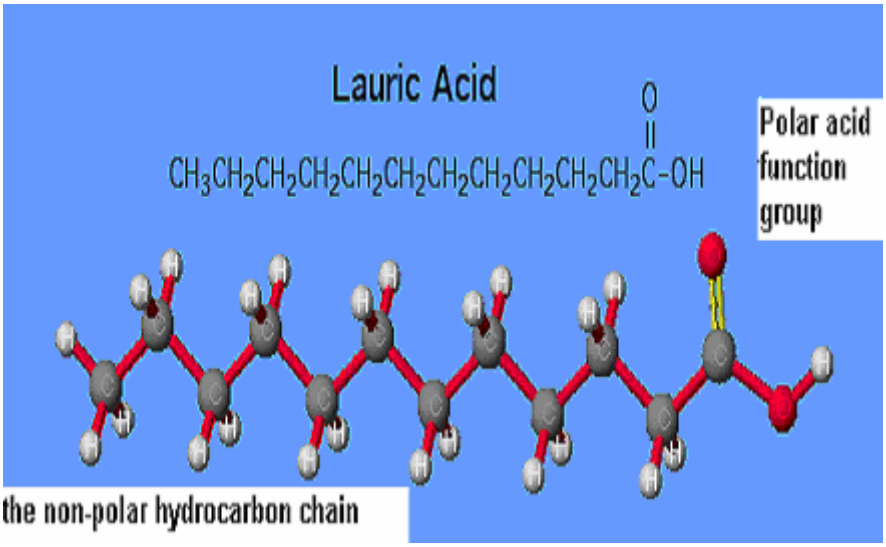

Figure 4.2. The sticker-ball model of lauric acid.

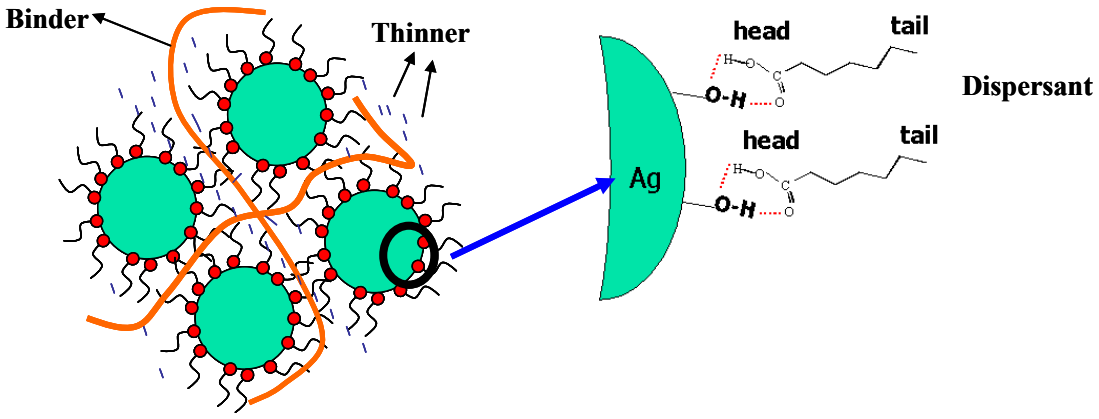

Figure 4.3. Schematic of nanoscale silver paste's composition.

Dispersion is one of the most important processes to prepare the paste. A good dispersion can permit particles to homogenously distribute into the matrix of organic components without cluster aggregation and/or agglomeration. A paste with good dispersion can obtain good flowability, printerability and sinterability. Two dispersion methods are applied to disperse nanoscale silver powder in my study. To gain fair

comparison, the same silver powder, the same organics ratio and the same dispersion time (listed in Table 4.2) are chosen for both dispersion methods.

Conventional milling is applied as the first dispersion method. Figure 4.4 shows how ball milling works: rotation of the jar was driven by rollers, which mechanically bring the balls inside the jar to mill the materials. Silver powders, organics and adequate acetone solvent were mixed together and milled by a milling machine (U.S Stoneware, model number CK-95030) for four hours. Al_2O_3 balls with a diameter of 2mm are used as milling balls. The milling time is also kept at four hours. After that, the prepared paste was obtained when solvent was evaporated. The prepared nanoscale silver pastes are stencil-printed on the Al_2O_3 substrate and sintered with same temperature profile shown in Figure 4.1.

Ultrasonic vibration is applied as the second dispersion method. Figure 4.5 schematically shows the nanoscale silver paste preparation procedure by ultrasonic vibration. To gain enough dispersion energy, both ultrasonic bath (Branson 3310) and agitator (Cole Parmer 6610) are used. Silver powders, organics and adequate acetone solvent were mixed together and ultrasonically vibrated. Figure 4.6 schematically shows the ultrasonic dispersion. Ultrasonic agitator has the stronger vibration energy and can locally deagglomerate the silver particles in the solution (mixture of silver power, organics and acetone). Ultrasonic bath can homogenously distribute the deagglomerated powders and form homogenous dispersion. The nanoscale silver particles are sensitive to the temperature, and ice water is put into the ultrasonic both to absorb the heat generated by ultrasonic vibration. After dispersion, the solvent is evaporated out. The prepared nanoscale silver pastes are stencil-printed on the Al_2O_3 substrate and sintered with same temperature profile shown in Figure 4.1.

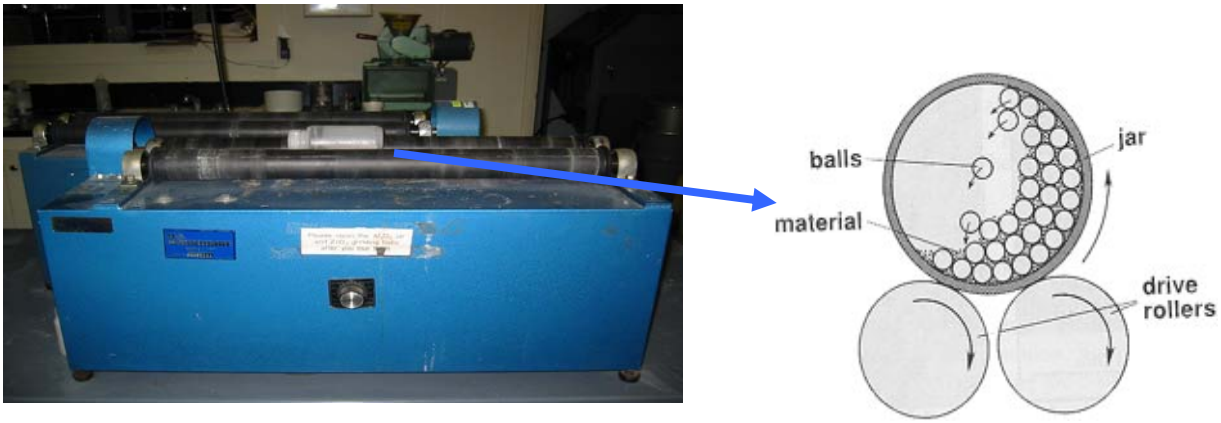

Figure 4.4. Dispersion by ball-milling: (a) facility for ball-milling, (b) schematic of ball-milling mechanism.

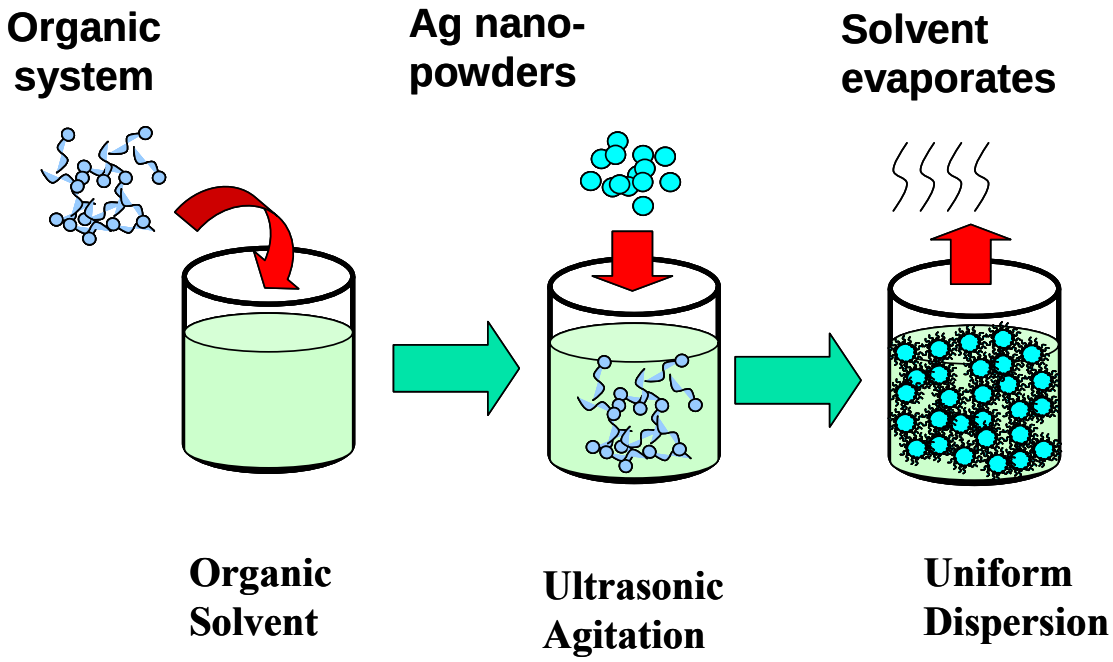

Figure 4.5 Procedure to disperse nanoscale silver paste using ultraonic vibration.

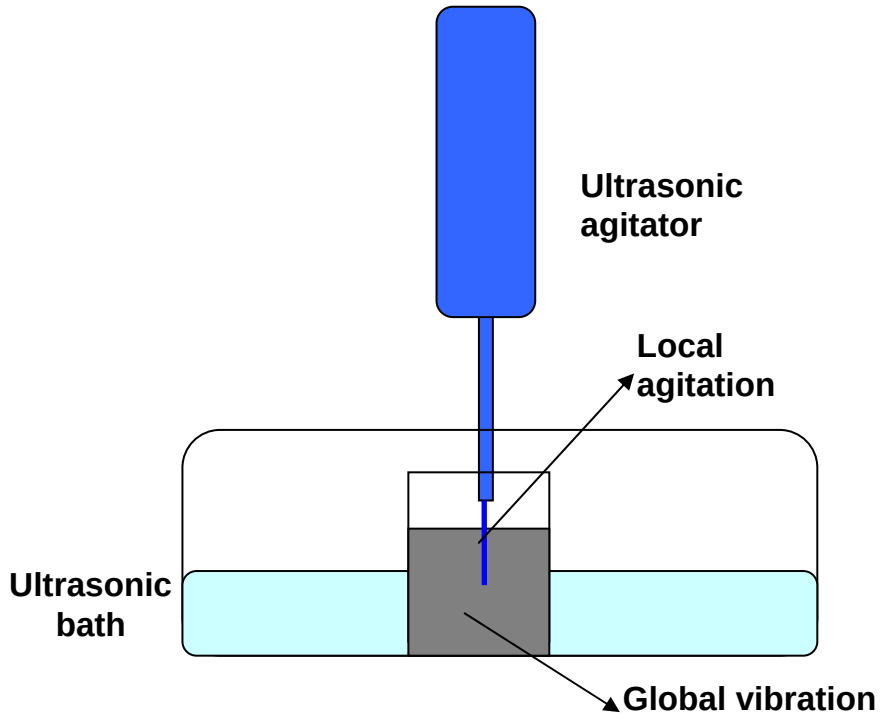

Figure 4.6 Schematic of ultrasonic dispersion.

4.1.3. Experiments to study organics burn-out as a means to realize rapid sintering

Sintering micron-size silver paste usually consists of two stages: first stage is to burn-out the organics components in the paste; the second one is to densify silver particles. Organics burn-out occurs as the powder compact heats through the temperature where the organics becomes unstable and evaporate. Heat first melts the organics, and then break down its molecular bonds, forming small molecules that evaporate out of the compact. The heating rate must be slow during organics burn-out to avoid damage to the compact of particles. The sintering profile of micron-size silver paste is schematically shown in Figure 4.7. The organics burn-out temperature (T1) is usually during the range of 250^{o}C to 450^{o}C, which depends on what kind of organics used in the paste. The

sintering temperature (T2) is usually higher than 750°C to accelerate the sintering processing. The organics burn-out temperature (T1) should be much lower than sintering temperature (T2) and thus the two stages can be separated. Organics burn-out temperature ramp (S1) keeps slow to let organics homogenously burn-out and thus prevent cracks being occurred in silver compact. The burn-out time (t1) also keeps long enough to permit all the organic components burn-out sufficiently. Sintering temperature ramp (S2) should be fast for the purpose of saving the processing time and sintering energy, and preventing non-densification diffusion. The sintering time (t2) can be very short if the sintering temperature is high enough.

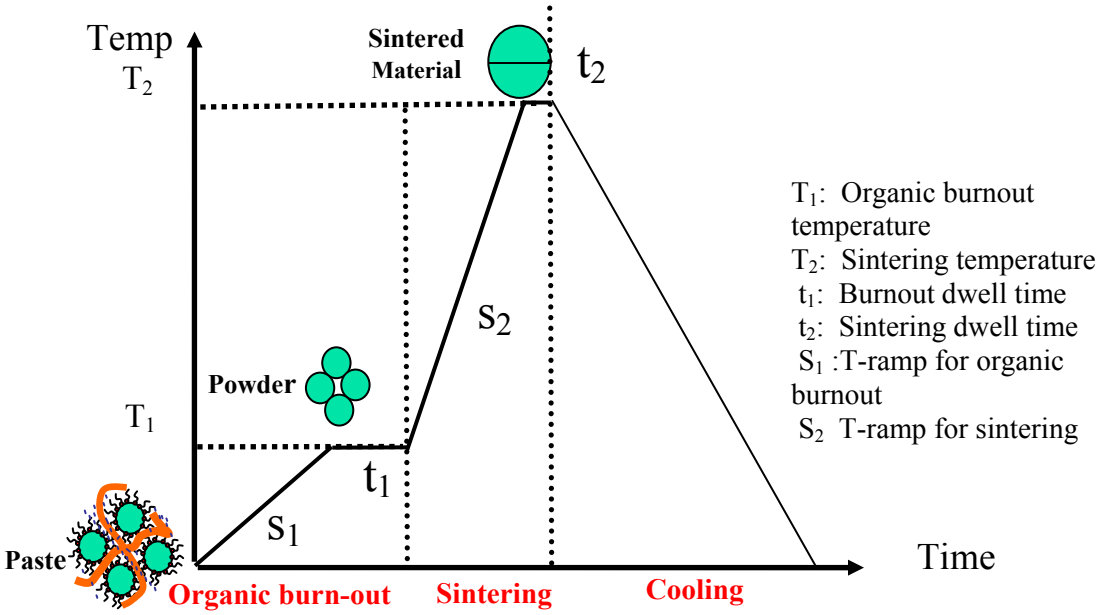

Figure 4.7 Sintering profile for micron-size silver paste.

The reason for using nanoscale silver paste, instead of micron-size one, is to lower the sintering temperature. The finer particle size of nanoscale silver powder can significantly increase the driving force and permit silver powder sintered at a much lower temperature than that of micron-size silver powders, if the sintering challenges such as aggregation, agglomeration and non-densification diffusion can be eliminated. With the lower sintering temperature, nanoscale silver paste can be applied as die-attach material to interconnect semiconductor devices onto the substrate. With such low sintering temperature (lower than 300^{o}C), the two-stage sintering profile, which is widely used to sintering micron-size silver paste, is difficultly used to sintering nanoscale silver paste. A temperature difference between sintering and burn-out is needed to separate these two stages. For micron-size silver paste, the sintering temperature higher than 750^{o}C and the organics burn-out temperature can be lower than 450^{o}C. The temperature difference between two stages can be is larger than 300^{o}C. For sintering nanoscale silver paste for die-attach application, the processing temperature should be lower than 300^{o}C to avoid damaging the devices. If temperature difference between sintering and burn-out is 300^{o}C, then the organics need to burn-out at 0^{o}C. This is almost unrealistic because paste system will be unstable even at room temperature. Even if we choose that the temperature difference between sintering and organics burn-out is 200^{o}C, the organics burn-out temperature should be 100^{o}C. It is difficult to find commercially available organics, which have such a low burn-out temperature and still can disperse the nanoscale silver particles. Even if we can synthesis such organics, the non-densification diffusion presents another challenge for low-temperature sintering nanoscale silver particles. The reason has been explained in Chapter 2. Briefly, the surface diffusion dominates at the low-temperature and consumes the driving force but does not contributes to the densification. At a relatively higher temperature, when densification diffusions such as grain boundary diffusion and lattice dominate, the driving force has already been consumed and thus the densification can not be realized. Fast heating rate is usually applied to resolve this problem when sintering ceramics materials. But in die-attach application, a fast heating rate brings the thermal shock and has a potential to damage devices and substrates. Thus, for nanoscale silver paste sintering, two stages have to be

merged together for organics burn-out and sintering to occur simultaneously. Figure 4.8 schematically shows the sintering profile of nanoscale silver paste sintering. This sintering profile is actually simpler than the one used for micron-size silver paste and only has one sintering temperature, one temperature rising ramp and dwelling time. The existing organics in the nanoscale silver paste has an additional benefit for sintering. These organics can retard the surface diffusion, occurs at relatively low-temperature when they do not burn-out. At relatively high temperature, the organics burn out and the densification mechanisms such as grain boundary diffusion and/or lattice diffusion have already dominate and abrupt sintering is realized.

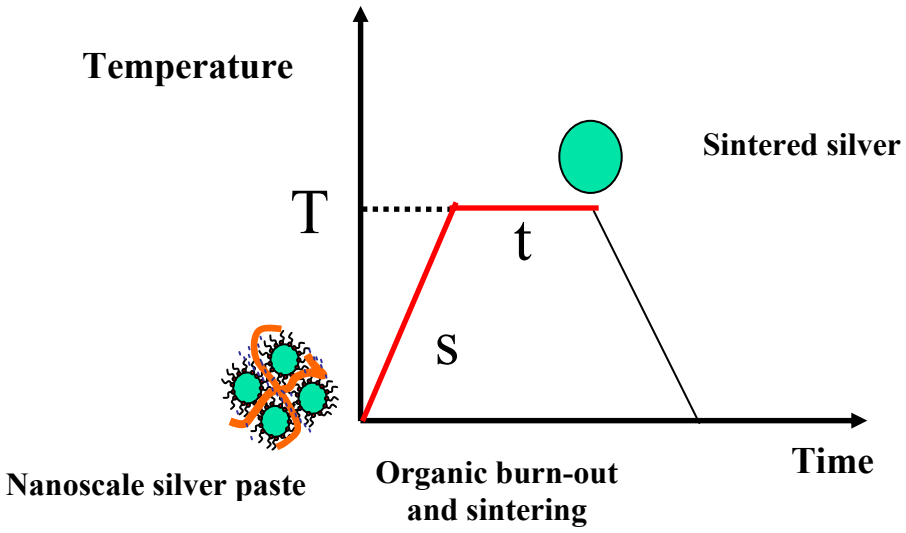

Figure 4.8 Sintering profile for nanoscale silver paste.

To experimentally verify this non-densification diffusion problem, the initial nanoscale silver powder should have no agglomeration and aggregation, plus be organics free. This kind of silver powder is not easily obtained commercially. The Carey Lea method is applied to prepare small amount of these powders. as adapted by Frens and Overbeek [52]. Sodium citrate was obtained from Sigma Aldrich and iron (II) sulfate and

silver nitrate were obtained from Alfa Aesar. The reducing agent was prepared by mixing freshly prepared sodium citrate and ferrous sulfate solutions in the ratio of 35 ml of 40% sodium citrate to 25 ml of 30% iron (II) sulfate. The solution was added with vigorous stirring to 25 ml of 10% silver nitrate to form a blue-black suspension. The suspension was then isolated by centrifugation. The sediment was redispersed in 50 ml of H_2O and reflocculated with 50 ml of the sodium citrate solution. The precipitate was redispersed, and then reflocculated three times with sodium citrate, and finally redispersed in water. The dried powder was examined using a scanning electron microscopy (LEO201 SEM) to determine the approximate size range of the silver particles. The prepared particles were sintered at 300^{o}C for 3 minutes at a slow heating rate of 5^{o}C/min and subsequently by rapid heating. A rapid heating rate was realized by putting small film samples into a heated furnace at 300^{o}C. The weight of the samples used was under 0.1 gram, and the thickness was less than 50 μm. The microstructure of each sintered sample was observed under the SEM. The prepared particles were sintered at 300^{o}C for 3 minutes at a slow heating rate of 5^{o}C/min and by rapid heating respectively. Rapid heating rate was realized by putting small film samples into a heated furnace at 300^{o}C. The weight of the samples used was under 0.1 gram and the thickness was less than 50 μm. The microstructure of samples before and after sintering is observed under the SEM.

To study the densification of nanoscale silver paste, the following experiment was conducted. The nanoscale silver paste with 30 to 50 nm was prepared using ultrasonic vibration approach shown in Figure 4.5. The organics ratio in the paste is listed in Table 4.2. The prepared paste is screen-printed on the p-type silicon substrates as observation samples. As a comparison, the sample of nanoscale silver paste with 100 nm was also prepared with similar procedure. A commercial micron-size silver paste (Herause C1075) was also printed on the silicon substrate as the third kind of sample. A SEM was applied to realize the in-situ observation of silver paste sintering. Here, SAM is not only served as an observation facility, but also supplies the accelerated electronics to sinter the pastes in the chamber. The accelerating voltage for scanning electron beams is 2 kV. The beam current is measured, using the Faraday Cup method to be 0.136 nA. The

scanning time per screen is 17.6 second and there are 1024*768 pixels in one screen. The image is produced by In-lens signal and the magnification is 100K. The vacuum pressure in the chamber of SEM is less than $2*10^{-6}$ Torr. No extra heating was applied in the chamber of SEM.

To study the organics burn-out effect on sintering nanoscale silver paste, the nanoscale silver pastes with particle size 30 to 50 nm were prepared using ultrasonic method. Two different organic systems are used to prepare the pastes respectively: organic system I has a lower organics burn-out temperature and organic system II has a higher burn-out temperature. Table 4.3 listed these two organic systems. The organics ratio (22 w%) and dispersion time (four hours) are kept the same for two pastes with different organic systems. The microstructure of silver pastes at different temperature was characterized by electronic scanning microscopy (SEM). Thermogravimetric analysis (TGA) is applied to study the organic burn-out of nanoscale silver pastes with different burn-out temperature.

The silver pastes with average particle size 100 nm were also prepared by using ultrasonic vibration method. Two different organics systems (organic system I and organic system II) listed in Table 4.3 are used to prepare the pastes respectively. The prepared pastes with different organics systems were sintered at the $450^{o}C$. The microstructure of the sintered silver paste were observed by electronic scanning microscopy (SEM).

Table 4.3 Two organic systems with different burn-out temperature.

	Surfactant	Binder	Thinner
Organics system I (Low burn-out T)	Fatty acid C12	PRV 914	PRV 912
Organics system II (High burn- out T)	Fatty acid C24	PVB	PRV 912

4.1.4. Experiments to characterize sintered nanoscale silver paste

To investigate the properties of sintered nanoscale silver layers, the electrical conductivity, thermal conductivity and shear strength of die-bonding were measured and compared with those of the solder reflowed layers.

In order to measure the resistivity of the sintered silver joints, silver prints formed like the resistor pattern were prepared by screen-printing. The resistor pattern is sintered with the profile listed in Figure 4.1. The resistance of the pattern is measured with a digital multi-meter. The cross-sectional area of the resistor line in the pattern was measured using a Dek-Tak3 profilometer. The average of three measurements was used to determine the cross-sectional area. The resistivity of the silver trace is calculated by: Equation 3.1.

The thermal conductivity is determined by measuring its thermal diffusivity, specific heat, and density. To prepare the samples for thermal property measurement, the silver paste was put into the die with one half inch diameter. The paste and die were then heated up to 100^{o}C to let thinner evaporate. After that, a 10MPa pressure was applied to get the pellets. The pellets were sintered with the profile listed in Figure 4.1. The thermal diffusivity was obtained using Parker's flash-light method [49]. The laser flash technique is schematically shown in Figure 3. 6. The specific heat was measured by

differential scanning calorimeter (DSC). The density was measured by the Archimedes method.

To measure the shear strength of sintered silver bonding, the following experiment was conducted. The nanoscale silver pastes with particle size 30 to 50 nm were prepared using ultrasonic method. The organics ratio was listed in Table 4.4. Compared with the organics ratio listed in Table 4.1, the organics ratio reduced from 22 w% to 16%. This is particular important for die-application, since in the die-attach sandwiched structure, the burn-out space for organics is limited. In Chapter 5, this issue of limited organics burn-out path will be detailed. The nanoscale silver paste was stencil-printed onto DBC substrate with silver coated surface with thickness 50 to 200 micron. The SiC die with the area 1.25 mm* 1.25 mm, was attached onto the printed silver paste film. The sandwiched die-attach structure was sintered up to 300^{o}C within one hour. The sintering profile is shown in Figure 4.1. The die-shear testing machine was made to measure the die-shear strength. Figure 4.9 schematically shows how to measure the die-shear force. The motor can be controlled to push the die with desired speed. The load cell measures the die-shear strength, and signal board samples the signal from the lad cell and sends to the lab-view software. With the known geometry of the die, the die strength can be obtained.

Table 4.4. Organics ratio of nanoscale silver paste for die-shear testing.

Nano Silver Powder (gram)	Surfactant (gram)	Binder (gram)	Thinner (gram)	Dispersion time
10	0.15	0.8	0.8	4 hours

Silver with particle size 30 to 50 nm Surfactant: fatty acid C12, binder: PRV 914, thinner: PRV 912

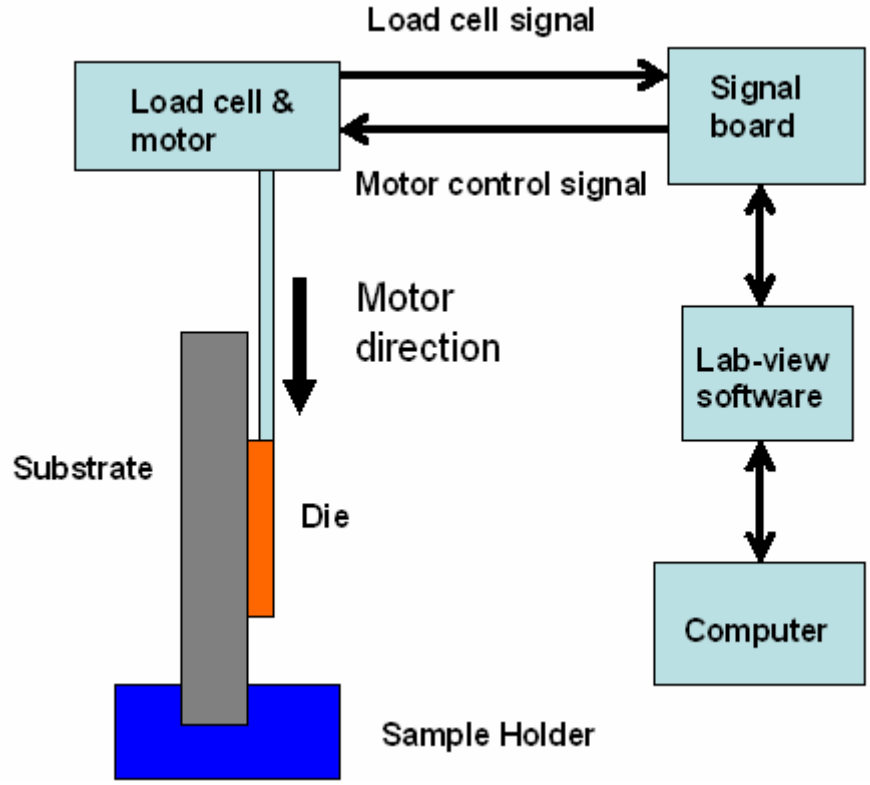

Figure 4.9. Die-shear testing machine

4.2 Results and discussion

4.2.1. Size effect of silver particles on sintering

Figure 4.10 (a) and (b) shows the TEM observation of nanoscale silver powder with the particle size 10 nm to 20 nm and powder with 30 to 50 nm respectively. Particle size of the two powders can be estimated from the observation of TEM and both of them match the data sheet. But the particles of both powers show a cluster microstructure: the particles are not individually separated, instead of gathering together. These clusters may be caused by aggregation or agglomeration depending on how strong the force between the individual particles. It is difficult to differentiate what is the exact reason to cause the cluster structure sole from the observation of TEM images. However, figuring out the reason for the cluster microstructure is important for sintering nanoscale silver. If these clusters are caused by aggregation, this type of silver powder can not be applied for low-temperature sintering. Because aggregates are the particles bonded by strong strength, and thus can not be redispersed by following dispersion process. The heavily aggregated silver powders have much larger effective radius than the real radius of individual particles, and thus the low-temperataure sinterability can be lost.

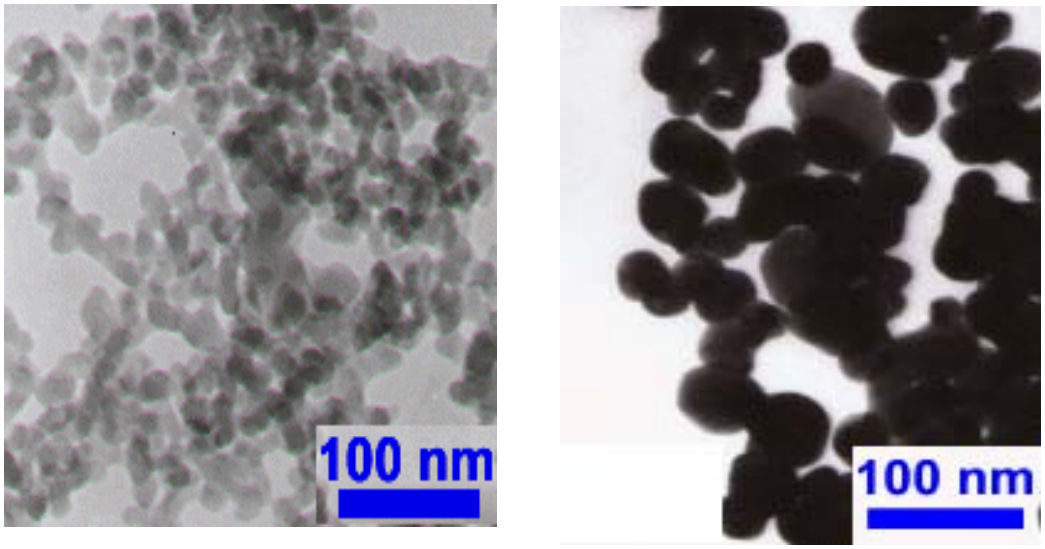

Figure 4.10 TEM observation of nanoscale silver particles: (a) 10 to 20 nm (b) 30 to 50 nm.

Three silver powders with particle size 10 to 20 nm, 30 to 50 nm and 100 nm respectively are pressed into pellets under 40 MPa pressure. These pellets are heated up to different temperature and the density of the pellets before and after heat treatment was measured. Figure 4.11 250^{o}C. Although the pellet with 100 nm silver particles has higher initial density than the pellet with 30 to 50 nm, the sintered density is significantly lower than that with 30 to 50 nm silver particles. Compared with 100 nm silver particles, the 30 to 50 nm silver particles have a much larger sintering driving force. The large sintering driving force can compensate the low mobility and boost the densification rate high at a relatively low temperature. Figure 4.12 shows the density of three types pellets made by different powders before and after heat treatment at 300^{o}C. With a higher sintering temperature (300^{o}C), the mobility can be higher than that in 250^{o}C, and thus the density of both pellets (the silver powders with particle size 30 to 50 nm and 100 nm respectively) increase. The density of pellets with 30 to 50 nm silver particles can reach almost 8.0 g/cc, which is 78% relative density of pure silver at 300^{o}C for only 10 minutes. As a comparison, the pellets 100 nm silver particle can only have 6.0 g/cc at the

same sintering condition. It is clearly shown that reducing particles size can significantly improve the densification rate and thus realize low-temperature sintering.

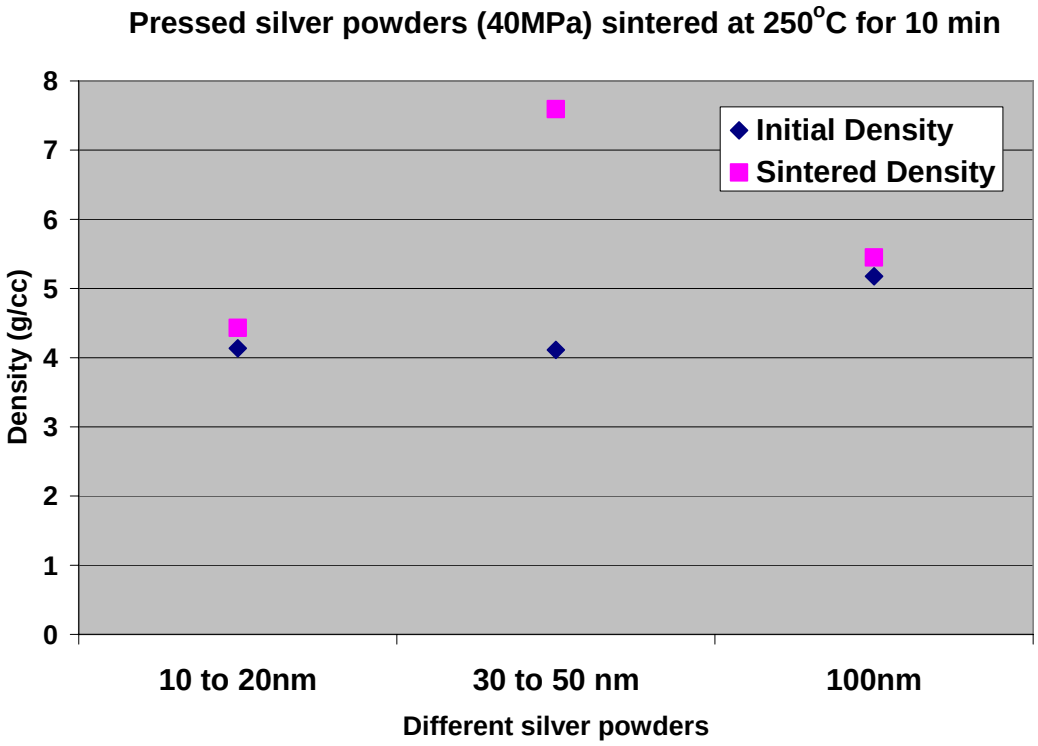

Figure 4.11. Silver pellets sintered at 250°C.

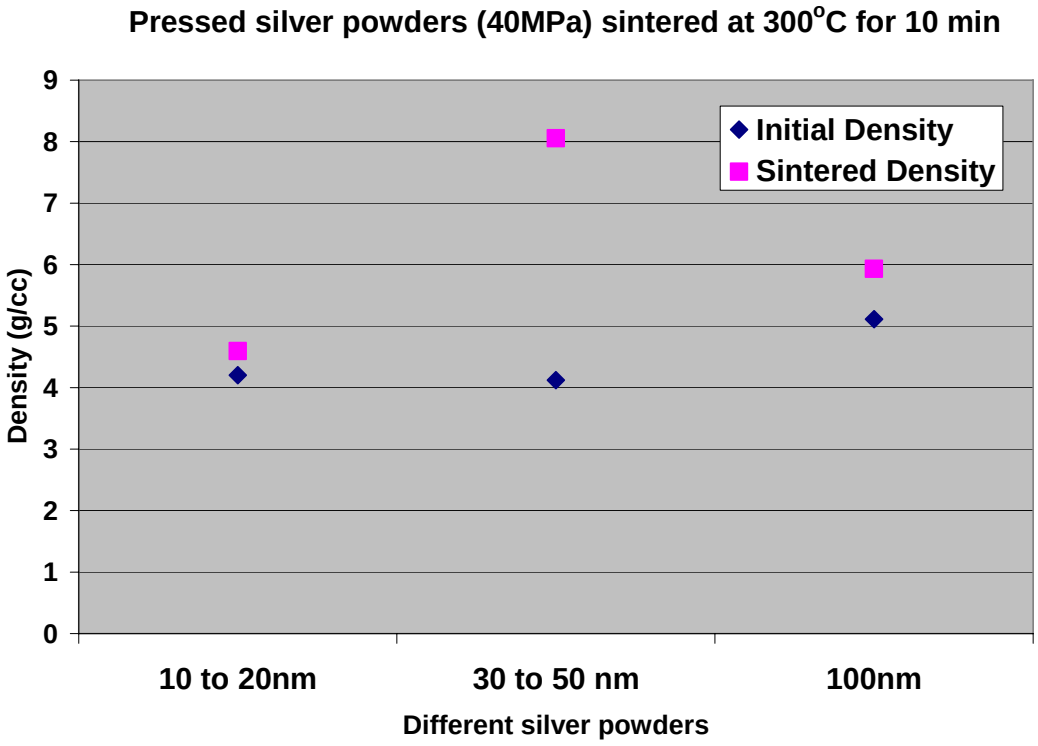

Figure 4.12. Silver pellets sintered at 300oC.

Theoretically, the pellets with 10 to 20 nm should have the highest density among three types of pellets after sintering. They, however, have the lowest sintered density at both heat treatment temperatures (250°C and 300°C). The following observation of paste preparation can explain that. Three silver pastes with particle size 10 to 20 nm, 30 to 50 nm and 100 nm respectively are prepared by ultrasonic vibration. The same processing time (four hours) and the same amount of organics (22 w%) are applied to prepare these pastes. The prepared pastes with 30 to 50 nm silver particles and 100 nm have similar flowability, which are just like commercial micron-size silver paste. Figure 4.13 shows the nanoscale silver paste with particle size 30 to 50 nm, with the comparison of commercial micron-size silver paste (Herease C1075). However, the 10 to 20 nm silver "paste" is like a gel and can not flow at all. This indicates that the initial silver powder has already been severely aggregated, and the ultrasonic vibration can not disperse them due to the strong bonding between particles.

(a) **(b)**

Figure 4.13. (a) Commercial micron-size silver paste; (b) Nanoscale silver paste with particle size 30 to 50 nm.

To verify aggregation of particles in the powder system is important. Because once powder aggregated, it can be sintered at a low temperature no matter what kind of dispersion method we use. To find dry powder aggregated at an early stage, the paste preparation and characterization time can be saved. The dry silver powders with particle size 10 to 20 nm and 30 to 50 nm respectively, were dispersed into pure acetone for four hours using ultrasonic variation. After that, fillers with go-though diameter 220 nm (MILLIPORE, Express^{TM} PLUS) were applied to fill the mixtures (dry powder and solvent). Figure 4.14 (a) is the filter to filter silver powder with particle size 10 to 20 nm. It shows that the container in filter has the clear water. This is because the silver powder with 10 to 20 nm can not go through this filter with DI water due to the severe aggregation. As a comparison, Figure 4.14 (b) is the filter to filter silver powder with particle size 30 to 50 nm. It shows that the majority of the powder with 30 to 50 nm can go through the filler with DI water. The TEM observation in Figure 4.10 shows the powder with 10 to 20 nm indeed has much smaller particle size than the powder with 30

to 50 nm, but the smaller particles aggregated together and even the long time ultrasonic vibration (four hours) can not redisperse them. These aggregated silver particles form clusters with much larger equivalent radius and prevent them from passing through a filter with 220 nm diameter.

(a) (b)

Figure 4.14 (a) Nanoscale silver powder with particle size 10 to 20 nm going through the filter; (b) Nanoscale silver powder with particle size 30 to 50 nm going through the filter.

Figure 4.15 shows the microstructure of sintered paste with the sintering profile shown in Figure 4.1. Figure 4.15 (a) is the microstructure of sintered paste with 10 to 20 nm silver particles; and Figure 4.15 (b) is that of paste with 30 to 50 nm. The microstructure difference is clearly shown and a very pores structure exists in the sintered silver paste with particle size 10 nm to 20 nm. This non-densification structure is due to the severe aggregation.

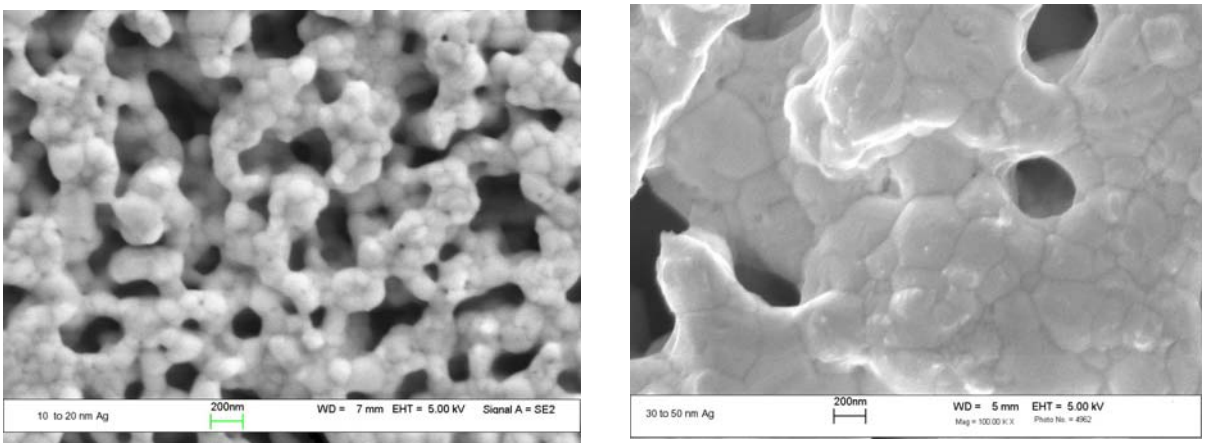

(a) **(b)**

Figure 4.15 (a) SEM observation of sintered silver paste with particle size 10 to 20nm, (b) SEM observation of sintered silver paste with particle size 30 to 50 nm.

The results of the above experiments show that the dry silver powder with particle size 10 to 20 nm has been aggregated severely when commercially obtained. And the aggregated silver particles can not be redispersed by ultrasonic vibration in limited time due to the strong bonding between particles. The aggregation can ruin the low-temperature sinterability of nanoscale silver. Unfortunately, the aggregation is actually easy to occur during nanoscale silver powders because they are unstable systems and have large surface energy. Large surface energy of nanoscale silver powder is the driving force for surface diffusion. When environment, such as press or vibration varies, there is a local non-uniform stress between the particles. This local stress will causes particles to form point contacts with the help of surface diffusion, but without densification. This is an irreversible process, which usually causes indispensable clusters, inhomogeneous distribution of particles and large voids. Micron-size particles have better resistance to aggregation because the large particles are not easy to form permanent local point-contacts under a small local stress. From this point view, the fundamental reason of aggregation and non-densification surface diffusion is actually the same. The difference is that aggregation usually happens in the processing of particles preparation, storage and/or shipping. The dry silver powder is so susceptible to aggregation, and even if the

fresh prepared powders do not have aggregation, any improper storage and/or shipping may cause aggregation. So, the data for commercial dry powder only lists the particle size and the distribution, but does not indicate the aggregation. Since aggregation is caused by local stress, any way that can release the stress can lower aggregation. The particles in the slurry form can have more flowability, and the solvent in the slurry can serve as a buffer to cushion and release the local stress. This approach is particular suitable for silver paste application since solvent needs to be added in the following paste preparation procedure. Figure 4.16 is the SEM observation of nanoscale silver particles with the particle size 30nm to 60 nm particle size in the slurry form [53]. According to the data from vender, about 29 w % of isopropyl alcohol (IPS) is added into the nanoscale silver powder. The SEM observation clearly shows that the tiny silver particles are homogenously distributed without aggregation. Shipping and storage is the major concern to use the IPS, instead of acetone, for the solvent in silver slurry. This is because acetone has a strong dissolvability and evaporability. Using acetone as the solvent requires more expensive containers and sealing technique.

The silver powder in isopropyl alcohol (IPA) is also prepared into the paste by the ultrasonic dispersion. During the dispersion, the dispersion time (four hours) is applied and the 22 w% organics is put into the powder systems. The silver to organics ratio listed in Table 4.2. The prepared pastes are sintered with sintering profile shown in Figure 4.1 respectively. Figure 4.17 shows the microstructure of the silver paste sintered at 300^{o}C. The dense microstructure indicates that the paste can be low-temperature sinterable.

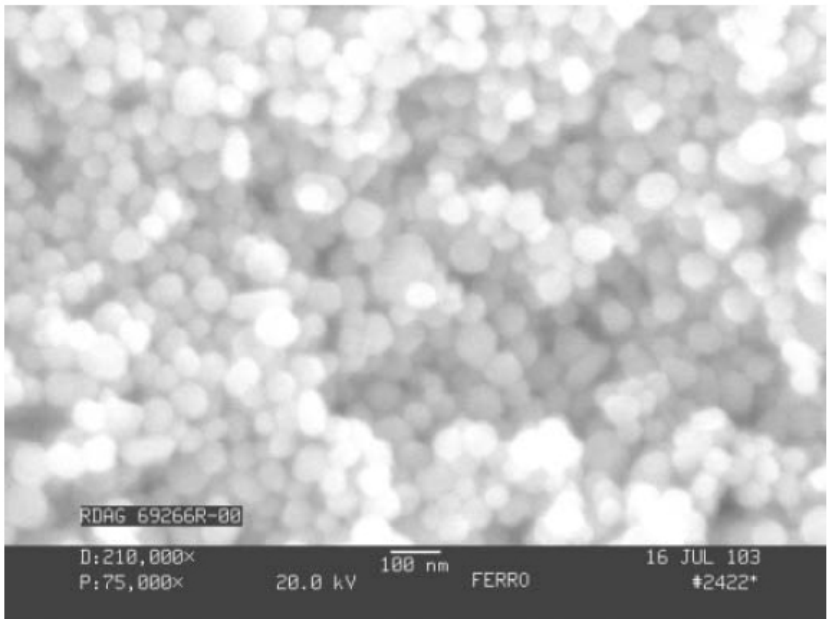

Figure 4.16 the nanoscale silver in the IPA .

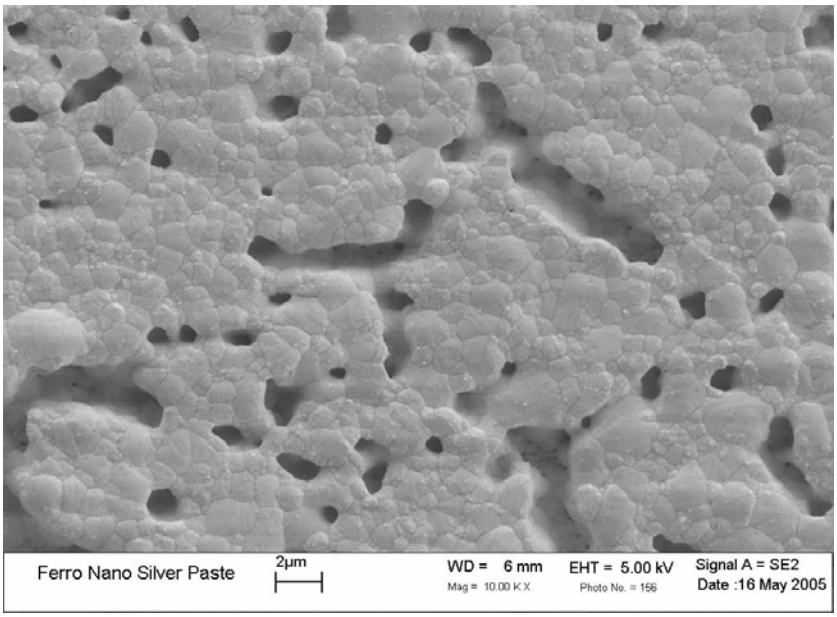

Figure 4.17. Microstructure of sintered silver at 300^{o}C.

4.2.2. Dispersion method to eliminate particles agglomeration

Both ball milling and ultrasonic vibration methods are applied to prepare the silver paste with the same nanoscale powder with particle size 30 nm to 50 nm. The dispersion time keeps the same (4 hours) for fair comparison of both methods.

Figure 4.18 (a) and (b) are the SEM observation of nanoscale silver pastes with 30 to 50 nm. The paste in Figure 4.18 (a) is dispersed by conventional ball milling method; and the paste in Figure 4.18 (b) is dispersed by ultrasonic vibration. The SEM observation clearly shows that the paste dispersed by ultrasonic vibration has significantly improved particle distribution than that dispersed by conventional ball milling. Ultrasonic uses the vibration of silver particles themselves to loosen the weak bonding between particles and permit them redistributed again in the solvent. The efficiency is higher and the dispersion energy is more uniform. The ball milling, however, uses external mechanical force to break the weak bonding. Compared with tiny silver particles with 30 to 50 nanometers, the milling balls are huge (2 mm, about 50,000 larger); the ball millings can not keep a uniform dispersion of the paste. And also, the mechanical milling may cause large local stress and cause further agglomeration and even aggregation of particles.

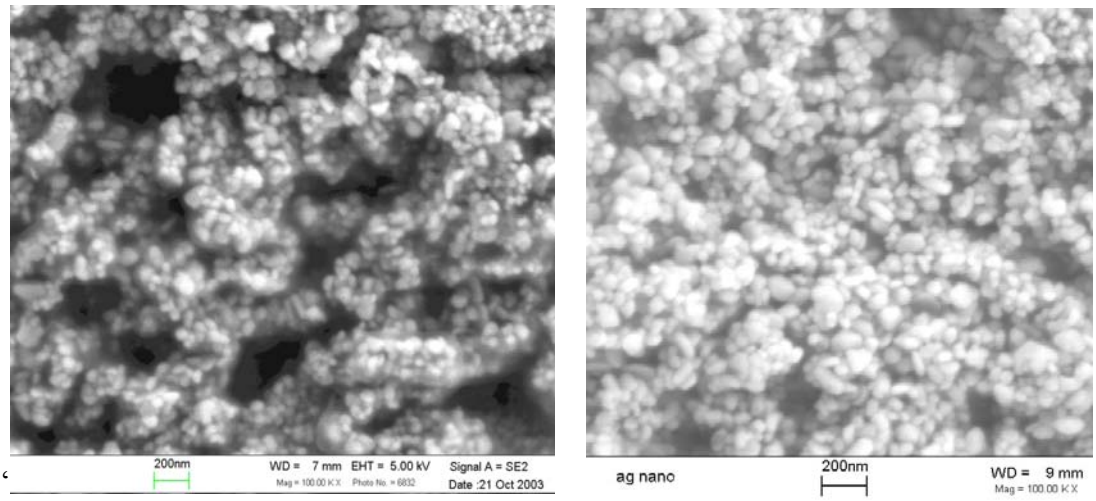

(a) **(b)**

Figure 4.18 SEM observation of nanoscale silver paste. (a) dispersed by ball milling (b) dispersed by ultrasonic.

The two prepared nanoscale silver pastes are stencil printed to the silicon substrate and heat up to 300^{o}C with the same sintering profile. Figure 4.19 shows the microstructure of two sintered pastes respectively: (a) dispersed by ball milling and (b) dispersed by ultrasonic. The observation of SEM clearly shows that the sintered paste with ultrasonic dispersion has much denser microstructure than the one with ball milling structure. This is because the agglomeration in the paste dispersed by ultrasonic vibration has already effectively redispersed and the particles have more uniform distribution.

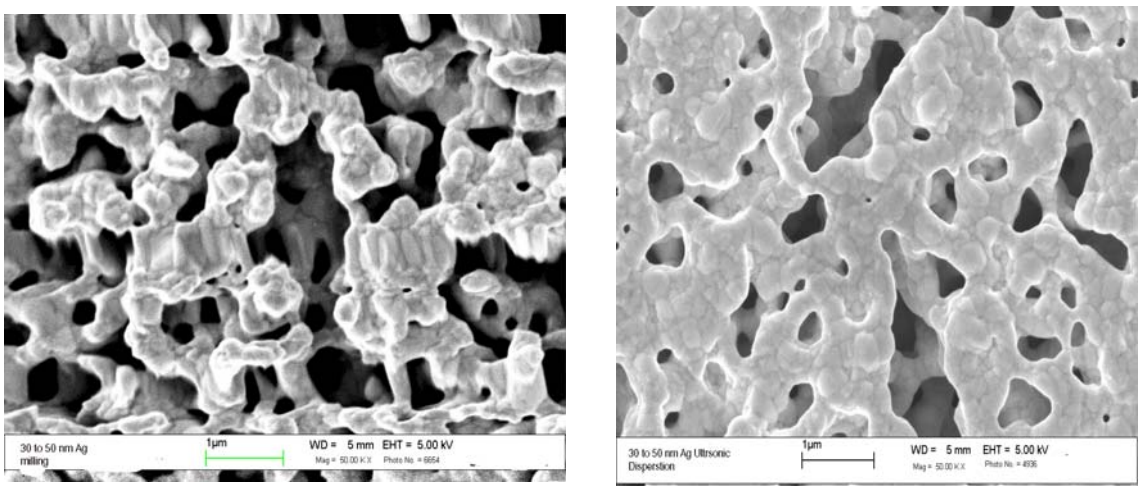

Figure 4.19 The SEM observation of sintered microstructure of nanoscale silver paste. (a) dispersed by ball milling (b) dispersed by ultrasonic.

4.2.3. Organics burn-out as a means to realize abrupt sintering

The raw silver powder prepared by the Carey Lea method was observed using scanning electronic microcopy (SEM) and shown in Figure 4.20. From the observation of SEM, we can see most of the particles appear to fall in the 10 nm to 30 nm range. The SEM observation also shows that there is no agglomeration or aggregation in the silver powders. Samples from the same powders were sintered at 300°C at a rapid heating rate and at a slower rate of 5°C/min respectively. The rapid heating rate was attained by dropping the sample directly onto a pre-heated furnace. The microstructure sintered samples with different heating rate is in the SEM micrographs in Figure 4.21 (a) and (b), respectively. From the SEM observation of the microstructure, it is clear that the sample sintered at the slow heating rate attained a lower density than one sintered under a rapid heating rate. With the slower heating rate, significant surface diffusion will occur. The surface diffusion consumes the sintering driving force and causes little densification. With rapid heating, the material is able to go past the low temperature regime in a very short amount of time, thus minimizing the occurrence of surface diffusion and the expenditure of the sintering driving force. This driving force will be consumed later at

the peak sintering temperature by densifying mechanisms that become active such as grain boundary diffusion, and to a lesser extent, bulk lattice diffusion.

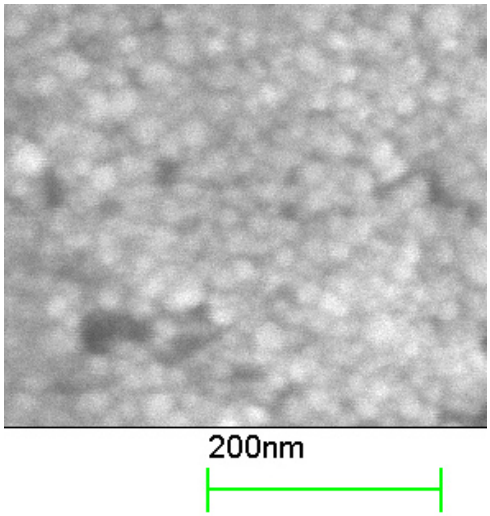

Figure 4.20 SEM image of nanosize silver particles prepared by the Carey Lea method with an estimated particle size range of 10 to 30 nm.

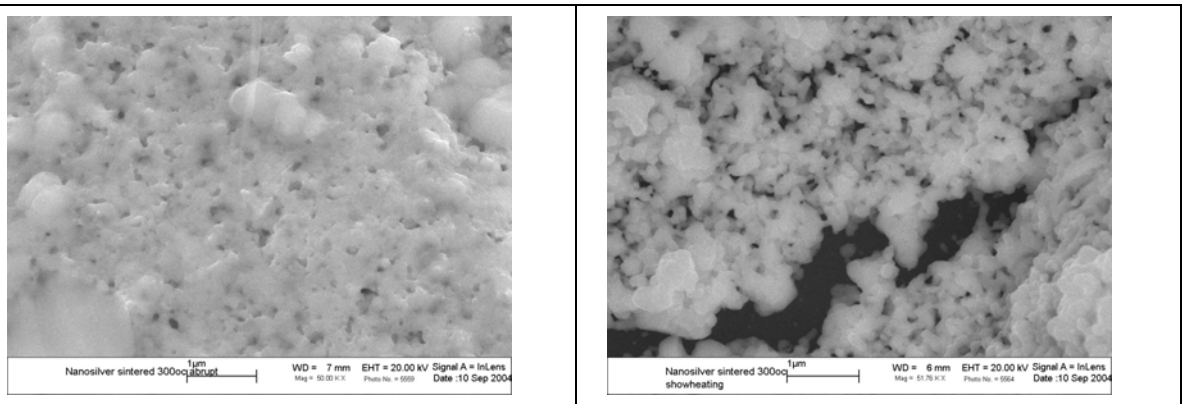

(a) (b)

Figure 4.21. SEM images of nanosize silver powder sintered at 300°C (a) with rapid heating, (b) with a slow heating rate of 5°C.

Fast heating rate is difficult to implement for die-attach because the thermal shock has the potential to destroy the device and / or substrate. The purpose of using fast heating rate is to pass the relative-low temperature zone fast and prevent non-densification diffusion from occurring. In the paste form, organics components are needed to prevent particles agglomeration, prevent paste cracking during handling and adjust viscosity for screen and/or stencil printing. When these organics exist, the diffusion can not occur between silver particles and thus the non-densification process is retarded at relatively low-temperature. At relatively high-temperature, these organics are burn-out. The densification processing such as grain boundary diffusion and/or lattice diffusion dominate, thus causing rapid densification to occur. Figure 4.22 illustrates this concept of controlling organics burn-out to realize abrupt sintering. If the organics burn-out temperature T_1 is equal or higher than the transition temperature between non-densification processing and densification processing, the non-densification diffusion can be avoided during nanoscale silver paste sintering and the actual sintering temperature is determined by organics burn-out.

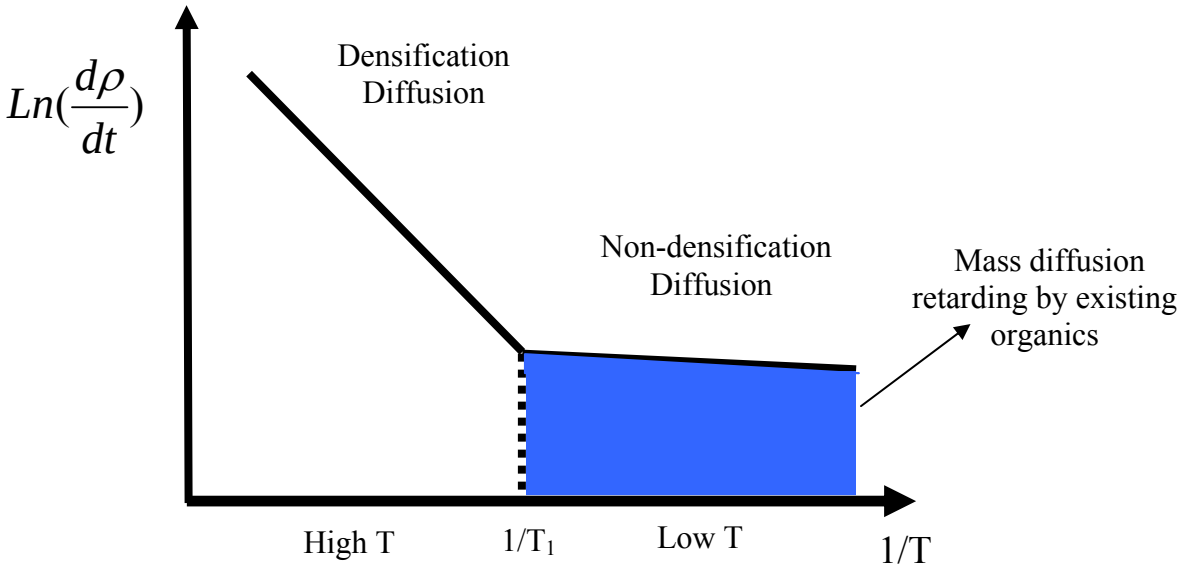

Figure 4.22. Controlling organics burn-out to prevent non-densification diffusion.

Nanoscale silver paste with particle size 30 to 50 nm was prepared by ultrasonic vibration method. The prepared silver paste was put into the chamber of SEM with high vacuum. To situ investigate the sintering/densification of nanoscale silver paste, the scanning electrons are applied to sinter the paste and reflected electronics supplies the images of sintered silver paste. Figure 4.23 shows that silver paste with 30 to 50 nm silver particles is sintered by the electron beams of the SEM. Figure 4.23 (a), (b), (c), and (d) indicate the silver paste after 1, 3, 5, and 7 screen scans, respectively. Since the scanning speed is 17.6 seconds per scan, the 1, 3, 5, and 7 screen scans corresponding the sintering time is 17.6 seconds, 52.8 seconds, 88 seconds, and 123 seconds. The SEM images show the progression of the densification and grain growth processes that take place in a relatively short period of time, e.g., in a matter of a few scans with the electron beams. Porosity is eliminated as the particles form increasingly larger necks and particles are pulled closer together. Eventually, pores are pinched off and shrink as the process shifts to the grain growth regime towards the end of the sintering process. Figure 4.24 (a) and (b) show the silver paste with particle size 100nm after 1 and 7 screen scans, respectively. Neck formation and grain growth were similarly observed, but the extent of the densification is substantially less than that observed in the 30 nm powder paste in relatively the same amount of time, as measured by the number of scans. However, no grain growth and densification were observed to take place in the commercial micron-scale silver paste under the same observation condition (shown in Figure 4.25).

There are two reasons that the nanoscale silver paste can be sintered with scanning electronics in a vacuum. The accelerated scanning electronics can ablate the organics in the paste and the vacuum condition in the SEM chamber can accelerate the organics evaporation. During the same time organics were removed, the electron beam energy can be absorbed by silver particles and thus activate the sintering process. Because the 30 nm silver particles have substantially more surface area, and hence more surface energy than the 100 nm particles, densification and grain growth are more likely to occur faster even at a low temperature under the beam spot. However, the densification barely occurs in the micron-size silver paste under the same electronic scanning conditions due to the absence of sintering driving force.

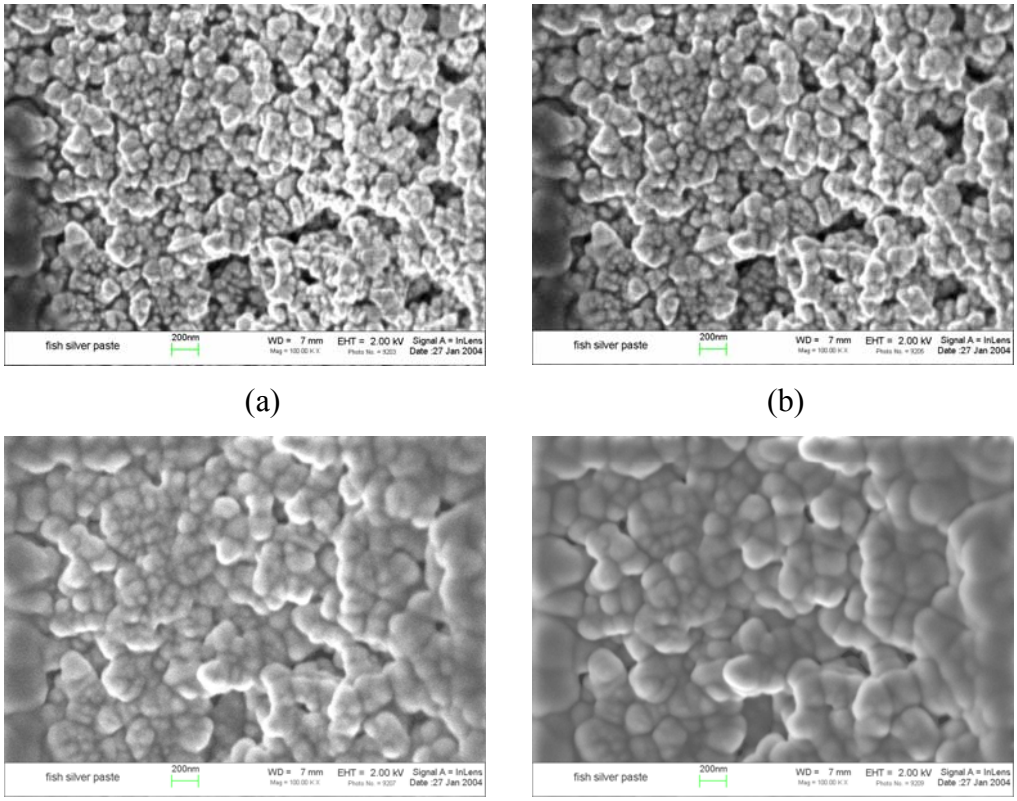

Figure 4.23 The in-situ observation of sintering of the 30 nm nanoscale silver paste by SEM. (a), (b), (c), and (d) are the images after 1, 3, 5, and 7 screen scans, respectively.

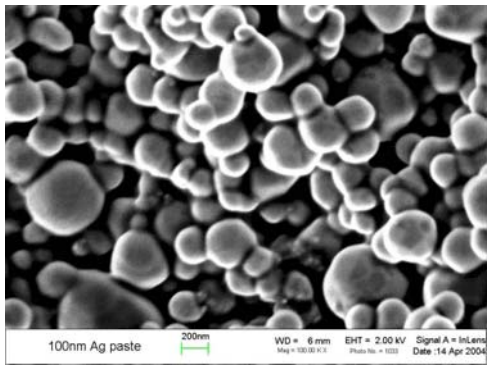

(a)

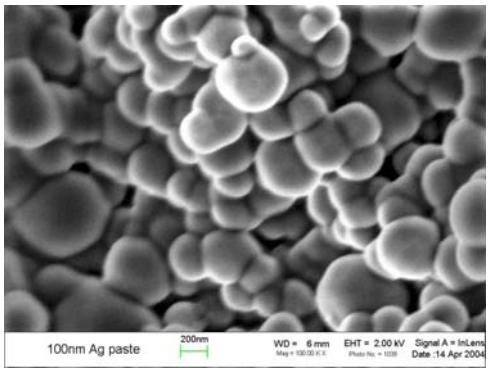

(b)

Figure 4.24 The in-situ observation of sintering of the 100 nm nanoscale silver paste by SEM. (a) and (b) are the images after 1 and 7 screen scans, respectively.

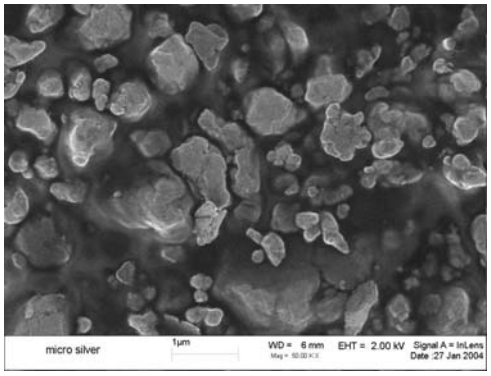

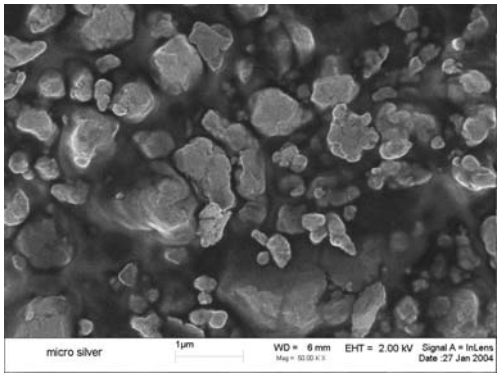

Figure 4.25. The in-situ observation of sintering of the micron-size silver paste by SEM. (a) and (b) are the images after 1 and 7 screen scans, respectively.

The nanoscale silver paste with particle size 30 to 50 nm was prepared using ultrasonic dispersion and the composition in the paste is listed in Table 4.2. To study how the organic burn-out affects the sintering of nanoscale silver, the prepared paste was sintered at different temperature and the sintered microstructure was observed by SEM. The heating rate is 17^{o}C / min. Figure 4.26 (a), (b), (c) and (d) are the microstructures of nanoscale silver paste with heated at 200^{o}C, 225^{o}C, 250^{o}C, and 275^{o}C for ten minutes, respectively. When the temperature is lower than 250^{o}C; there is little change in the microstructure. When the temperature is over 275^{o}C, rapid densification occurs. Figure 4.27 shows the thermogravimetric Analysis (TGA) of nanoscale silver paste. Below 250^{o}C, the paste loses weight quickly, due to volatilization and/or burn out of the organics. Beyond 250°C, the loss rate drops substantially. By the time most of the organics have burned out, the paste has already passed through the low temperature regime where surface diffusion dominates, and entered the high temperature zone where densification mechanisms dominate. Therefore, in applications where the nanoscal silver can be deposited in the paste form, it is possible to attain significant densification without the need for rapid heating rate.

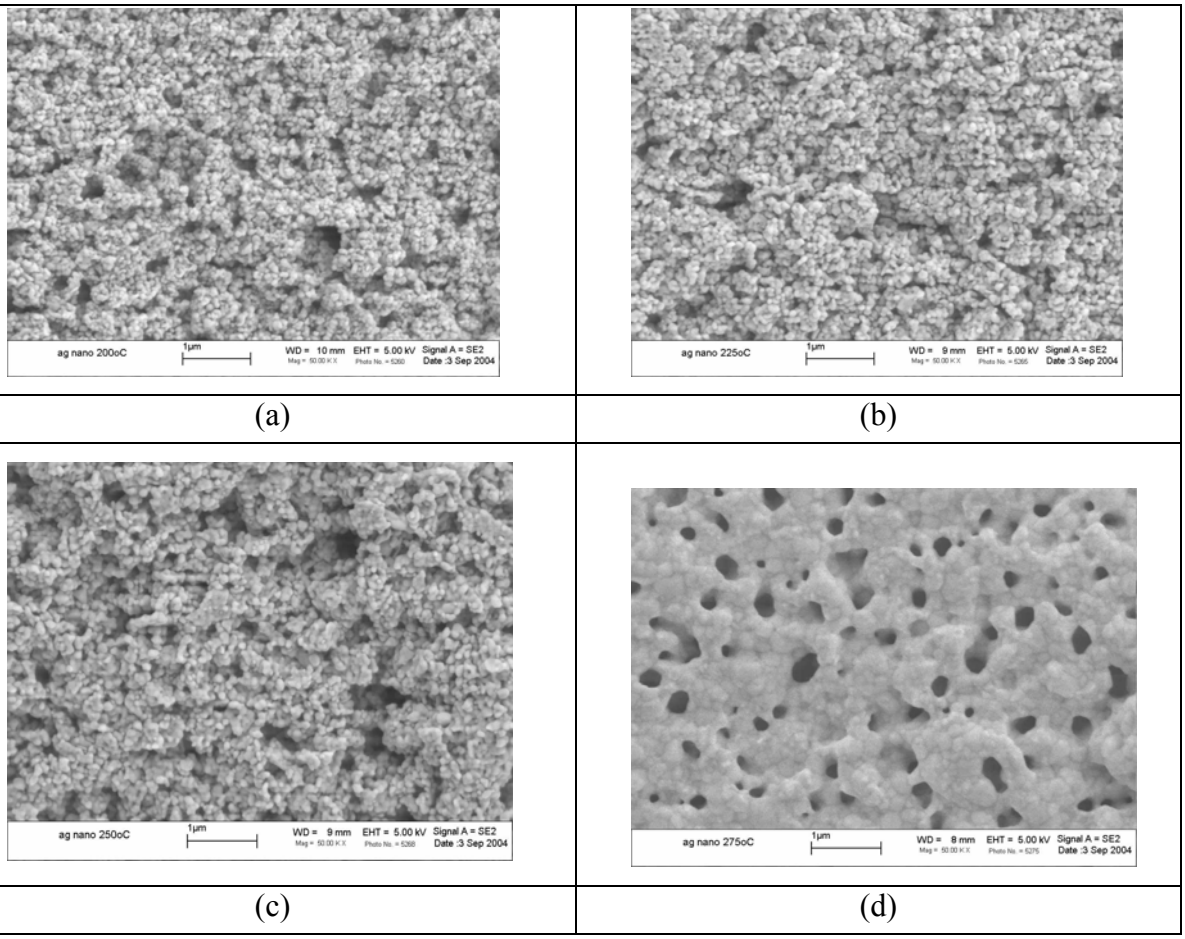

Figure 4.26. Nanoscale silver paste with particle size 30 to 50 nm sintered at different temperature for 10 minutes: (a) 200^{o}C, (b) 225^{o}C, (c) 250^{o}C, (d) 275^{o}C.

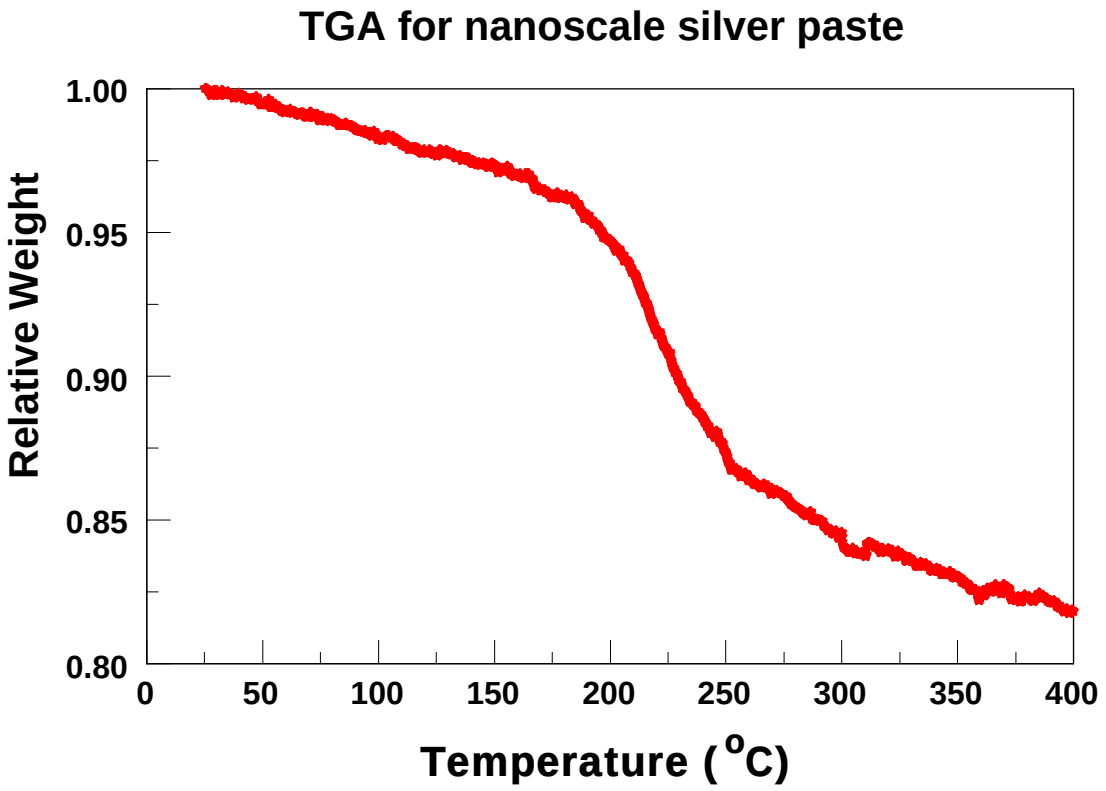

Figure 4.27. TGA of nanoscale silver paste with particle size 30 to 50 nm using low-burn-out temperature organics.

Two types of nanoscale silver pastes with particle size 30 to 50 nm were prepared using ultrasonic vibration. The two pastes have the same nanoscale silver particles (30 to 50 nm), the same dispersion time (four hours), and the same organics ratio (22 w%). The only difference is that they have different organic systems: one has the organic system with low burn-out temperature (type I) and another one has organic system with high burn-out temperature (type II). Two pastes were printed on the direct-bonded copper (DBC) substrate with gold-coated substrates and sintered at the temperature at 300°C. Figure 4.28 shows the films of both the pastes with high-burn out temperature organics (Figure 4.28 (a)) and low-burn-out temperature organics (Figure 4.28 (b)) sintered at

300°C respectively. Although the pastes have same silver powders with particle size 30 to 50nm and are sintered at the same temperature, the paste with high burn-out temperature organics still appears brown in color and seems not densified at all. The reason is that the paste shown Figure 4.28 (b) has the organics with high burn-out temperature; at 300°C within a few minutes the organics can not be burn-out, and thus the existing organics prevent silver particles from having any mass diffusion and the densification processing can not occur below the burn-out temperature of organics. The Figure 4.27 and Figure 4.29 show the thermogravimetric analysis (TGA) of the two pastes with different organic systems respectively. It can be clearly seen that the organics with high-burn out temperature can not be burn-out at 280°C. The SEM was applied to observe the microstructure of the two pastes sintered at 300°C and is shown in Figure 4.30. The nanoscale silver paste with organics of low burn-out temperature (shown in Figure 4.30 (a)) has a dense microstructure after heating up to 300°C. However, the paste with organics of high burn-out temperature (shown in Figure 4.30 (b)) still presents individual particles and undensified microstructure after the 300°C temperature. The undensified microstructure is caused by the high burn-out temperature organics in the paste. The organics with high organic burn-out temperature can still exist at 300°C. With the existing organics, the diffusion can not occur between silver particles and thus the dense microstructure can not be obtained.

(a) (b)

Figure 4.28. Images of sintered nanoscale silver paste with particle size 30 to 50 nm at 300^{o}C. (a) with high burn-out temperature organics (b) with low burn-out temperature organics.

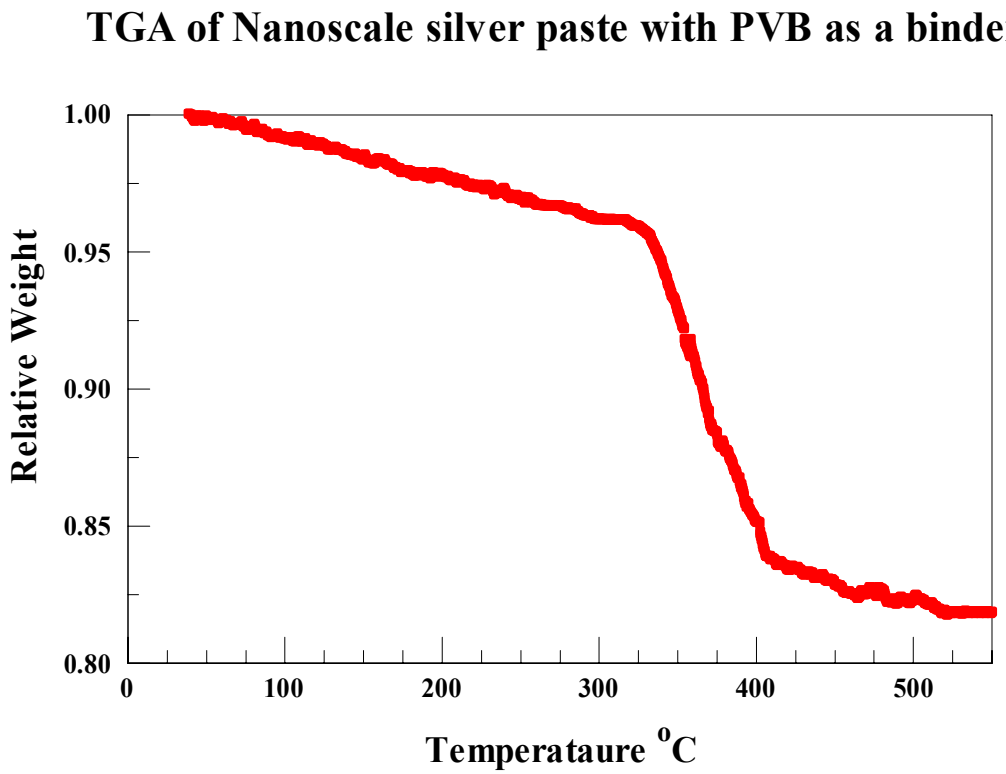

Figure 4.29. TGA of nanoscale silver paste with particle size 30 to 50 nm using high-burn-out temperature organics.

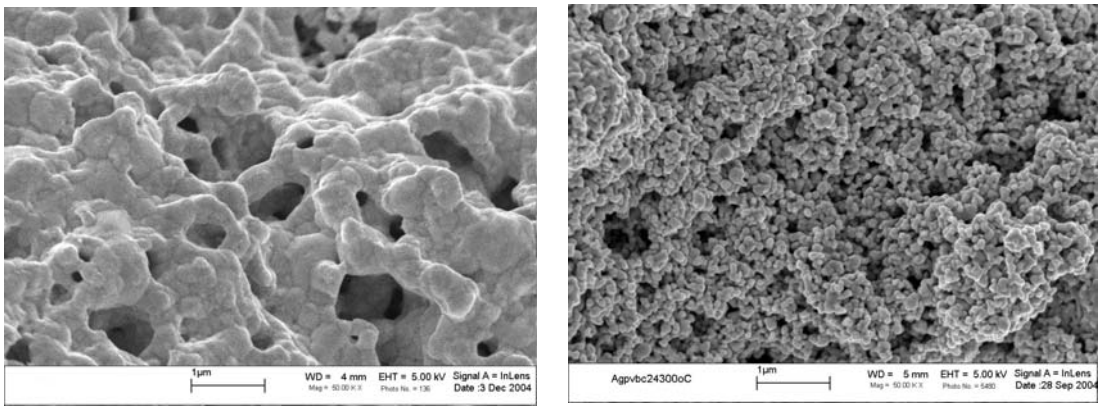

(a) (b)

Figure 4.30. The SEM observation of two pastes with different burn-out temperature of organics: (a) with low organic burn-out temperature; (b). with high organic burn-out temperature.

Two types of nanoscale silver pastes with particle size 100 nm were also prepared using ultrasonic vibration. The two pastes have the same nanoscale silver particles (100 nm), same dispersion time, same organics ratio (22 w%). The only difference is that they have different organic systems: one has the organic system with low burn-out temperature (type I) and another one has high burn-out temperature (type II). Both prepared silver pastes were sintered at 450^{o}C. Figure 4.31 shows the microstructure of sintered nanoscale silver paste with particle size 100nm. Figure 4.31 (a) is the sintered paste with the low burn-out temperature organics, and (b) is the sintered one with high organics burn-out temperatures. The SEM observation of these microstructures shows that the paste with high burn-out temperature organics has significantly denser microstructure that the one with low burn-out temperature organics. This is because the 100nm silver particles can not be densificated at the temperate as low as 280^{o}C, which is roughly the temperature low burn-out temperature organics can burn out. But at that temperature, if the organics have already been burn-out, the non-densification diffusion

such as surface diffusion, will occur and consume the sintering driving force. With a surface diffusion occurring at a relatively low temperature, the paste can not be sintered at a relatively high temperature. On the other hand, the paste with high temperature burn-out organics will retard the non-densification at relatively low-temperature and at a relative high temperature, the densification mechanism can dominate and thus an abrupt densification can be realized.

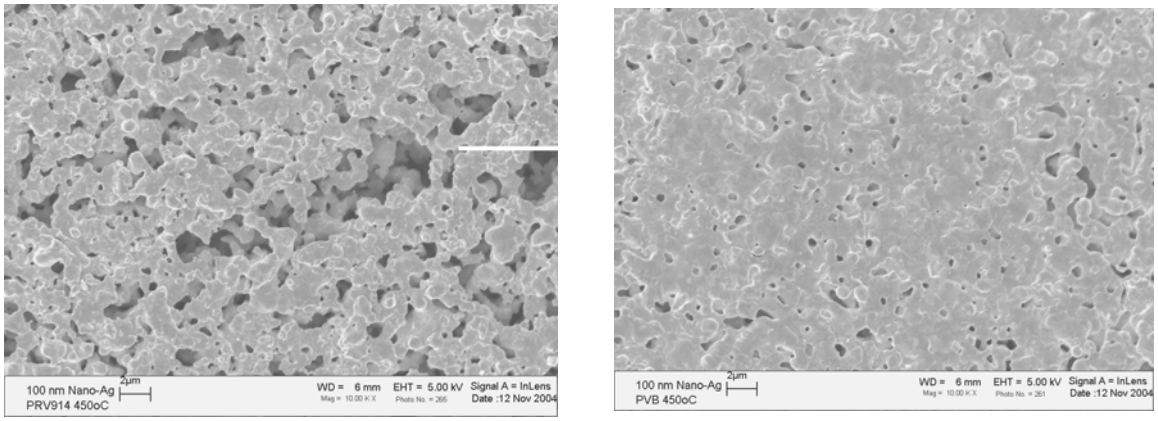

Figure 4.31. Microstructure of sintered nanoscale silver paste with particle size 100nm (a) with low temperature burn-out organics (b) with high temperature burn-out organics.

4.2.4. Properties of sintered nanoscale silver paste

Table 4.5 shows the properties of sintered nanoscale silver paste with the comparison with lead-tin solder and gold-tin solder. From this table, we can see that the processing temperature of solders is higher than the melting temperature, which is the maximum temperature solders can be used. In the liquid form, the solder bonding will be totally lost. The processing temperature of nanoscale silver is a little bit higher than lead-tin and compatible with gold-tin, however, the melting temperature of silver is 961^{o}C,

much higher than solders. The working temperature is higher than the processing temperature making the sintered nanoscale silver a very good candidate for high-temperature packaging material. Compared with solders, the sintered silver has much better electrical and thermal properties. The sintered silver joints have the compatible die-shear strength with lead-tin solder. Gold-tin has much stronger shear strength, but it belongs to the hard solder. The die-attach layer of gold-tin solder interconnection is stiff, instead of cushioning the strength between die and substrate like lead-tin solder and sintered silver. The stiff die-attach layer transfers the thermal-mechanical strength to the die and has the potential to damage the brittle semiconductor devices.

Table 4.5. The properties of sintered nanoscale silver paste with the comparison of lead-tin solder and gold-tin solder.

	Processing temperature	Working temperature	Electrical conductivity 10^5 (Ω -cm)-	Thermal conductivity (W/K-cm)	Shear Strength (MPa)
63Sn37Pb	213ºC	<183ºC	0.69	0.51	20-40
80Au20Sn	~310ºC	<280ºC	0.625	0.58	80MPa
Sintered nanoAg	300ºC	<650ºC	3.8	2.4	>30MPa

4.3 Conclusion

In this chapter, a nanoscale silver paste which can be sintered at the temperature as low as 300^{o}C was developed. Compared with micron-size silver particles, nanoscale silver particle have much larger driving force and thermodynamically can be densified at low-temperature. In practice, there are several challenges existing in the nanoscale materials sintering such as aggregation, agglomeration and non-densification sintering at relatively low temperature.

After that, experiments are conduct to understand low-temperature sintering challenges of nanoscale silver paste and several approaches are developed and/or suggested to overcome sintering problems: aggregation, agglomeration and non-densifying diffusion at initial stage of sintering.

Storing nanoscale silver powders in the solvent with surfactant coating is suggested to avoid aggregation / agglomeration of silver powders during the storage and shipping of powders. This slurry form will not further increase the difficulty of paste preparation, because we need solvent and surfactant to prepare paste any way.

Ultrasonic vibration dispersion is developed to reduce particles agglomeration. Compared with the paste prepared by conventional ball-milling processing, the silver paste prepared with ultrasonic dispersion has more uniform distribution and much denser microstructure after sintering.

Controlling the burn-out temperature is developed to reduce non-densifying diffusion and thus realize abrupt sintering. With slow heating rate, even the nanoscale silver powder without agglomeration and/or aggregation still has the difficult to be sintered to high density. By adding organics with proper burn-out temperature, the non-densifying surface diffusion can be retarded at low-temperature; after organics burn out, densifying diffusion such as lattice and or bulk diffusion can take over and an abrupt densification can be realized.

The prepared nanoscale silver paste was sintered at 300^{o}C within one hour, the measured electrical and thermal properties are significantly better than solder joints. And the shear strength is compatible with solder joints.

Chapter 5 Application of sintering nanoscale silver paste: attaching SiC devices for high-temperature application

5.1 Introduction

Traditional (IPEMs) can only operate at a temperature below 125^{o}C. To cool power modules down, bulky heat-sink and complicated thermal design are needed. The additional cooling system increases the cost and lowers the power density for power conversion system. On the other hand, the emerging applications require the next generation integrated power electronic modules to work at higher temperature [54-57]. Figure 5.1 shows a few high-temperature applications for power electronics, such as jet engine sensor and control, spacecraft power conditioning, transmitters for deep well drilling, industrial process measurement and control and automotive engine sensors. Figure 5.2 schematically shows the major advantages for high-temperature application: 1) reduce the bulk cooling system; 2) function at harsh environment for emerging applications.

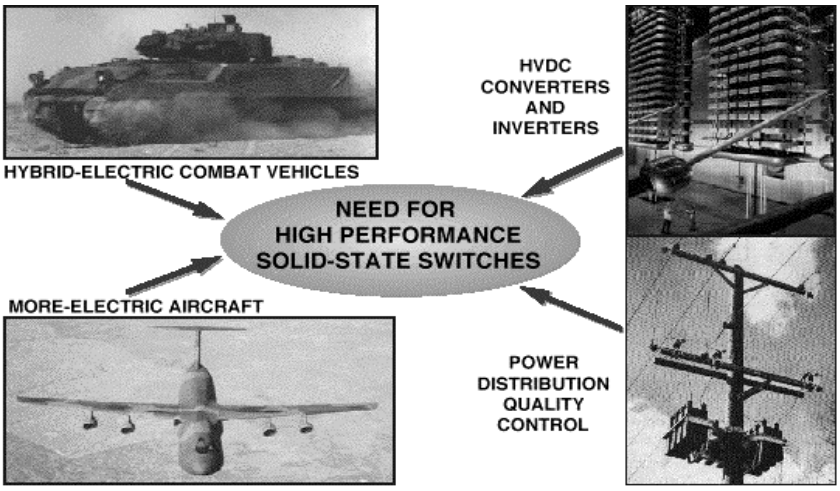

Figure 5.1 High temperature applications of power electronics.

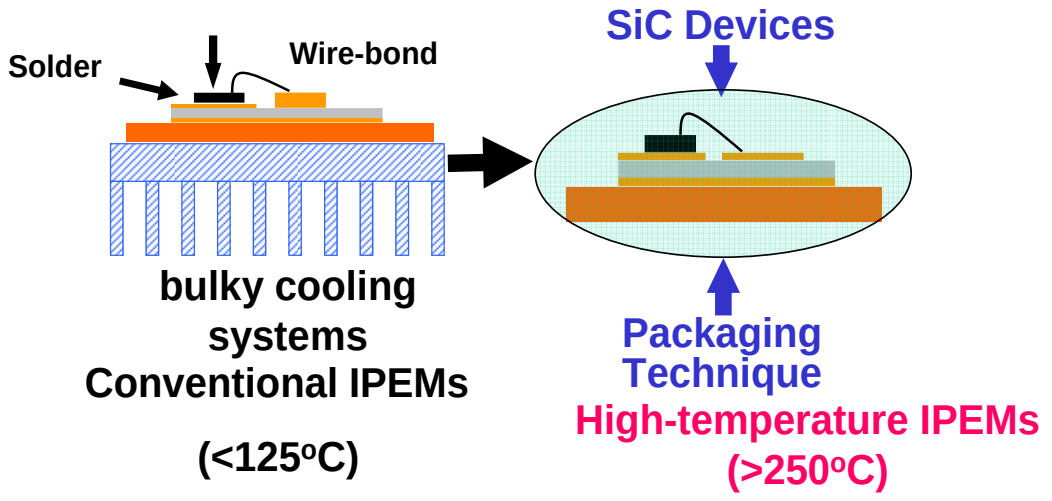

Figure 5.2. (a) Conventional IPEMs, which only can work at the temperature below 125°C, (b) high-temperature IPEMs, which can work the temperature higher than 250°C.

Figure 5.2 also indicates that to design IPEMs working at a high temperature, we not only need power devices which can function at high-temperatures, and also the novel packaging techniques enabling high-temperature operation. Table 5.1 is the properties of SiC material with the comparison with Si and some other semiconductor materials. The combination of several advantageous material properties such as high temperature stability, high thermal conductivity, high breakdown field and high saturation velocity makes Silicon Carbide (SiC) a very promising material for high power and high temperature applications. High-temperature characteristics of those devices enable integrated power electronics modules (IPEMs) to work in harsh environments and dramatically decrease the cooling requirement of power electronic system. Recent studies on SiC devices have shown promising results on their switching characteristics and their ability to function at elevated temperatures up to 450ºC or even higher [58-61]

Table 5.1. Properties comparison of semiconductor materials.

Material	E_g eV	ε_r	μ_h $cm^2/V \cdot s$	E_c $10^6 V/cm$	v_{sat} $10^7 cm/s$	λ $W/cm \cdot K$	n_i cm^{-3}
Si	1.1	11.8	1350	0.3	1.0	1.5	1.5×10^{10}
Ge	0.66	16.0	3900	0.1	0.5	0.6	2.4×10^{13}
GaAs	1.4	12.8	8500	0.4	2.0	0.5	1.8×10^{6}
GaP	2.3	11.1	350	1.3	1.4	0.8	7.7×10^{-1}
GaN	3.39	9.0	900	3.3	2.6	1.3	19×10^{-10}
3C-SiC	**2.2**	9.6	900	**1.2**	2.0	**4.5**	**6.9**
4H-SiC	**3.26**	10	720[a] 650[c]	**2.0**	2.0	**4.5**	**8.2×10^{-9}**
6H-SiC	**3.0**	9.7	370[a] 50[c]	**2.4**	2.0	**4.5**	**2.4×10^{-5}**
Diamond	5.45	5.5	1900	5.6	2.7	20	16×10^{-27}
AlN	6.2	8.5	300		1.8	2.8	9×10^{-34}

Note: a – mobility along a-axis, c-mobility along c-axis

High-temperature packaging technique is another challenge for high-temperature IPEMs. Conventional packaging materials / techniques such as printing circuit board (PCB) substrate, solder interconnection, epoxy underfill, etc can not meet the high-temperature requirement [62-65]. During these challenges, die-attachment is one of the largest. Die-attach layer is only several mils, but it mechanically supports the power devices and also supplies the electrical interconnection and majority heat dissipation. So, its performance and reliability essentially effect the operation of the power devices during the field. Thus far, solders of the Pb-Sn binary system are widely used as interconnection materials to attach power devices. The Pb-Sn solder, however, has low-melting temperatures (melting point 187°C). Such a low melting temperature prevents its

application to interconnect devices functioning at high temperature. Right now, only a few gold-rich solders have the melting temperature higher than 250^{o}C, such as gold-tin solder. But these solders are expensive due to large percent gold contents and none of them can bear temperature over 350^{o}C. Additionally, they have relatively low electrical, thermal conductivities and fatigue resistance. Futher more, these rigid gold-contained solder during the cyclic loading, transfer rather than cushion the thermal mechanical stress to the device and easily crack the die. Sintered silver has high temperature stability, high electrical and thermal conductivity, and high fatigue resistance. Its high sintering temperature (>600^{o}C), however, has prevented its application as a die-attach material. Some studies have evaluated the use of pressure to lower the sintering temperature of silver powder compacts for attaching power semiconductor devices. The application of pressure, however, does have a drawback because it makes automation in manufacturing very difficult to implement and thus appreciably increases the cost. Furthermore, pressure applied on the devices may cause physical damage, such as device cracking. Ricky W. Chuan and Chin C. Lee [66]develop a silver-indium joining technique which can enable low-temperature processing and high-temperature application. The long process time may cost this technique expensive, and the addition of In may be detrimental to the joint's performance.

In this Chapter, an alternative method – sintering nanoscale silver paste – is developed as an alternative die-attach solution for high-temperature application. The challenge for sintering die-attach technique – limited organics burn-out path - is presented. This problem is significantly lessened by reducing organics ratio in the paste. The effects of die-size and heating rate were also investigated by measuring the shrinkage profile (relative die position) of the die-attach silver film during heating treatment. The single Silicon Carbide (SiC) Schottky barrier diode (SBD) packaging was achieved by sintering die-attach and gold wire-bonding. The measured forward and reserve characteristics show that the sintering technique can enable high-temperature applications.

5.2 Experimental procedure

Chapter 4 has already developed a nanoscale silver paste which can be sintered at a temperature as low as 300°C. The organic contents in the paste and existing organics have multiple functions such as adjusting viscosity for printing process, retarding non-densification diffusion at relatively low-temperature, etc. Before the organics burn out, the silver particles in the paste can not densified and thus the desire properties can not be obtained. Figure 5.3 schematically shows the sintering conditions of nanoscale silver paste for different applications. Figure 5.3 (a) is the condition for conductive trace application. In this application, the paste is open to air and the organics have enough space to be burn-burn at elevated temperature. Figure 5.3 (b) shows the condition for die-attach application. In this application, the paste is sandwiched between the substrate and device and organics can only be burn-out from the side way. The limited organics burn-out path challenges sintering die-attach application.

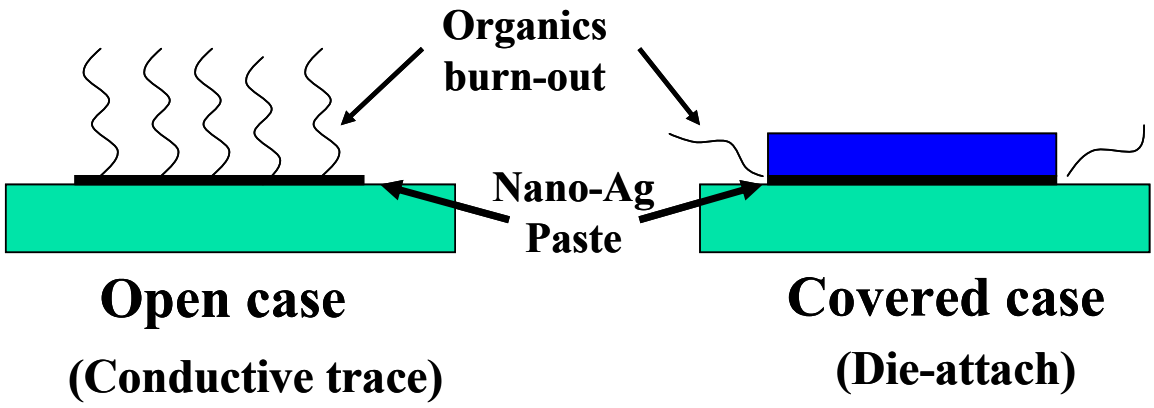

(a) (b)

Figure 5.3. Sintering conditions of nanoscale silver paste for different applications: (a) conductive trace application (paste open to air), (b) die-attach application (paste sandwiched between die and substrate).

To verify that the die-attach application does suffer the limited burn-out path for die-attach application, the following experiment was conducted. The silver paste with 22 w% of organics was prepared using ultrasonic vibration method. The silver powder has the particle size 30 to 50 nm. The organic contents and ratio are listed in Table 4.2. The prepared nanoscale silver paste was stencil-printed to form two films on the same Al_2O_3 ceramics substrate. The thickness of the film is about 50 to 100 micron meter. One film was covered by the glass with the area 4 mm * 4 mm; and the thickness of the glass is 0.75 mm. Another film was just open to the air without coverage as a comparison. In this experiment, glass, instead of a real semiconductor device was selected to cover the printed paste, because the glass is transparent and thus the changing of paste, can be observed by naked eyes during the heat-treatment. Both of the samples are sintered by the sintering profile shown in Figure 4.1. The optical microscope and SEM were applied to investigate the coverage effect of the sintering.

For conductive trace application, silver paste usually needs to be printed to fabricate very small features. Printerability is one of the key characteristics for this kind of application. To enhance the printerability, more organics, especially binders need to be added into the paste. The additional organics do not result in burn-out problem since the printed paste is open to the air. On the other hand, the die-attach has a large-area interconnection, and the printed die-attach layer usually has the regular shape with area larger than the die. The regular die-attach silver film can be printed with reduced organics in the paste. With reduced organics, the sinterability of silver paste in the sandwiched die-attach structure can be enhanced. Reducing the organics can reduce the problem of limited organics burn-out path. To investigate the organics ratio effect on the paste sintering during the sandwiched structure, the pastes with different organics ratio were prepared. During the organic components, the binder is the most difficult burn-out one due to the long carbon chain. And thus, four silver pastes with different binder ratio were prepared using ultrasonic vibration method, and the detailed organics ratio was listed in Table 5.2.

Table 5.2 Silver pastes with different organic ratios.

Silver powder	Binder	Thinner	Surfactant
10g	1.5g	0.8g	0.1g
10g	1.2g	0.8g	0.1g
10g	0.8g	0.8g	0.1g
10g	0.4g	0.8g	0.1g

The prepared pastes were stencil-printed on the Al_2O_3 substrate to investigate the processability. A rectangle thin film with 6 mm * 9 mm was printed, and naked eyes and optical microscopy were applied to investigate whether the paste can be processed for die-attach application. The paste with the lowest organics ratio that can still be processed was chosen as the candidate for sintering die-attach application. The chosen silver paste was printed to form the two films onto the Al_2O_3 ceramic substrate and one of the films was covered with glass (4 mm*4 mm) and another one was exposed to air as a comparison. The two films were sintered using the profile shown in Figure 4.1. The optical microscope and SEM were applied to investigate the coverage effect of the sintering.

How easy and how fast the organics can burn-out is also related with the size of the die and heating profile. Figure 5.4 schematically shows the die-size effect on burn-out of organics. The mass of organics in the die-attach layer is proportional to the area of the die; however, the burn-out path of organics is proportional to the perimeter of the die. The larger the die, the more difficult the organics can burn-out efficiently because the ratio of mass to the burn-out path becomes larger. On the other hand, the heating rate internally determines how fast the organics can burn into the gas. If the gas can not evaporate externally, it can accumulate and increase the gas pressure. A fast heating-up ramp leads to high pressure and pushes the die up to release the pressure. This procedure reduces the contact area of the die and paste. With reduced contact area, the die bonding strength will be significantly reduced. A slow heating rate however leads the die-attach

processing time too long and make it not practical for application. An optical system schematically shown in Figure 5.5 will be applied to detect the relative die position in the vertical direction during the sintering die-attach processing. The optical part of the system consists of a low power HeNe laser (4 mW), mirrors, lenses, and silicon photodetectors. The heating part includes a high plate with precise-temperature control. The temperature profiles are maintained by a temperature controller within ±1^{o}C up to 400^{o}C. The tilt angle of the silicon piece is placed over the die-attach sample. This variation in tilt angle is monitored by reflecting a HeNe laser beam off the silicon surface and detected by a position sensitive detector. With this optical setup, a tiny die position can be magnified and detected by the detector. The effective length of this detector is 13 mm and corresponds to an electrical signal with -10V and +10V. The electrical signal is digitized by an A/D converter and recorded by a program. For the experiment, two types of dies with area 2 mm * 2mm and 4 mm *4 mm respectively are used with three different heating rate (20 ^{o}C / min, 10 ^{o}C / min and 5 ^{o}C / min).

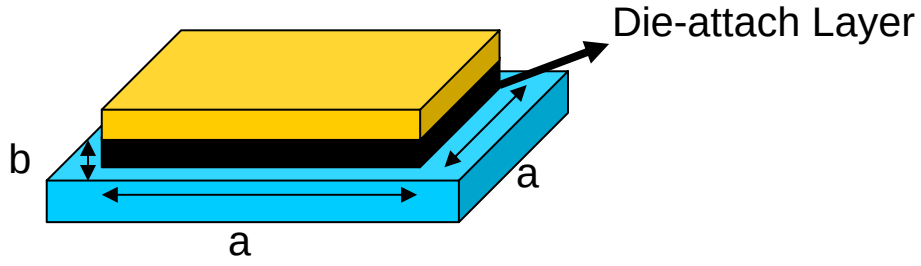

Figure 5.4. Schematic of die-size effect to organics burn-out.

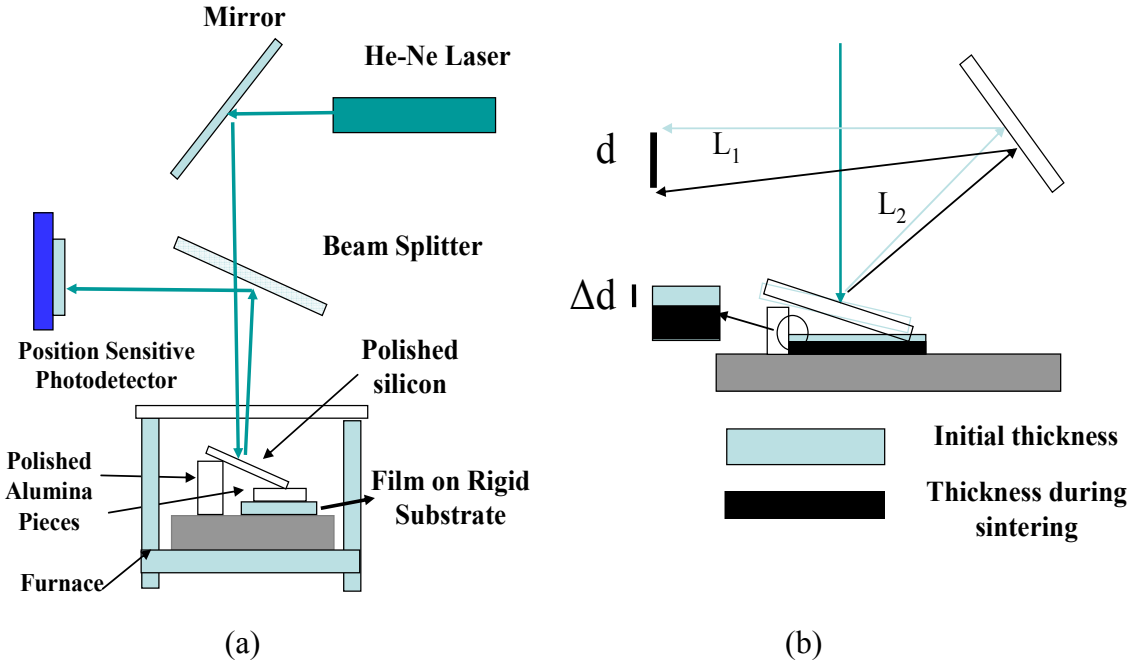

Figure 5.5. Optical setup to measure to shrinkage profile.

Schottky Barrier Diode (SBD) consists of a metal-semiconductor rectifying contact with an N-drift region designed to support the required reverse blocking voltage. When a positive bias is applied to the metal with respect to the N-type semiconductor, forward conduction occurs by the thermal emission of the majority carrier electrons across a metal-semiconductor barrier. The on-state voltage drop of the SBD therefore consists of the sum of the voltage drop across the barrier and the voltage drop across the N-drift region. There is no modulation of the drift region in the SBD structure due to the negligible minority carrier injection and thus can eliminate the reverse recovery problem associated with P-i-N rectifiers. Compared with P-i-N diode, the Si SBD also has two disadvantages: high forward voltage drop for high block-down die and larger reverse leakage current and very sensitive to the temperature. These drawbacks result in seldom application of Si SBD at the blocking voltage higher 200 v. Silicon carbide (SiC) has a band-gap about three times wider than that of silicon (3.0 ev for 6H-SiC and 3.25 eV for 4H-SiC), high avalanche breakdown electric field (2-4 $*10^6$) V/cm, high saturated electron drift velocity of $2*10^7$ cm/sec, and high thermal conductivity (4.9 W/cm-K).

Wider band-gap enables SiC devices function stably at high-temperature. The high breakdown electric field allows the use of much higher doping and thinner layers for a given blocking voltage than silicon devices, resulting in much lower specific on-resistance. SiC SDB is superior to that of the silicon P-i-N power rectifier for a blocking voltage up to 3000 voltage and even can work at a higher temperature. It also has excellent reverse recovery and reverse bias leakage characteristics even at high operation temperature. Compared with other types of silicon carbide devices such as SiC MOSFTETs, SDB is easier to be fabricated due to the absence of the oxidation layer. The application of SiC SDB can improve the power conversion system performance (no reverse recovery problem and high-temperature stable) and lower the system cost (eliminating snubber circuits for rectifiers). Due to its excellent performance and relative low cost, the SiC SDB is already commercially available and its application has been demonstrated in power factor compensation (PFC) circuitry [67]. Figure 5.6 shows the turn-off characteristics of SiC SBD (600V, 10 A) with the comparison of Si FRED (IXYS DSEI 12-06A). The SiC diode, is a majority carrier device, and thus does not have any stored minority carriers. Therefore, there is no reverse recovery current associated with the turn-off transient of the SBD. However, there is a small amount of displacement current required to charge the Schottky junction capacitance (< 2 A), which is independent of the temperature, current level and di/dt. In contrast to the SiC SBD, the Si FRED exhibits a large amount of the reverse recovery charge, which increases dramatically with temperature, on current and reverse di/dt. For example, the Qrr of the Si FRED is approximately 160 nC at room temperature and increases to about 450 nC at 150°C. This excessive amount of Qrr increases the switching losses and places a tremendous burden on the switch and diode in typical PFC applications. At the same time, the SiC transistors such as JFETs, MESFET and even MOSFET are also successfully fabricated [68, 69]. How to interconnect these devices and enable the high-temperature application, however, still presets a challenge due to the lack of high-temperature packaging technique.

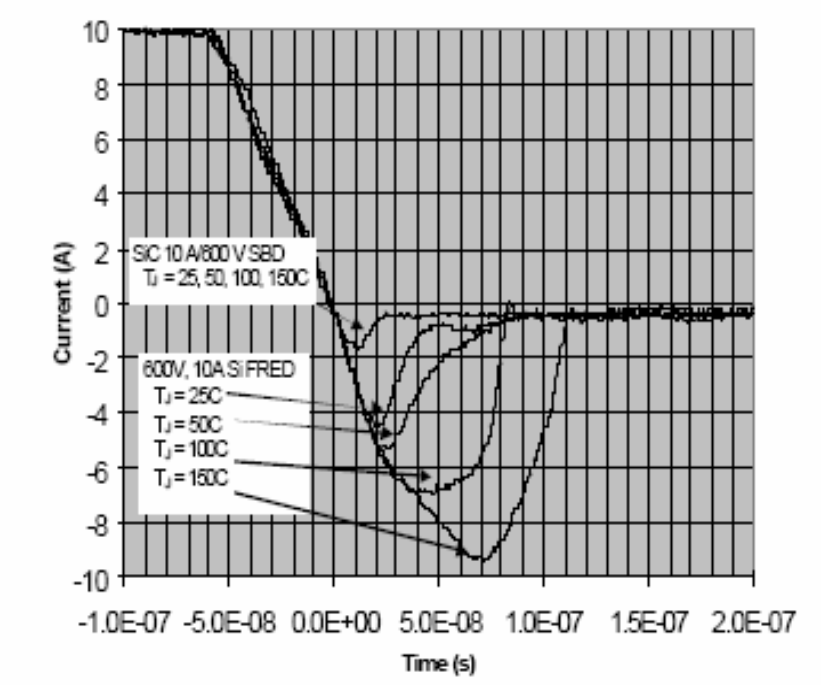

Figure 5.6. Turn-off switching waveform of the 10 A / 600 V SiC SBD in comparison to Si FRED (IXYS DSEI 12-06A).

In this chapter, sintering die-attach technique was demonstrated as an alternative high-temperature packaging technique by packing single chip packaging SiC SDB. The bare SiC SBD was obtained from Cree with die size 2 mm * 2mm (600 V breakdown voltage, 20A current rating by common temperature application). The obtained die was characterized by a high-temperature probe station. The single chip packaging has four steps and Figure 5.7 schematically shows these steps: Ag or Cu thin film deposition, nanoscale silver paste printing, sintering die-attach and Au-wire bonding. For the film deposition, a thin gold or silver film was electron plated on the DBC substrate. If the surface of DBC is copper, a thin Ni was electron-less plated to increase the adhesion between silver and copper. After that, nanoscale silver paste was stencil-printed on DBC substrate with the thickness 20 to 80 microns. And the bare dies were attached onto the DBC substrate with noble metal coating. The sintering profile shown in xx as applied to

bond dies and substrate. Finally, wire-bonding is applied to connect the top side of the devices with the thin gold wire with an one micron diameter. The hand high current, eight gold wires are paralleled to interconnect the top side the die and the substrate.

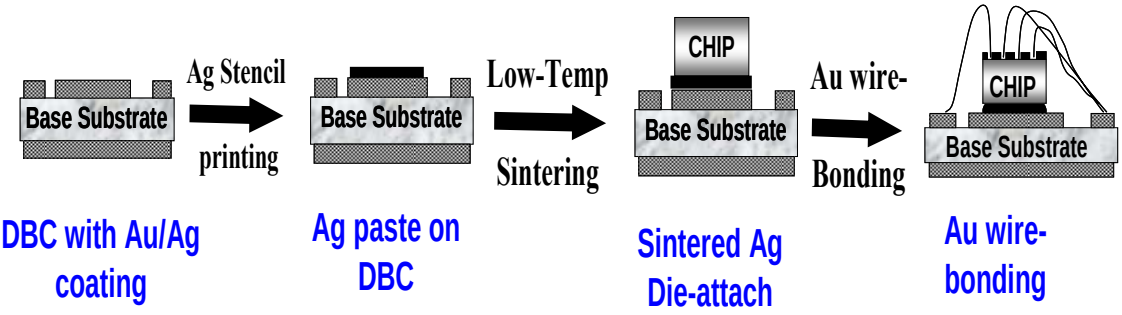

Figure 5.7. Chip scale packaging processing of SiC die for high-temperature application.

To measure the high power characteristics of the packaged die at variable temperature, a setup was built to power the devices at elevated temperature. The schematic of the experimental setup is shown in Figure 5.8. The high temperature device or module was put into a heating chamber in order to test the temperature in a thermal equilibrium environment. The device or module was measured with only one voltage pulse of 300 ms to avoid too much power input because any large amount of power input would change the thermal equilibrium environment.

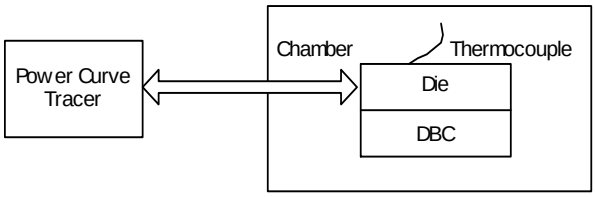

Figure 5.8. Setup to measure high-temperature characterization of devices.

5.3 Results and discussion

5.3.1. Reducing organics ratio for sintering die-attach

Figure 5.9 shows the printed nanoscale silver paste with 22 w% organics before and after sintering. Figure 5.9 (a) is the silver film with glass coverage; and Figure 5.9 (b) is the film without glass coverage. Both of the films were sintered at 300^{o}C within one hour, and the sintering profile was shown in Figure 4.1. The paste in the open area turns to silver color with only a few minutes at 300^{o}C, which indicates the silver particles have already been sintered. With the coverage of glass, the paste still presents a brown color at 300^{o}C within an hour, which indicates the silver particles still do not be sintered. This observation is an evidence that the 22 w % of organics in the paste can not be sufficiently burn-out. With the coverage of glass, the organics in the die-attach film can not burn-out from the top side, the only way the burn-out gas can evaporate is from the side way. The limited burn-out space challenges the silver paste sintering in the sandwiched die-attach. Increasing sintering time can eventually burn-out the organics and sinter the silver particles, but the long processing time is not practice for die-attach application.

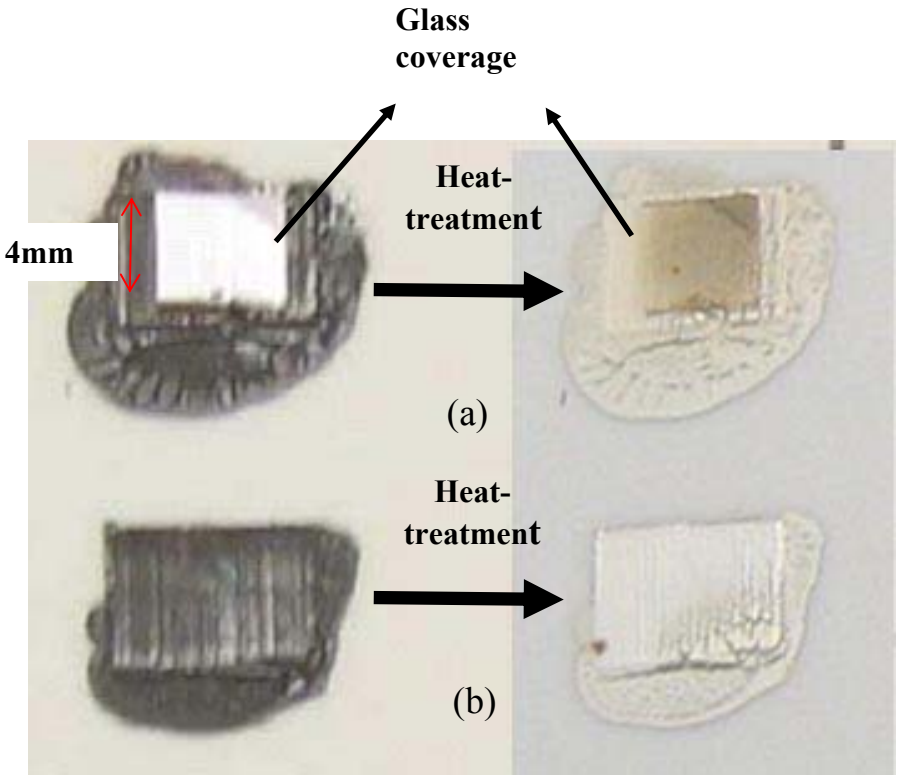

Figure 5.9. Nanoscale silver film with organics ratio 22 w% before and after sintering: (a) film with glass coverage, (b) film open to air.

Reducing the organics ratio in the paste is the simple way to assist the paste sintering during the sandwiched die-attach structure. The pastes with organics ratio listed in Table 5.2 have been prepared. The prepared silver pastes were printed to form the film with area 6 mm * 9 mm. The prinerbility testing shows that paste with 16 w% organics has the lowest organic ratio and still can be printable to form the silver film. Further reducing the organics ratio has the difficult to obtain good film for die-attach applications. The printed silver films with only 16 w% organics were printed on the Al_2O_3 substrate to form two films: one with glass coverage and another is not. These films are sintered using the sintering profile Figure 4.1. Figure 5.10 shows the sintered silver film with 16 w% organics: Figure 5.8 (a) is the film with glass coverage; and Figure 5.10 (b) is the film without glass coverage. Without coverage, the silver paste with 16 w% organics, similar with paste having 22 w% organics, can also be sintered at

300^{o}C within only a few minutes. Unlike the film with 22 w% organics ratio shown in Figure 5.9 (a), the silver film with 16 w% of organics can be sintered within one hour shown in Figure 5.10 (a). The SEM observation of these sintered silver films with coverage is shown in Figure 5.11. Figure 5.11 (a) is the film with higher organics ratio (22 w%), and Figure 5.11 (b) is the film with lower organics ratio (16 w%). The SEM observation clearly shows that the particles in the silver film with higher organics ratio are still not sintered due to the existing organics. With the comparison, the silver particles with lower organics ratio have already formed the dense microstructure. This observation indicates that reducing organics ratio from 22 w% to 16 w% can significantly enhance the sinterability of silver paste in the sandwiched structure and can control the die-attach processing within an hour.

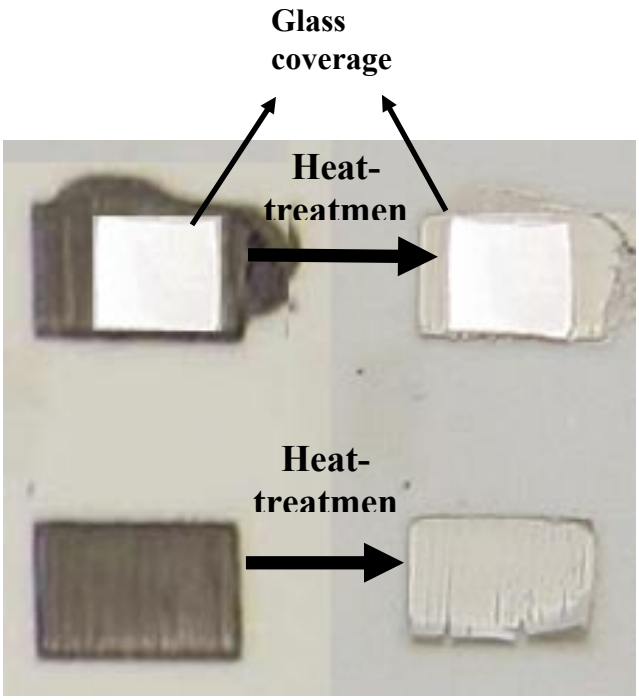

Figure 5.10. Nanoscale silver film with organics ratio 16 w% before and after sintering: (a) film with glass coverage, (b) film open to air.

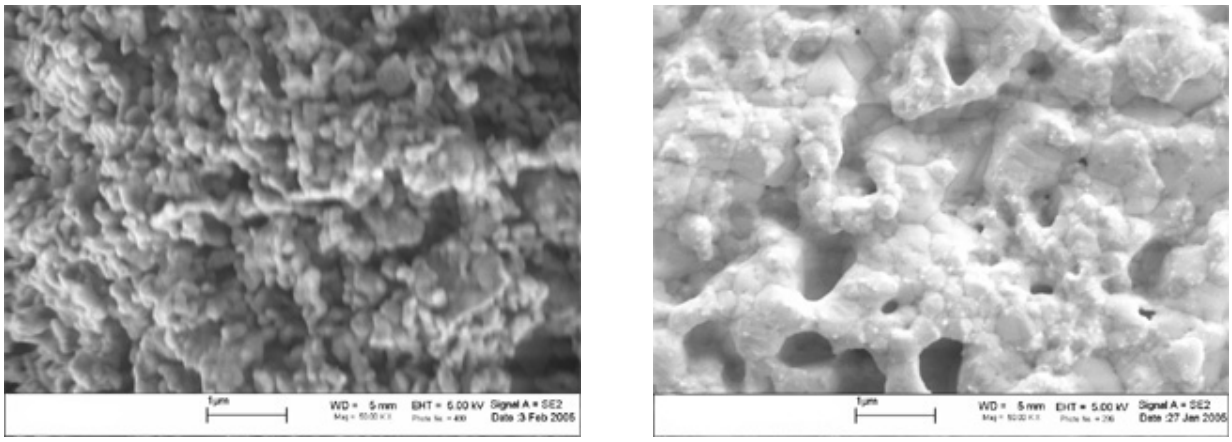

(a) (b)

Figure 5.11. SEM observation of sintered nanoscale silver film with glass coverage. (a) with high organics ratio (22 w%) and (b) with low organics ratio (16 w%).

With only six weight percent of organics reduction (from 22 w% to 16 w%), the sinterability of the silver film in the sandwiched structure is significantly improved. This is because the density of silver is much higher than the density of organics. Figure 5.12 shows the density of components in the nanoscale silver paste. The density difference makes the binder occupy 32 volume percent in the paste with 22 w% organics and is the largest part during all the components (shown in). However, in the paste with 16 w% organics, volume of binder drops to only 22 volume percent. The large volume percent of binder volume percentage drop makes the paste with 16 w% organics much easier to be sintered at sandwiched structure than the one with 22 w% organics.

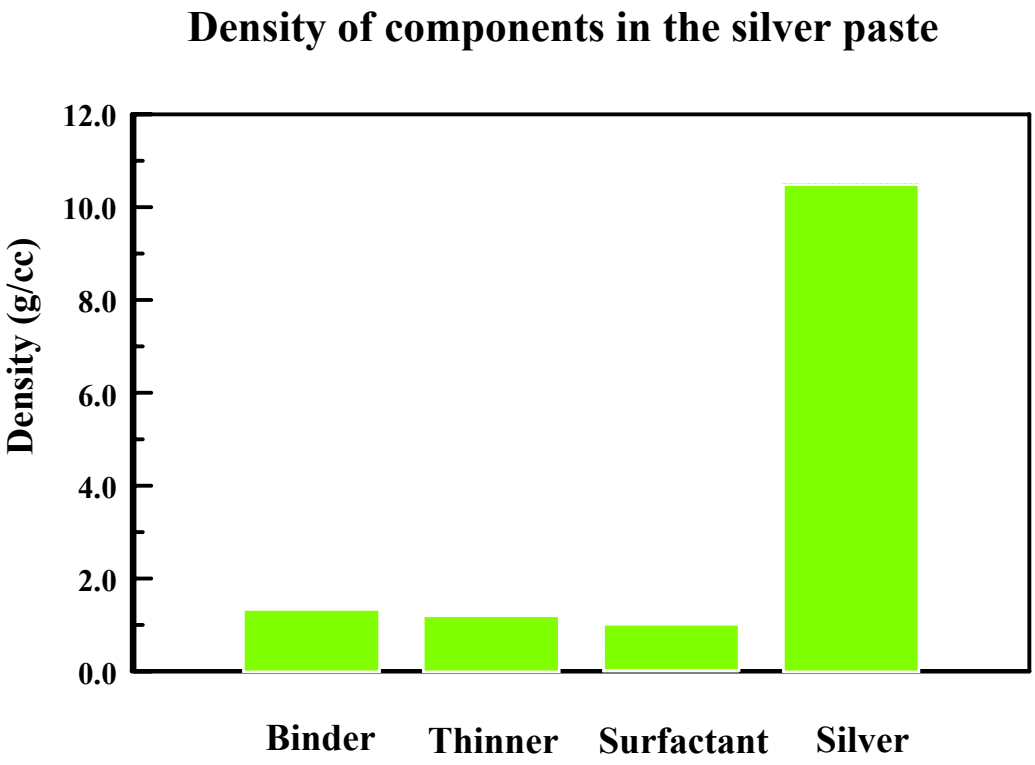

Figure 5.12 Density of components in the nanoscale silver paste.

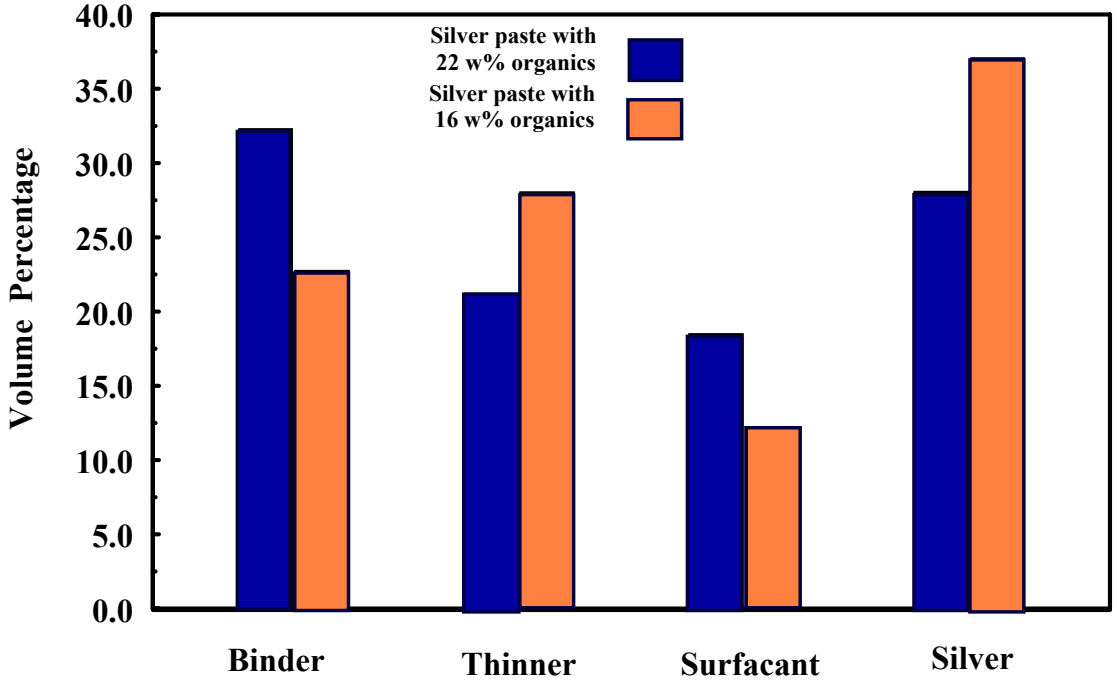

Figure 5.13. Voltage percentage of components for two different nanoscale silver paste.

5.3.2. Die-size and heating rate effect on the sintering die-attach

The relative position of the semiconductor device during sintering die-attach was measured using optical system shown in Figure 5.5. The paste contains 16 w% organics and heating rate is 20^{o}C / min. Two different type of dies with die-size 2 mm * 2 mm and 4 mm * 4 mm are chosen respectively. Figure 5.14 shows the relative die position of the die with size 4 mm * 4mm. The initial die position corresponds to a -4V voltage signal shown the y-axis of Figure 5.14. After heat treatment, the organics in the silver die-attach layer turns out gas and Figure 5.15 shows the shrinkage profile of silver paste under coverage of die with size 2 mm * 2 mm. With larger die (4mm * 4 mm) coverage,

the silver film has the difficulty to burn-out organics from the side-way. The fast heating rate (20°C / min) causes the large burn-out pressure and pushes the die up to release the burn-out gas. The dynamical change of die position shown in Figure 5.14 reduces the contact area between die and silver film and results in the poor die-attach bonding. For the smaller die (2mm * 2mm), the burn-out path for unit organics is larger, and the organics can burn-out from the side-way. Figure 5.15 shows that the die position has no dynamical change during the organic burn-out. After the organics burn-out, the die position becomes down due to densification of silver particles and the shrinkage of die-attach film.

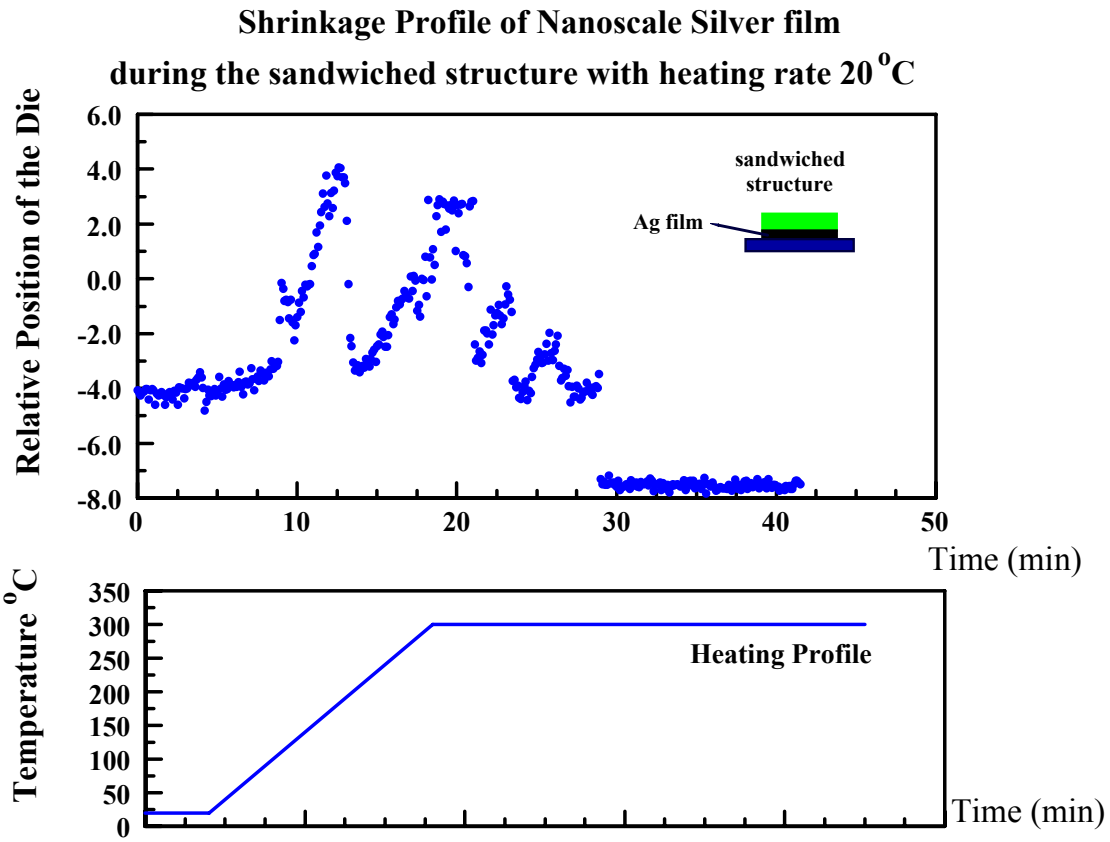

Figure 5.14. Shrinkage profile of silver film with 20°C heating rate and 4 mm * 4 mm die coverage.

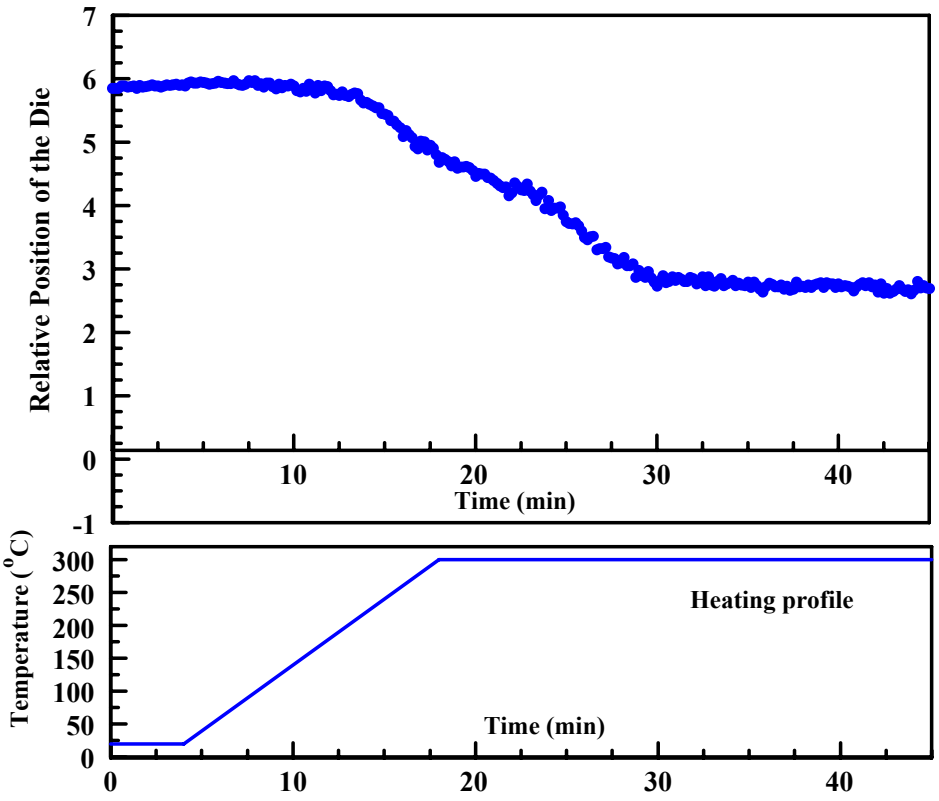

Figure 5.15. Shrinkage profile of silver film with 20°C heating rate and 4 mm * 4 mm die coverage.

Figure 5.16 and Figure 5.17 shows the shrinkage profile (die-position) of silver paste under coverage of die with size 4 mm * 4mm using heating rate 10°C / min and 5°C / min respectively. By reducing the heating rate, the organics burn-out pressure becomes low and the dynamic change of die position can be significantly reduced. For the die with die-size 2 mm * 2 mm, 20°C / min heating rate can be used and the whole processing time can be easily controlled within one hour (heating up for 14 minutes and dwelling for 30 minutes). However, for the larger die with size 4 mm * 4mm, the heating up time can be as long as 60 minutes (5 °C / min heating rate applied) and the processing time can be significantly longer.

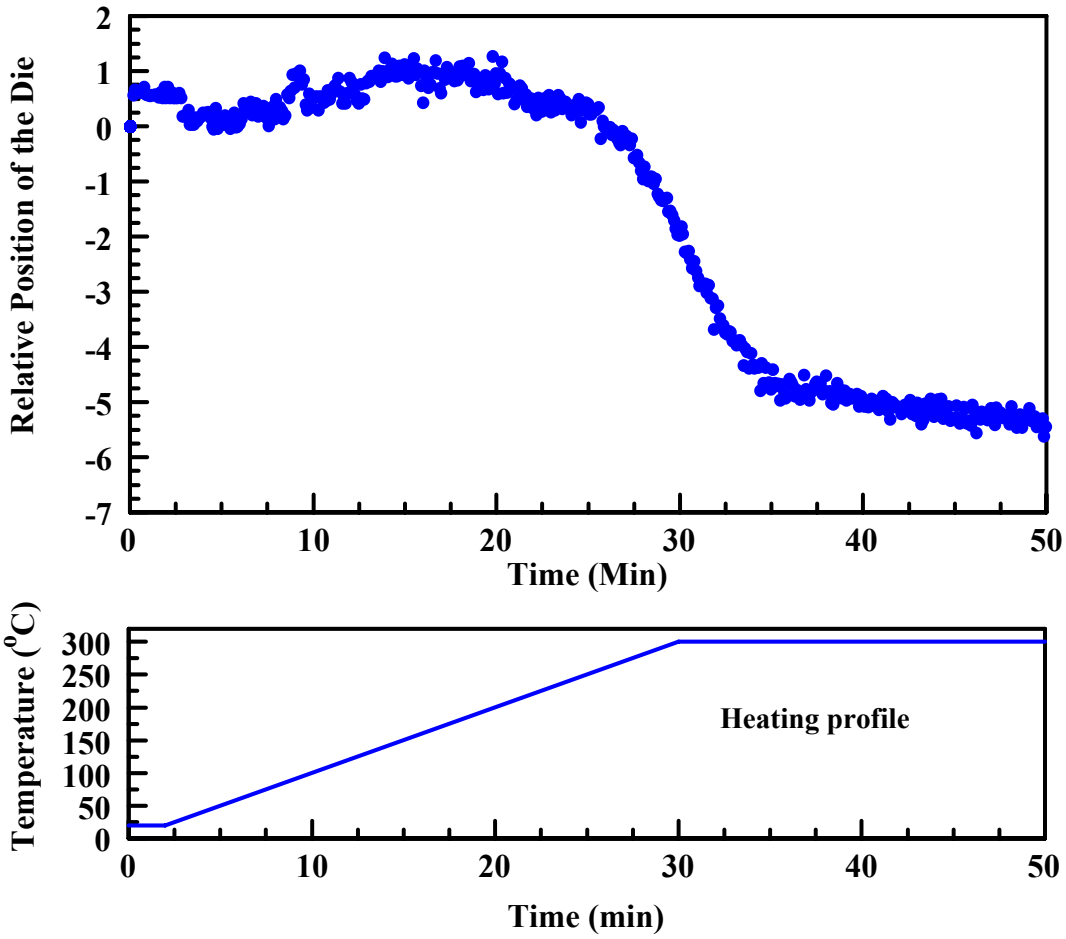

Figure 5.16 Shrinkage profile of silver film with 10°C heating rate and 4 mm * 4 mm die coverage.

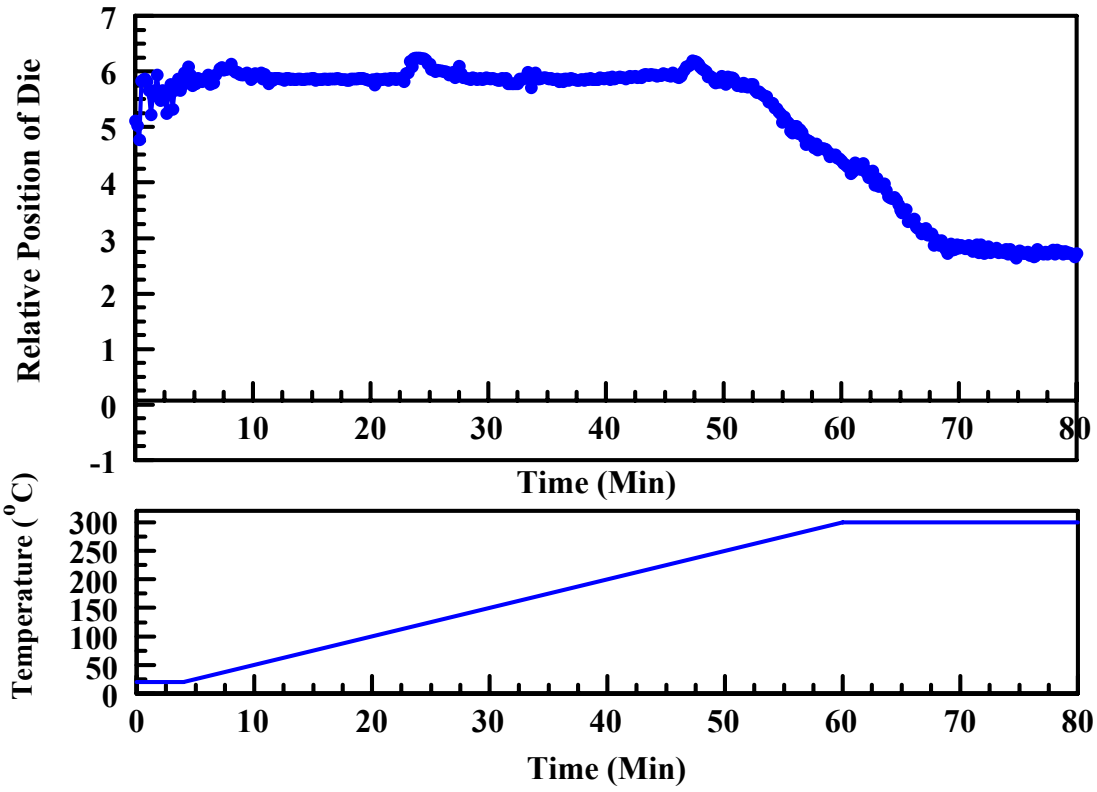

Figure 5.17 Shrinkage profile of silver film with 5°C heating rate and 4 mm * 4 mm die coverage.

The bare SiC schottky diodes (size 2 mm * 2mm) obtained from Cree were characterized and the forward and reverse characteristics were shown in Figure 5.18 (a) and (b) respectively. These bare diodes were attached by nanoscale silver paste sintering technique and the top sides were connected by gold wire-bonding. According to the previous shrinkage profile study, the fast heating rate such as 20°C / min can be applied to sintering attaching these SiC diodes with die-size 2 mm * 2mm. To ensure reliable die-attach joints, the 30 minutes sintering dwelling time was applied and the whole sintering profile was controlled within one hour. Gold wire with 1 micron diameter was applied to interconnect the attached die and DBC substrate. Eight gold wires are

paralleled to enhance the current capability. The forward and reverse characteristics of the packaged SiC SDB were measured and shown in Figure 5.19 (a) and (b) respectively. These measured results show that the sintering attachment can enable the packaged SiC SDB diode work at high-temperature (> 250^{o}C), while solders can barely function at such a high-temperature. Another interesting thing is that the SiC SDB diodes have the positive temperature coefficient when the forward current is over one Amps, however, the Si diodes usually have the negative temperature coefficient. With a positive temperature coefficient, several SDBs can be easily paralleled together to handle larger current because the current can equally distribute automatically with feedback mechanism.

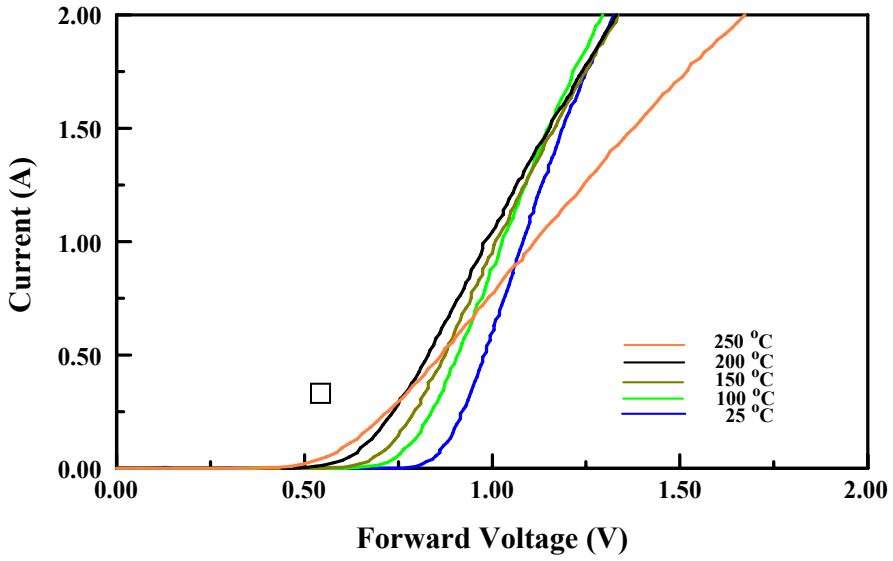

(a)

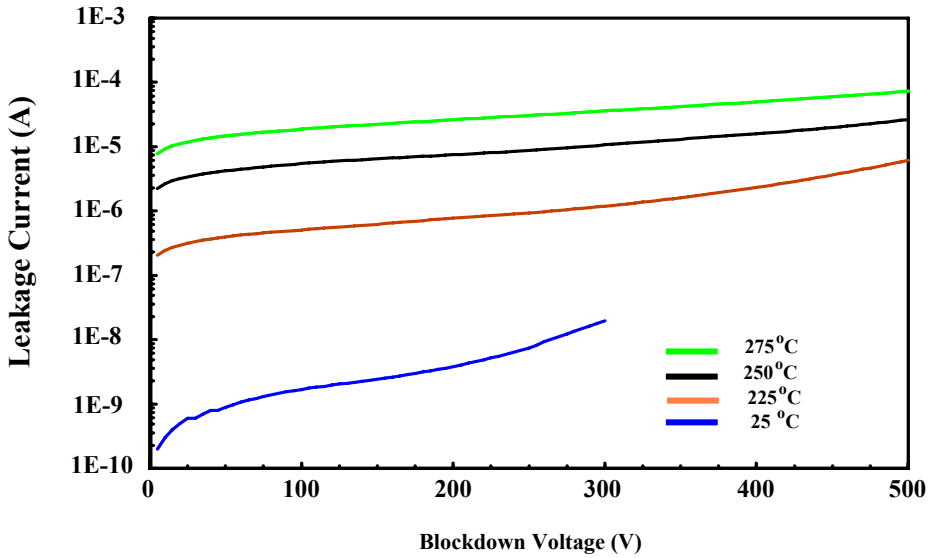

(b)

Figure 5.18. Bare SiC SBD (a) forward and (b) reverse characteristics.

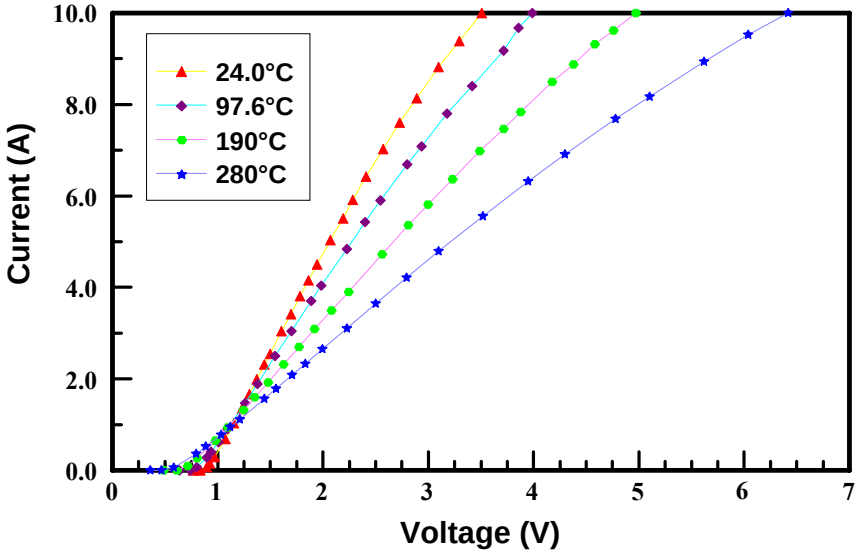

(a)

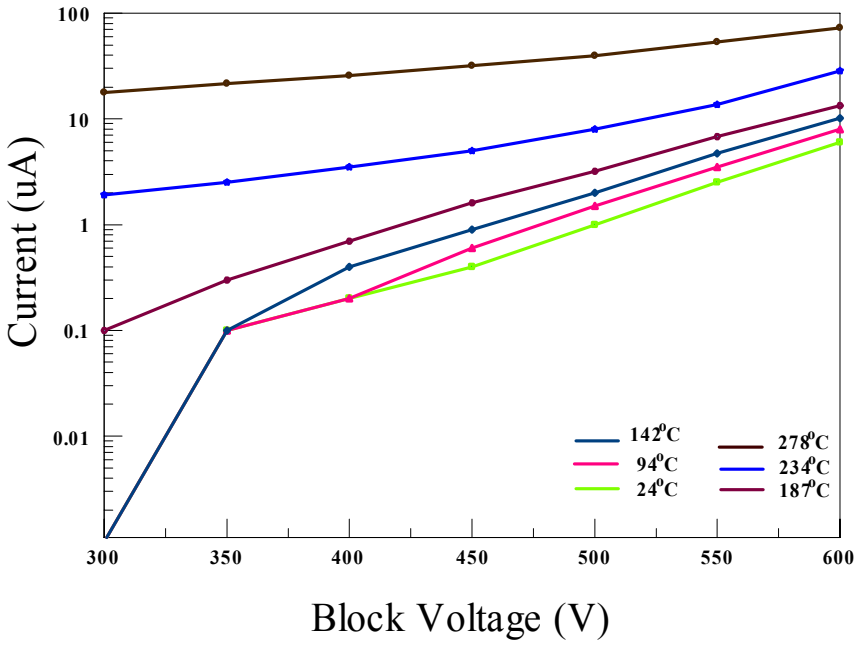

(b)

Figure 5.19. Packaged SiC SBD (a) forward and (b) reverse characteristics.

Figure 5.20 shows some other die-attach samples such as attaching SiC PiN diode on gold coated substrate, die-size 2 mm * 2 mm (a), SiC SBD on silver coated substrate, die-size 1.25 mm * 1.25 mm (b).

(a) (b)

Figure 5.20. The sintered attached SiC die. (a) SiC PiN diode on gold coated substrate, die-size 2 mm * 2 mm, (b) SiC SBD on silver coated substrate, die-size 1.25 mm * 1.25 mm.

5.4 Conclusion

The high-temperature power modules can work at harsh environments with significantly improved power density by eliminating the bulky cooling systems. These modules can find numerical advanced applications such as in air-space power conversion, military electrical-magnetic guns, deep-core drilling, etc. Development of high-temperature power modules depends on not only advanced power devices, but also high-temperature packaging techniques. Current solder interconnection technique hardly meets the high-temperature packaging requirement due to low-melting temperature and bad performance of solders.

In this chapter, a sintering joint technique – low-temperature sintering nanoscale silver paste - was developed as a viable die-attach technique to attach SiC devices for high-temperature application. The organics in the silver paste is difficult to burn-out because of the limited burn-out space in the sandwiched die-attach structure. Organics ratio in the paste was reduced to accelerate the die-attach processing. The effects of die-size and heating profile were also investigated by monitoring the relative die-position during the heating-treatment. The chip scale packaging of SiC device is achieved by attaching the SiC device onto the DBC substrate and wire-bonding on the top side. The characteristics of packaged device such as forward characteristic and block-down characteristic are measured at high-temperature. The measured results show that the sintering nanoscale silver paste is a promising technique for high-temperature application.

Chapter 6 Summary and future work

6.1 Summary and conclusion

Attachment of power semiconductor devices is one of the critical processes in the power device and/or module packaging since it is the limiting factor for thermal management, power density, reliability and cost of power systems. The existing die-attach materials / technologies such as conductive adhesives and reflowed solders can not meet the future of power electronics requirements, especially at high-temperature due to their inherit limitations. Advanced die-attach technology for semiconductor power devices is highly demanded.

In this dissertation, low-temperature sintering silver paste technique is developed as viable die-attach solution to replace current solder reflow die-attach practice. Silver, instead of solder alloy, is selected as die-attach material because it has high thermal and electrical conductivity, good mechanical properties and high melting point, which enables silver joints having excellent performance and reliability even at high temperature. Sintered silver has widely been used in microelectronic packaging and the high performance has been demonstrated. The high melting temperature (961^{o}C), however, challenges its application to interconnect semiconductor devices, since the reflow approach can not be used due to the simple fact that no device can withstand such high processing (reflow) temperature. Sintering supplies an opportunity for silver die-attach because sintering can be formed at a temperature lower than the melting point of materials. Lowering sintering temperature is the key thing to develop silver die-attach technique. Micron-size silver paste commercially available can only be sintered a temperature higher than 750^{o}C to gain a desire properties for die-attach if without external pressure assistance. Sintering is a mass diffusion process, and thus the densification rate not only depends on the mobility which is thermally activated (higher the temperature, higher the mobility), but also depends on the driving force. The solid-state sintering theory indicates that the application of external pressure and reducing

particles of silver can increase the sintering driving force and thus lower the sintering temperature.

Author developed two silver die-attach techniques by low-temperature sintering micron-size silver paste with external pressure and nanoscale silver paste respectively in this dissertation. The processing parameters such as pressure, temperature and time of pressure-assisted sintering die-attach was investigated, the measured properties and reliability show a significant improvement with the comparison of solder joints. To develop nanoscale silver paste sintering, the paste sintering mechanisms are studied. The sintering difficulties for nanoscale materials are evaluated and numerous approaches are developed to address these difficulties. The sintering nanoscale silver paste was finally applied to attach SiC diodes and enable their high-temperature applications. The measured results show that sintering nanoscale silver paste as viable die-attach solders, especially at high-temperature.

The conclusion and significance of this work are summarized in the following three sections.

6.1.1. Pressure-assisted low-temperature sintering die-attach

Pressure-assisted low-temperature sintering micron-size silver paste was developed as an alternative to die-attach approach. Semiconductor materials such as silicon and silicon carbide are brittle materials just like some ceramics. Local stress concentration can easily destroy these devices. A fix with silicone gel filled was designed to transfer the mechanical force and avoid the stress concentration. The processing parameters such as temperature, pressure and time, were evaluated. It was found that the application of pressure can significantly lower the sintering temperature and obtain the desire properties for die attach. It was also found that the pressure-assisted die-attach process is a relative fast processing, with only a few minutes, the sintering joints can be formed. The measured properties show that the sintering joints are superior to the solder interconnection. Not like solder reflow having solid/liquid phase transition and trapped flux to resist oxidization, sintering silver joints are formed by atomic diffusion with only solid phase existing during the die-attach processing. Large voids, which usually exist in the solder die-attach, can be avoided in silver sintering die-attach. The chip swimming

problems can also be overcome and thus the die placement accuracy can be improved. There are about twenty percent of small voids with sub-micron size existing in the sintered die-attach silver layer. These voids cushion the thermomechanical stress generated by mismatch of coefficient of thermal expansion (CTE) between substrates and semiconductor devices. The thermal cycling test also shows the improved reliability of sintered silver layer than that of the solder joints. The characteristic of pressure-assisted sintering die-attach are summary in xx with the comparison of reflowed solders.

Table 6.1.The comparison of pressure-assisted sintering die-attach and solder reflow.

	PLS silver Die-attach	Reflow solder Die-attach (Sn63Pb37)
Processing temperature	240^{o}C	210^{o}C
External pressure	40MPa	N/A
Working temperature	>350^{o}C	<183^{o}C
Electrical conductivity (10^5 W^{-1} cm^{-1})	2.4E-6	1.4E-5
Thermal conductivity (W/cm K)	80	43
Mechanical property (MPa)	50	20 to 40
Attach layer uniformity	Uniform	Existing large voids
Toxic	No	Yes
Chip-swimming	No	Yes

PLS: Pressure-assisted low-temperature silver sintering

The application of large external pressure makes this technique difficult for auto manufacture implementation and also has a potential to damage the semiconductor devices.

6.1.2. Low temperature sintering nanoscale silver paste

Besides large external pressure, reducing silver particles is another alternative to increasing the sintering driving force. The nanoscale silver has larger excess surface energy and theoretically can be densified at low temperature. However, the fact that sintering is a solid mass transport process and the densification is accomplished by atomic diffusion may result in several low-temperature sintering problems for nanoscale materials such as agglomeration, aggregation and non-densification diffusion. The agglomeration and aggregation mean that the tiny particles gather together to form bigger clusters. The existing clusters have equivalent radius which may be significantly larger than the particle size of nanoscale particles and ruin the low-temperature sinterability of nanoscale materials. Unfortunately, the agglomeration and aggregation are particularly easy to occur in the nanoscale materials during their preparation, shipping and storage due to the nature of nanoscale – tiny particle size and large excess surface energy. The difference between agglomeration and aggregation is that the agglomeration is bonded by a weak force and the bonding can be redispersed by applied external energy. The aggregation is bonded by strong force and the bonding can not be redispersed. Storage of nanoscale silver powder in the organic solvent such as with a little surfactant is an efficient way to prevent aggregation of silver particles. The additional solvent dose not increase the difficulty for paste preparation since the solvent is required to add in the following paste preparation. Ultrasonic vibration, instead of ball-milling, was developed to de-bond the agglomeration and redisperse the nanoscale silver particles. Ultrasonic vibration can homogenously displace energy to the individual particles and thus the agglomeration existing in the nanoscale silver powders can be efficiently redispersed. Densification of nanoscale particles is also determined by how atoms diffuse. Only several atomic diffusion mechanisms such as grain boundary diffusion and lattice

diffusion can result in densification, and others only consume the sintering driving force and not contribute to the densification. But, the non-densification mechanisms dominate the relatively low-temperature zone, consuming the sintering driving force and resulting in the densification diffusion such as grain boundary diffusion difficult to occur at a relatively high-temperature. Controlling organics burn-out temperature is applied to overcome this non-densification issue. With the existing organics in the silver paste, the mass diffusion such as surface diffusion was prevented at a relative low temperature. After organics burn-out, temperature has reached a relatively high-temperature zone where densification mechanisms have already dominated, and a rapid densification can occur.

A nanoscale silver paste can be successfully prepared by applying these approaches to overcome sintering difficulty. The sintered silver showed significantly better electrical and thermal properties than those of solders and the mechanical property is compatible with that of solder.

These sintering difficulties not only exist in silver particles, but also other metal particles. The sintering mechanism study of nanoscale silver paste gives a better understanding of sintering nanoscale noble metal powders and offers an opportunity to develop other metal sintering techniques.

6.1.3. Sintering nanoscale silver paste to attach SiC devices for high-temperature application

Silver has the high melting point and high-temperature stability, making the sintered silver die-attach particular suitable for high-temperature application. The sintering nanoscale silver paste was developed to attach silicon carbide diode and enable the high-temperature application. One sintering challenge existing in the die-attach processing is that the organics under the die coverage can not be efficiently burn-out due to the limited burn-out space. Organics ratio in the paste was adjusted to lessen this problem. A fast heating rate with a large die also presents a problem for sintering die-attach, because the accumulated burn-out gas can push the die up to release the pressure. The contact area between semiconductor device and the silver film will be reduced and the die-bonding will be weak. The effect of die size and heating rate on sintering die-attach was

investigated by measuring the relative die position. The single chip SiC diode packaging was fabricated by silver sintering die-attach and gold wire-bonding and the measured characteristics show that the sintering die-attach is a viable packaging technique for high-temperature application.

6.2 Future work

The sintering silver interconnection technique presents superior characteristics over solder joints such as better electrical, thermal and mechanical properties. The sintered silver is also environmentally friendly and stable at high-temperature. Without liquid / solid phase transition, the chip swimming problems can also be avoided and the accuracy of die placement can be improved. This technique has broader applications and does obviously not limit to attach power semiconductor devices. This technique offers an opportunity to manufacture high performance, more reliable electronics suitable for new applications.

Interconnection of solders, especially lead-tin eutectic solder has been widely used in electronic industry for several decades, their performance and reliability (failure mechanisms) have already be extensively studied. The silver sintering interconnection technique also needs to be carefully studied and the impact of this application needs to be evaluated.

6.2.1. Large die interconnection

It was found in the previous chapter that the sintering technique still makes it difficult to attach large semiconductor devices due to the limited organics burn-out path. The nanoscale silver paste in a large area interconnection that can hardly burn-out the organics and the existing organics prevent silver particles diffusion together and result in poor bonding. One solution is to pattern the silver paste into smaller film arrays; and the gaps or grooves between the arrays are left to evaporate organic gas. Figure 6.1 schematically shows the arrayed films for large-die attachment; during the die-attach process, the organics in the individual silver film array can be burn-out through these

grooves. How to array these smaller silver films needs to be studied carefully by considering thermal, mechanical and reliability issues. Actually, the grooves may offer a potential opportunity for better reliability of die-attach. The biggest challenge for large die attachment is the stress concentration generated by the difference of coefficient of thermal expansion (CTE) between substrate and the die during the cycling load. The larger the die, the more stress concentrated. Instead of bonding the whole device with large area onto the substrate, the arrayed die-attach leaves grooves. These grooves may release the stress concentration and avoid die cracking. These grooves may also offer a better thermal management because the forced air and even liquid can directly flow into these grooves, circulate and suck more heat out from the devices. All these benefits can not be gained by clearly understanding the failure mechanism and thermal conduction mechanism and thus both finite element modeling (FEM) and experiments need to conduct.

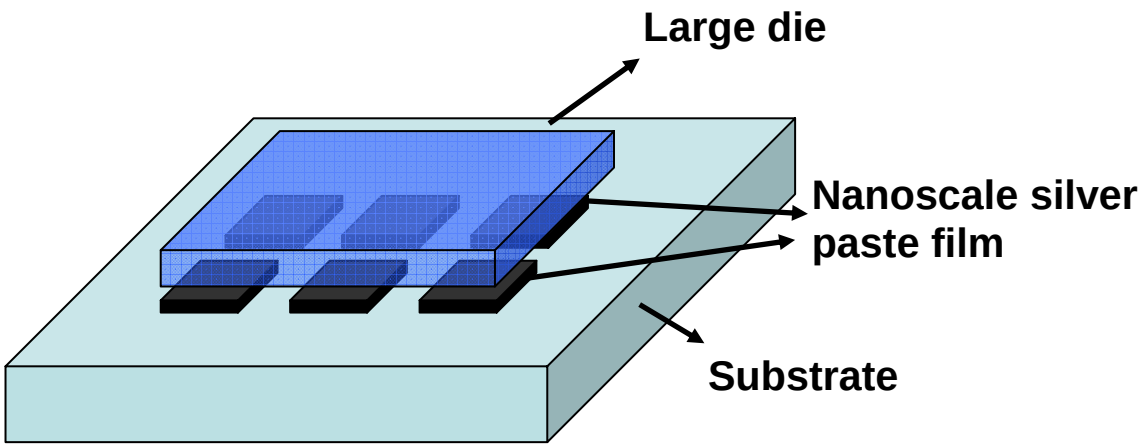

Figure 6.1. A schematic of silver film array to attach large size device.

6.2.2. Silver migration

Silver migration is an infamous problem and needs to be investigated for any silver applications. There are two silver migration mechanisms occurring: ionicmigration (IM) and electromigration (EM). Ionicmigration prefers to in the moisture environment, where Ag is ionized by water [70]:

$$Ag \rightarrow Ag+, \quad H_2O \rightarrow H+ + OH-$$

Ag+ and OH- deposit as generating AgOH on the side of an anode. Ag_2O decomposed from AgOH is dispersed for colloid on the side of anode.

$$2AgOH = Ag2O + H_2O$$

after this, by a hydrate reaction,

$$Ag_2O + H_2O = 2AgOH = 2Ag+ + 2OH-$$

As the reaction is advanced, silver ion moves on the side of a cathode and a deposit of dendrite formed of silver is advanced. Bolger et al. [71] identified three conditions for silver ionicmigration: presence of silver in the system, existing DC bias with the existing silver constituting the anode and a medium for transport for ions (in the most practice situations, humid conditions suffice).

Electromigration refers the migration of atoms in a metal interconnect line due to momentum transfer from conduction electrons. The metal atoms migrate in the direction of current flow and can lead to failure of the metal Line. Electromigration may be due to diffusion in the bulk of the material, the grain boundaries or on the surface. Silver electromigration is primarily grain boundary due to the higher grain boundary diffusivity.

Silver migration places a more serious problem when develop sintering silver technique for top size interconnection due to the narrower pitch and higher current rate. Adding noble metal with high-melting temperature such as gold and platinum can significantly reduce the migration of silver. But the additional metal may detrimentally affect the sinterability of nanoscale silver and the performance of sintered silver. Carefully passivating and encapsulating silver may also reduce the risk of silver migration. Further studies need to be carried out in order to investigate how serious the migration problem, especially in high-temperature and high power density applications.

6.2.3. Future applications for sintering silver interconnection technique

Several flip-chip packaging techniques based on solder paste interconnection have already been developed by collegians in center of power electronics systems (CPES). The sintering silver interconnection technique can use the similar concept and implement a complete interconnection solution for high-temperature solution. Figure 6.2 (a) shows the dimple array structure [72] and Figure 6.2 (b) is the triple stacked high standoff structure [73]. Both structures use hourglass shape instead of barrel shape of solder joints to increase the reliability of interconnection. By simply replacing solder paste and solder ball into silver paste and silver ball, these structures can easily realized. Both structures also use flexible substrate (flex) as interconnection layer. The flex substrate is a double-sided, copper-clad laminate, which is an adhesiveless composite of polyimide film bonded to copper foil. This copper-clad is commercially available. The flexible substrate can absorb the mismatched thermomechanical stress and improve the reliability of the whole structure. The flex substrate, however, presents a challenge for high-temperature application. The polyimide film existing in the flexible substrate can not withstand high-temperature. Although industry has already pushed very hard to improve the temperature stability, and several flex substrates have already been commercially available such as Kaptona-E (a registered trademark of the E.I. DuPont de Nemours & Co.), Upilexb-S/SGA (a registered trademark of Ube Industries, Ltd.), Apicalc-HP (a registered trademark of Kaneka Corporation). But none of them can stably function at a temperature higher than 200^{o}C [74]. The bonded copper foil also can resist high-temperature and be easily oxidized. A high-temperature flexible substrate needs to be developed to adopt these interconnection techniques.

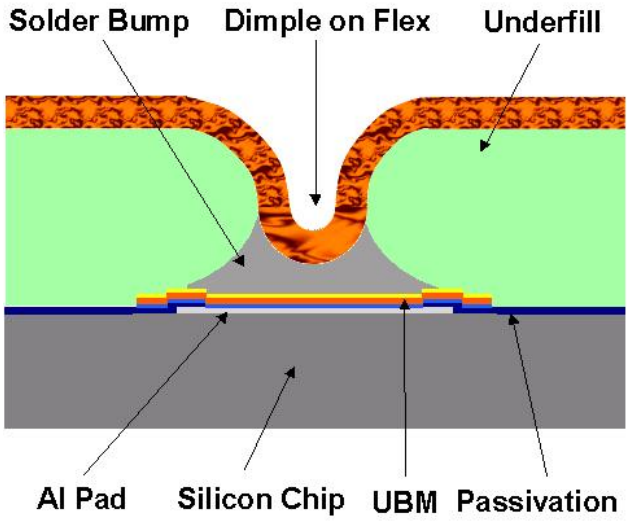

(a)

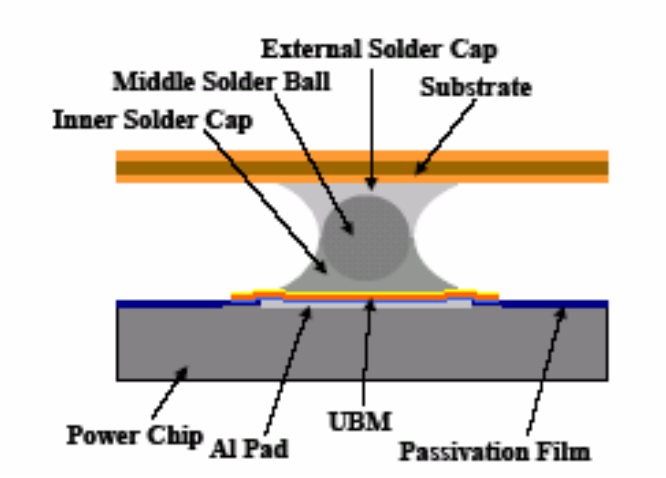

(b)

Figure 6.2. Schematic of flexible substrate flip-chip interconnection: (a) dimple array, (b) flip-chip on flex.

Based on the fact that the coefficient of thermal expansion of silicon carbide (3.2 mmp/^{o}C) is almost the same with aluminum nitride (3.3 mmp/^{o}C), a double rigid-substrate structure is worth looking into. A schematic of this simple structure is shown in Figure 6.3. From the macroscopic point of view, there is almost no thermomechanical stress between substrates and the die since both aluminum nitride substrates and die expand and shrinkage at the almost same rate. But the rigid of aluminum nitride substrates still present a big problem for reliability due to the large coefficient of thermal expansion (CTE) difference between silver interconnection layer and the substrates or silicon carbide die. During the cycling load, the expansion and shrinkage of silver are clamped by two rigid restrictions: silicon carbide die and substrates. The stress caused by these restrictions may fail the interconnection. The failure mechanism of the double rigid-substrate structure may be significantly different from the one side rigid substrate silicon die interconnection and the research needs to investigate the feasibility of this simple interconnection technique.

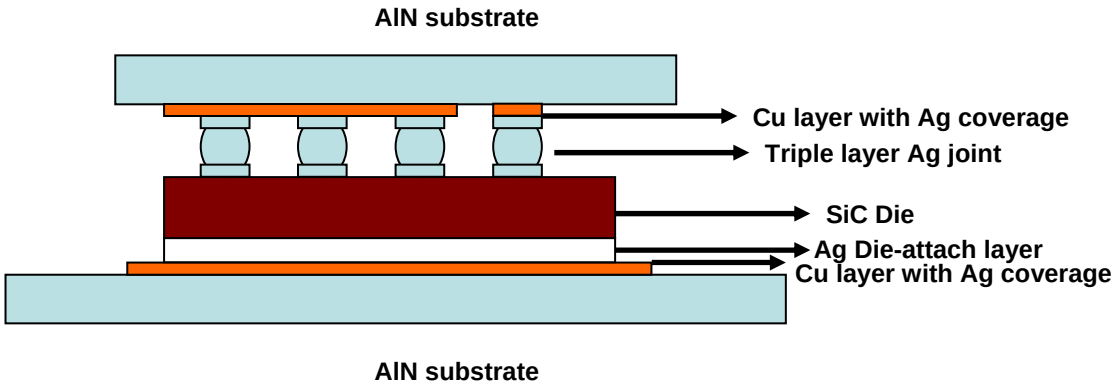

Figure 6.3. A schematic of double rigid-substrate interconnection implemented by silver sintering.

Although photolithograph has better solution, the printing systems such as screen printing, stencil printing and ink-jet printing still found large applications in microelectronics because they are fast, cost efficient and flexible. Thin, flexible, and cheap plastic electronics could have many applications, from solar cells to radio frequency identification labels in product packaging. Printing is an attractive manufacturing option because it deposits materials quickly and cheaply over large areas [75]. One of the key barriers to develop economical-efficient plastic electronics is the low-temperature sinterable (curable) ink. Several companies and research institutes such as Sumitomo Electric Industries [76], Ltd., Xerox Research Centre of Canada [77], Xink Laboratories [78] and University of California, Berkeley, are developing the low-temperature ink system. Due to the low temperature sinterability, the nanoscale silver paste is suitable for this application. Figure 6.4 shows the nanoscale silver paste sintered at only 280^{o}C for ten minutes. By adjust the viscosity, the nanoscale silver paste can be suitable for various printing facilities such as ink-jet printing or screen printing. To optimize the fine-pitch printerability and low-temperature sinterability, future research needs to study the compatibility of organics and nanoscale silver powders

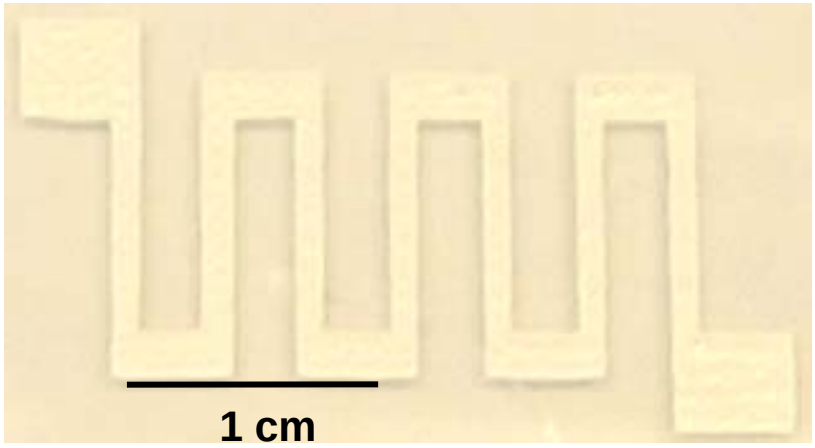

(a)

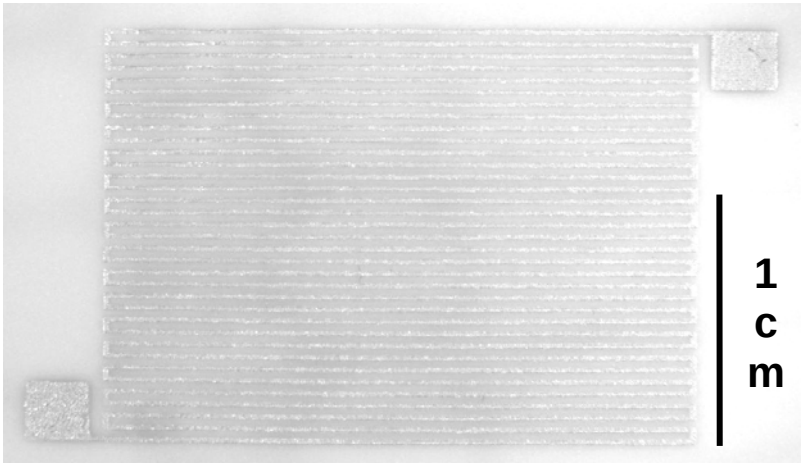

(b)

Figure 6.4. Silver conductive trace sintered on the glass substrate with 280^{o}C: (a) on glass substrate and (b) on the ceramics substrate.

Due to the distinguish properties of sintering silver die-attach such as high thermal conductivity, high-temperature stability and without chip swimming problems, the sintering silver die-attach offers a promising die-attach solution for laser chip or light

emitting diode (LED). These chips usually have a small size (< 2 mm* 2 mm) and very high power density. A 10 w light emitting diode with size 1 mm *1 mm has the power flux 1kw/cm^2, and the power density is about eight times higher than that of current microprocessors, which has the highest power density in the digital chips. Stabilizing the junction temperature of these devices is also critical since the optical spectrum is highly correlated with the junction temperature. Get ridding of the heat from the chips to stabilize the junction temperature is thus the key factor for these optical devices. Sintered silver has high thermal conductivity and high temperature stability, and thus can stably supply an attachment with minimum thermal impedance. These optical chips also need to be precisely placed, especially for communication application. Sintering silver die-attach eliminates the chip-swimming problem and the accuracy can be greatly improved.

Appendix : Nanoscale noble metal films preparation using layer by layer self-assembly technique

Printing nanoscale noble paste can build the film with the thickness of tens of micron. This technique, however, is difficult to build film with nanoscale range. The self-assembly technique can prepare film within nanoscale without fashion equipment. This process was first introduced by Iler et al. [79] about forty years ago. Decher has demonstrated the layer-by-layer electrostatic self-assembly of cationic and anionic polyelectrolytes as well as multilayer structures consisting of combinations of charged colloidal particles, including biomacromolecules such as DNA [80]. Many groups have now used electrostatically driven layer-by-layer assembly to realize assemblies containing proteins/polyeletrolytes [81] and inorganic nanoparticles such as magnetite[82], SiO2, TiO2, and CeO2 [83]. This appendix will apply the self-assembly technique to prepare noble metal films such as gold and silver.

The self-assembly technique utilizes the electrostatic attraction and complex formation between anions and cations to form supramolecular assemblies of polyelectrolytes and colloids. Figure A 1 schematically shows the layer by layer self-assembly procedure. The substrate was firstly dip into the metal colloid solution with positive charge (Figure A 1 (a)). The immersion time can be as short as tens of seconds to a few minutes. After that, the substrate is removed, rinsed, and dipped in an aqueous solution of an oppositely charged ion solution at room temperature (Figure A 1 (b)). The surface film is grown monolayer by monolayer, by repeating the dipping cycle as many times as needed, until the desired number of layers has been produced (Figure A 1 (b)).

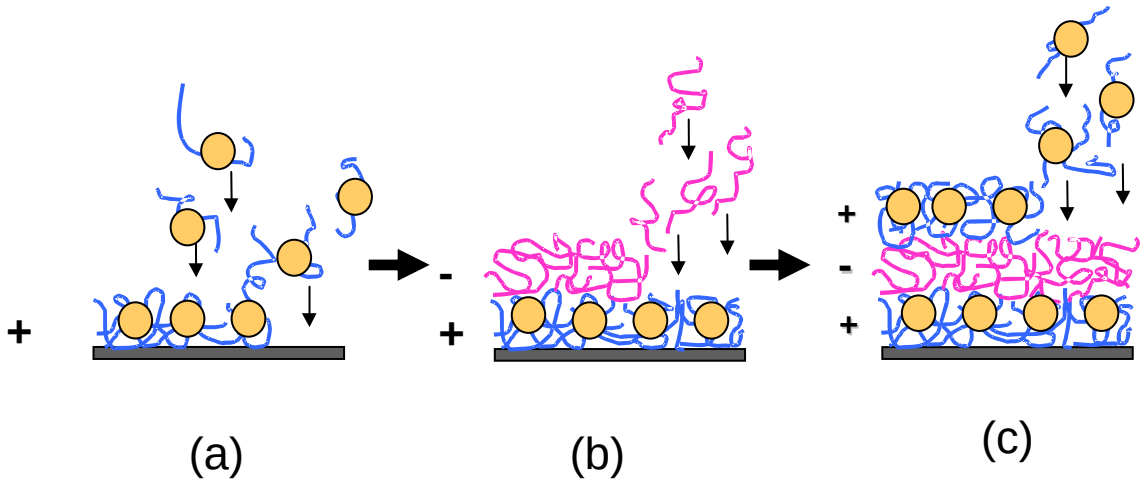

Figure A 1 Schematic of layer by layer self-assembly: (a) first layer of metal colloid with positive charge; (b) second layer of organic with negative charge; (c) repeating layer by layer fashion.

Gold self-assembly film

Gold colloid preparation

The self-assembly gold film requires two types of solution. The first layer deposited contains the gold nanoclusters attached to the PDDA molecules and has an inherent positive charge (Au colloid). The second layer contains the poly s-119 and has a negative charge. Figure A 2 (a) and (b) shows the molecular structures of PDDA and poly-S-119 respectively. The synthetic route to prepare gold colloid involves the reduction of halide in solution in the presence of stabilizer. The concentration of reducer ($NaBH_4$), gold salt ($HAuCl_4$) and PDDA was listed in Table A. 1 Two processing procedures (a) and (b) were applied to prepare the gold colloids and listed in Figure A 3 (a) and (b) respectively. In the procedure (a), the gold particles are firstly reduced out and then put the PDDA to stabilize. To prepare the second solution, we dissolved poly s-

119 in deionized water and the acidity was adjusted to pH 5 using HCl. We used a concentration of 120 mg per 60 ml of water (0.0021 M).

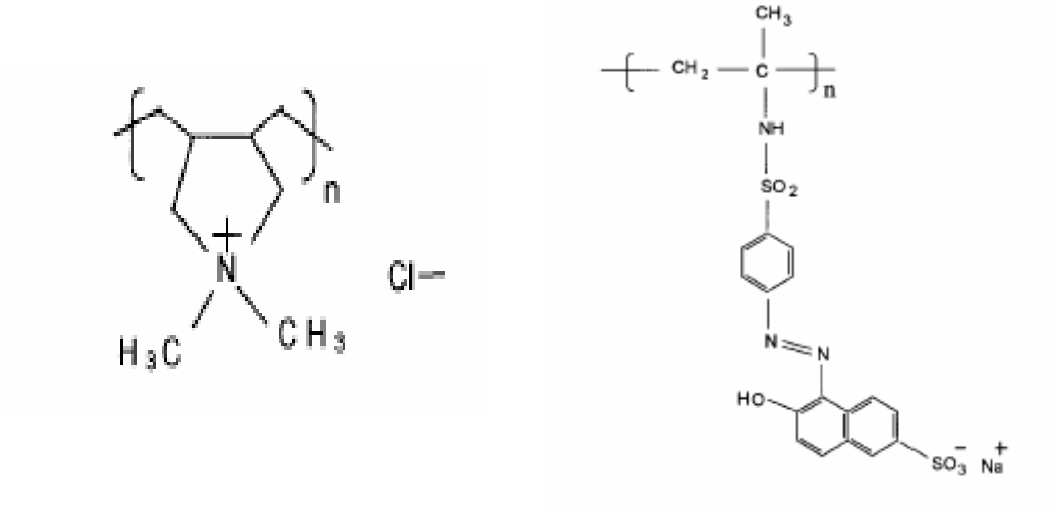

(a) **(b)**

Figure A 2 Molecular structures of PDDA (a) and poly-S-119 (b).

Table A. 1. List of solution parameters and concentration investigated to prepare gold colloid. .

PDDA (Molar)	$NaBH_4$ (Molar)	$HAuCl_4$ (Molar)
3.6*10E-3	1.8*10E-4	9*10E-4

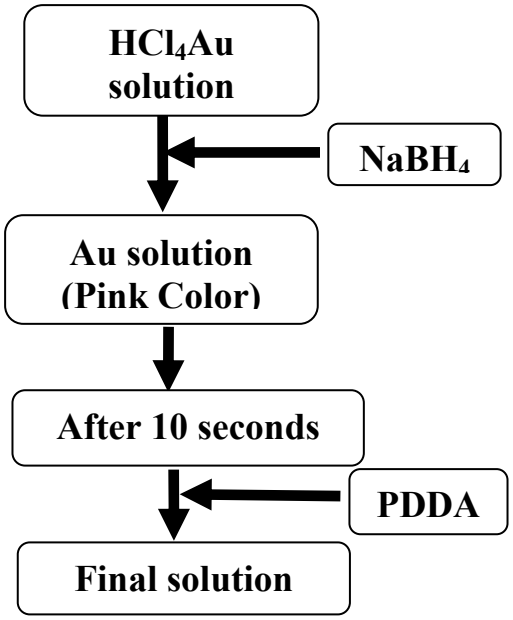

(a)

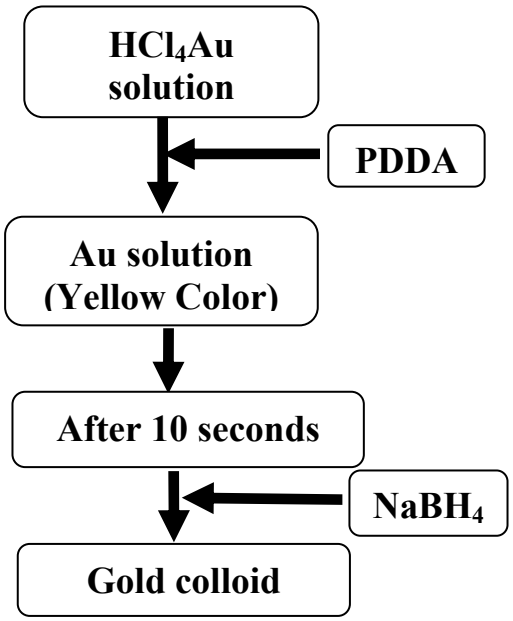

(b)

Figure A 3. The processing procedure to prepare gold colloids: (a)gold particles firstly reduced out; (b) Gold particles finally reduced out.

The gold colloids prepared by procedures (a) and (b) respectively were observed the stability in the same room temperature condition. It was found out that the gold colloid prepared by procedure (b) is much more stable than those prepared by procedure (a). After only half hour, the colloid prepared by procedure (a) starts to precipitate the gold particles out, and the colloid prepared by procedure (b) can last more than three months and even longer. This is because the $NaBH_4$ is a strong reducer and the reduced gold atoms can nucleate and grow rapidly, if no organic protection. With the existing PDDA in the solution, the reduced gold particles can be efficiently protected by attached PDDA and the further grain growth is prevented. The prepared gold colloids prepared by procedure (b) were analysis by a UV- absorption analyzer and the UV spectrum was shown in Figure A 4**.** The observation of UV spectrum indicates that the gold particles is below 20 nm.

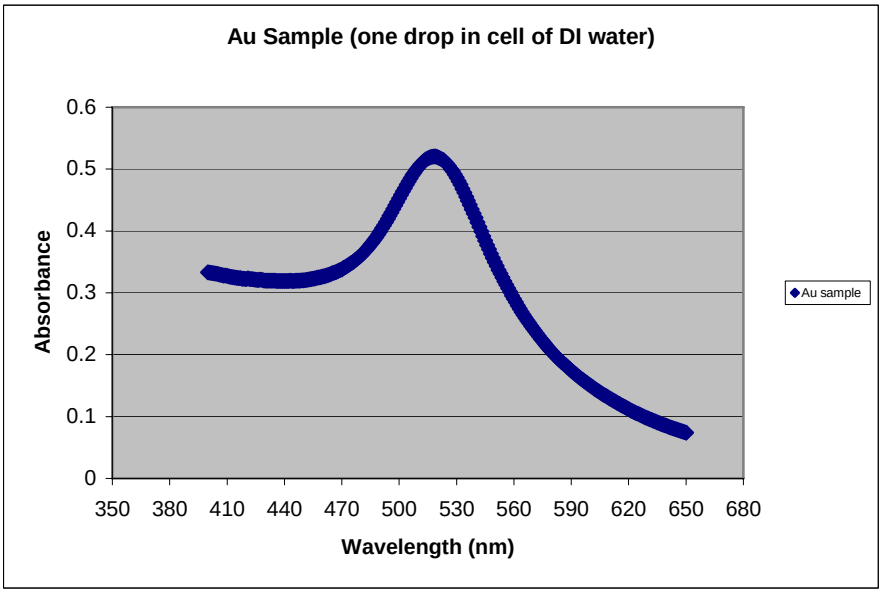

Figure A 4 UV spectrum of colloid gold solution.

To investigate the effect of PDDA concentration on the stability of gold colloids, different gold colloids were prepared by adjusting the concentration of PDDA. The prepared gold colloids are analyzers by Horiba particle size analyzer. The instrument uses laser scattering to determine and particle size and the distribution. The best resolution of this particle size analyzer can reach 100 nm and is not particularly sensitive to the very fine clusters. For the gold colloid with 3.6 E-3 mol / L concentration of PDDA, the particle size analyzer can not detect any particle size information during the four days aging period. However, for the gold colloid with 3.6E-4 mol / L concentration of PDDA, the particle size analyzer can detect the particles with 500 nm particle size after two days. After another two days, the gold colloid has a bi-model distribution: one peak locates on 130 nm and another one locates on 5000 nm. And also, the gold precipitation can be observed can naked eyes. These measures and observation indicate the concentration of PDDA has a significant effect on the stability of gold colloids. With little PDDA protection, the nanoscale gold particles have a strong tendency to grow to micron size and finally precipitate out from the solution.

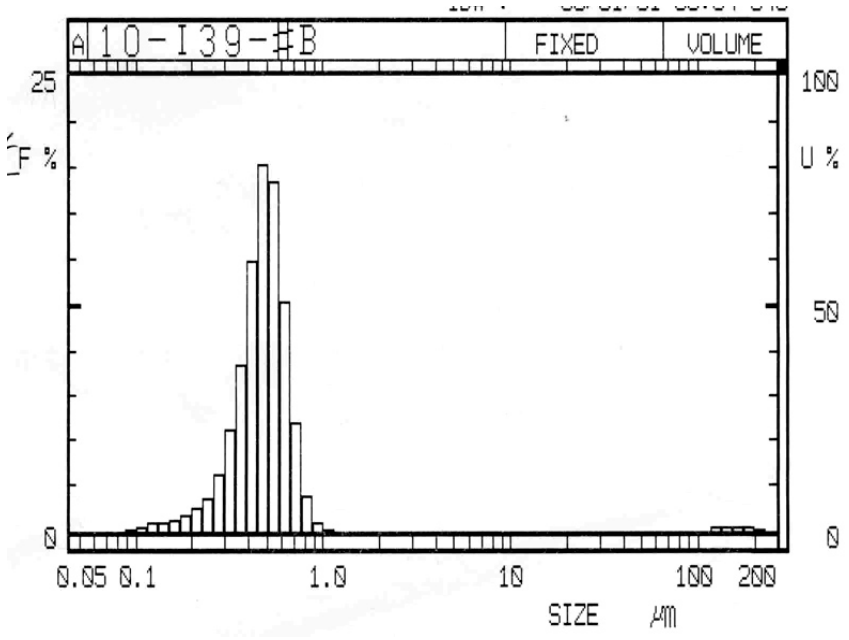

(a)

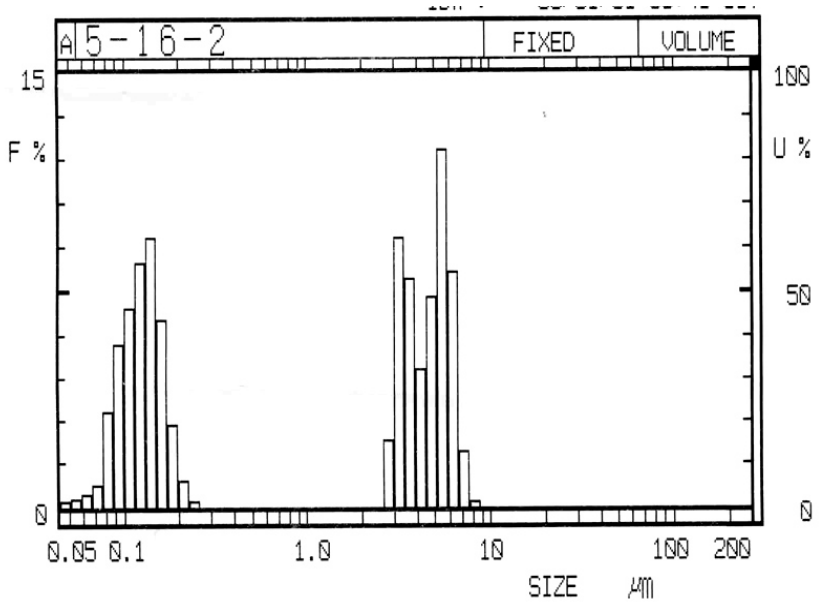

(b)

Figure A 5 Particle size distribution of a solution with a relative PDDA concentration of 0.1 (a) After two days aging period; (b) After four days aging period.

Self-assembled gold film preparation

A clean substrate with negative charge is necessary for self-assembled gold film preparation. Firstly, silicon substrates were ringed in piranha solution (the mixer with 98% H_2SO_4 and 30 % H_2O_2, the volume ratio is 7:3). After that, the pure water with resistivity of 18 M ohm cm washes the substrates three times in an ultrasonic bath. The procedure for depositing the films is as follows. Firstly, dipping the washed silicon substrate into the gold colloid solution with positive charged PDDA for 3 to 5 minutes. Then, the substrate was rinsed thoroughly with DI water. After that, the substrate was dipped into s-119 solution for 1 to 2 minutes. By repeating this fashion, the multi-layer gold film can be assembled into the substrate. The deposition process does not require any special equipment or facilities and can be as simple as hand dipping as shown in Figure A 6 (a). Figure A 6 (b) shows a 80 bi-layer gold film on silicon. The gold coverage was observed by scanning electronics microcopy.

(a) (b)

Figure A 6. Preparation of self-assembled gold film: (a) dipping procedure; (b) a 80 bi-layer gold film on silicon.

Figure A 7 (a) shows the SEM observation of deposited gold film. The EDS analysis showed in Figure A 7 (b) indicates that there are nanoscale gold particles attached onto the silicon substrate, but the coverage is very little.

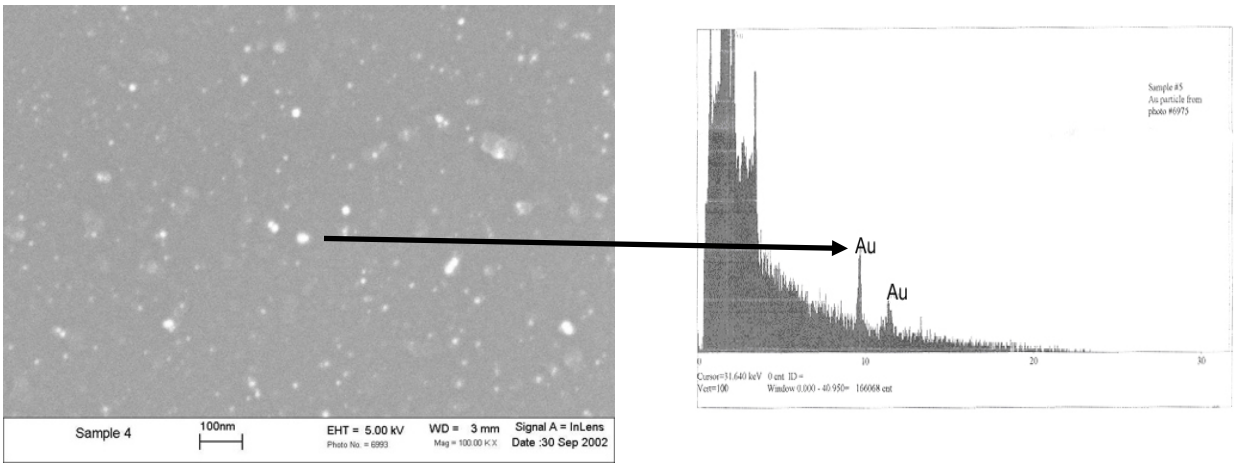

Figure A 7. (a) SEM image of an ISAM film on silicon substrate deposited from a solution with a relative PDDA concentration of 3.6E-3 mol/L. (b) EDS of the film indicates the bright spots are gold particles.

To increase the gold coverage of self-assembled film, an applied electrical field was applied. A simple fixture shown in Figure A 8 (a) was built to realize electrical filed assisted self-assembling. Figure A 8 (b) shows a 80 bi-layer gold film on silicon prepared by electrical filed assisted self-assembling. The thickness of the self-assembled gold film was measured by Tek-Tak 3. The gold coverage was observed by scanning electronics microcopy.

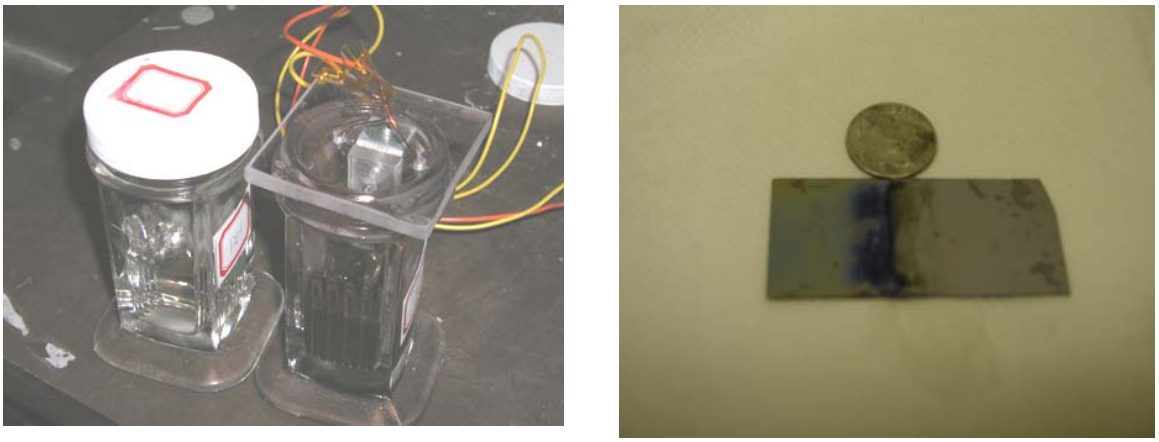

(a) (b)

Figure A 8 Preparation of self-assembled gold film with electrical field assistance: (a) dipping procedure; (b) a 80 bi-layer gold film on silicon.

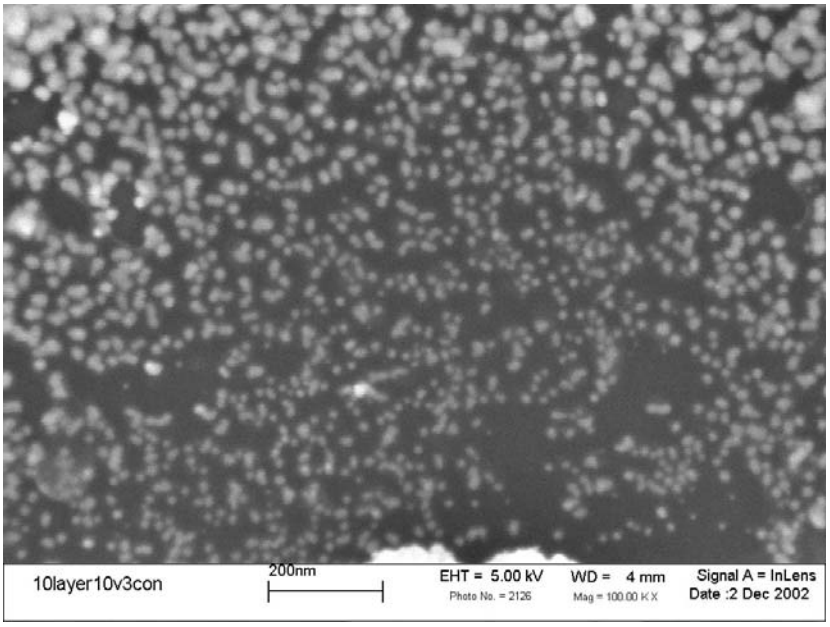

Figure A 9 SEM image of an ISAM film on silicon substrate deposited from a solution with electrical field assistance.

Silver self-assembly film

Silver colloid preparation

The self-assembly silver film requires two types of solution. The first layer deposited contains the silver nanoclusters attached to the PAA molecules and has an inherent positive charge (silver colloid). The second layer contains the PSS and has a negative charge. Figure A 10 (a) and (b) shows the molecular structures of PAA and PSS respectively. PAA, instead of PDDA, was used to stabilize the nanosclae silver particle, is due to the Cl^- in PDDA can react with Ag^+ in the silver salt and procedure precipitation AgCl. The concentration of reducer ($NaBH_4$), silver salt ($AgNO_3$) and PAA was listed in Table A. 1 The preparation procedure was shown in Figure A 11. To prepare the second solution, we dissolved PSS in deionized water and the acidity was adjusted to pH 5 using HCl. We used a concentration of 120 mg per 60 ml of water (0.0021 M).

(a) **(b)**

Figure A 10. Molecular structures of PAA (a) and (b) PSS.

Table A. 2 List of solution parameters and concentration investigated to prepare gold colloid.

PAA (Molar)	$NaBH_4$ (Molar)	$AgNO_3$ (Molar)
3.6*10E-3	1.8*10E-4	9*10E-4

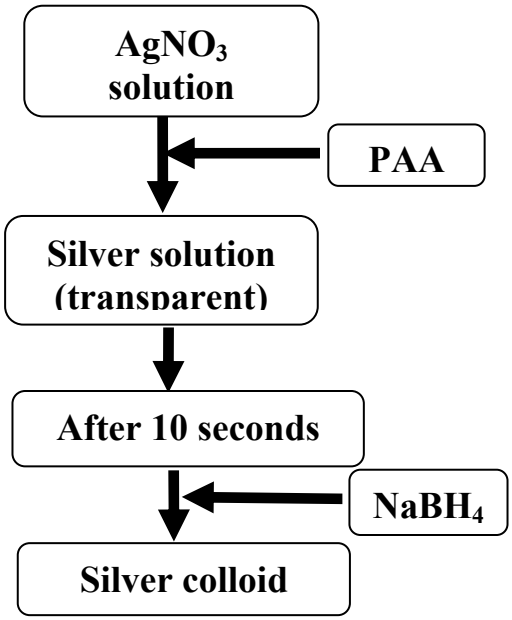

Figure A 11 The processing procedure to prepare silver colloids.

The prepared silver colloid can be stable for more than three month without precipitation. When the concentration of PAA was reduced, the instability was also observed just like the gold colloid with reduced PDDA concentration.

Self-assembled silver film preparation

Firstly, silicon substrates were ringed in piranha solution. After that, the pure water washes the substrates three times in an ultrasonic bath. The procedure for depositing the films is as follows. Firstly, dipping the washed silicon substrate into the silver colloid solution with positive charged PAA for 3 to 5 minutes. Then, the substrate was rinsed thoroughly with DI water. After that, the substrate was dipped into PSS solution for 1 to 2 minutes. By repeating this fashion, the multi-layer silver film can be assembled into the silicon substrate. The silver coverage was observed by scanning electronics microcopy. Figure A 12 shows the SEM observation of self-assembled silver film. The flexible Kapton© film was also applied as substrate to deposit the nanoscale silver film. Figure A 13 shows a 50 bi-layers silver film self-assembled on the Kapton© film.

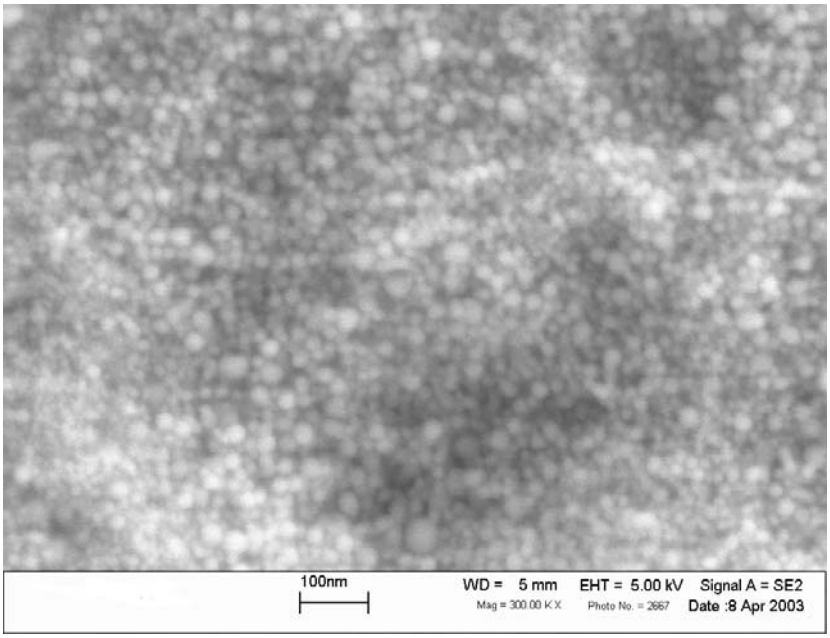

Figure A 12. SEM image of an ISAM film on silicon substrate deposited from a solution with PAA 3.6E-3 mol/L.

Figure A 13. A 50 bi-layers silver film self-assembled on the Kapton© film.

Reference:

[1] J. Vanfleteren, "Adhesive flip-chip technology," *IMAPS Benelux Spring Event – Gent*, 2004 May 14.

[2] C. o. t. E. Communities, "Proposal for a Directive of the European Parliament and the Council on Waste Electrical and Electronic Equipment: Proposal for a Directive of the European Parliament and of the Council on the restriction of the use of certain hazardous substances in electrical and electronic equipment," in *WEEE Directive Brussels*, vol. 13, 2000 June

[3] Florenz, Karl-Heinz, and W. Directive, "Committee on the Environment, Public Health and Consumer Policy Draft Report," European Parliament, 2001 February.

[4] J. H. Lau and S.-W. R. Lee, "Reliability of wafer level chip scale package (WLCSP) with 96.5Sn-3.5Ag lead-free solder joints on build-up microvia printed circuit board," *Electronic Materials and Packaging, 2000. (EMAP 2000). International Symposium.*, pp. 55 - 63 2000.

[5] "IPC Roadmap: A guide for assembly of lead-free electronics. draft IV," *International Packaging Consortium*, 2000 June.

[6] D. Suraski, K. Seelig, and I. Volume "The current status of lead-free solder alloys," *Electronics Packaging Manufacturing, IEEE Transactions on [see also Components, Packaging and Manufacturing Technology, Part C: Manufacturing, IEEE Transactions*

vol. 24, pp. 244 - 248, 2001.

[7] K. Stinson-Bagby, "Microstructural evolution in thermally cycled large-area lead and lead free solders," *Masters Thesis of Virginia Tech*, 2002 July.

[8] O. Rusanen and J. Lenkkeri, "Reliability issues of replacing solder with conductive adhesives in power modules," *Components, Packaging, and Manufacturing Technology, Part B: Advanced Packaging, IEEE Transactions on*, vol. 18, pp. 320 - 325, 1995 May.

[9] J. Liu, Z. Lai, K. H., and C. Khoo, "Overview of conductive adhesive joining technology in electronics packaging applications," *Adhesive Joining and Coating*

Technology in Electronics Manufacturing, 1998. Proceedings of 3rd International Conference, pp. 1 - 18, 1998.

[10] H. Takezawa, M. Itagaki, T. Mitani, Y. Bessho, and K. Eda, "Development of solderless joining technologies using conductive adhesives," *Advanced Packaging Materials: Processes, Properties and Interfaces, 1999. Proceedings. International Symposium* vol. 14-17, pp. 11 - 15, 1999.

[11] D. D. Chang, P. A. Crawford, J. A. Fulton, R. McBride, M. B. Schmidt, R. E. Sinitski, and C. P. Wong, "An overview and evaluation of anisotropically conductive adhesive films for fine pitch electronic assembly," *Electronic Components and Technology Conference, 1993. Proceedings., 43rd*, vol. 1-4, 1993 June.

[12] D. C. V. Katsis, J.D, "A finite element modeling of dynamic hot spot effects in MOSFET dies due to voiding in the solder die-attach," *IEEE 34th Annual Power Electronics Specialist Conference*, vol. 2, pp. 828 - 833, 2003 June.

[13] N. Zhu, "Thermal impact of solder voids in the electronic packaging of power devices," *15th Annual IEEE SEMI-THERM Symposium Proceedings, San Diego*, pp. 22-29, 1999.

[14] D. C. Katsis and J. D. van Wyk, "Void Induced thermal Impedance in Power Semiconductor Modules: Some Transient Temperature Effects," *Industry Applications Conference, 2001. 36th IAS Annual Meeting. Conference Record of the 2001 IEEE, Vol. 3*, vol. 3, pp. 1905 –1911, 2001.

[15] E. R. Brown and M. C. Shaw, "Thermomechatronics of Power Electronic Packages," *Conference Proceedings, Las Vegas*, 2000 May.

[16] T. A. Nguty, B. Salam, R. Durairaj, and N. N. Ekere, "Understanding the process window for printing lead-free solder pastes," *Electronics Packaging Manufacturing, IEEE Transactions on [see also Components, Packaging and Manufacturing Technology, Part C: Manufacturing, IEEE Transactions*, vol. 24, 2001.

[17] C. H. Tung, P. S. Teo, and C. Lee, "Interface Microstructure Evolution of Lead-Free Solder on Ni-Based Under Bump Metallizations During Reflow and High

Temperature Storage," *Device and Materials Reliability, IEEE Transactions*, vol. 5, pp. 212 - 216 2005 June.

[18] Z. Hou, G. Tian, C. Hatcher, R. W. Johnson, E. K. Yaeger, M. M. Konarski, and L. Crane, "Lead-free solder flip chip-on-laminate assembly and reliability," *Electronics Packaging Manufacturing, IEEE Transactions on [see also Components, Packaging and Manufacturing Technology, Part C: Manufacturing, IEEE Transactions*, vol. 24, pp. 282 - 292, 2001.

[19] C. M. L. Wu and M. L. Huang, "Microstructural evolution of lead-free Sn-Bi-Ag-Cu SMT joints during aging," *Advanced Packaging, IEEE Transactions on [see also Components, Packaging and Manufacturing Technology, Part B: Advanced Packaging, IEEE Transactions*, vol. 28, pp. 128 - 133, 2005.

[20] G. Y. Li and B. L. Chen, "Formation and growth kinetics of interfacial intermetallics in Pb-free solder joint," *Components and Packaging Technologies, IEEE Transactions on [see also Components, Packaging and Manufacturing Technology, Part A: Packaging Technologies, IEEE Transactions*, vol. 26, pp. 651 - 658, 2003.

[21] Y. Fukuda, M. G. Pecht, K. Fukuda, and S. Fukuda, "Lead-free soldering in the Japanese electronics industry," *Components and Packaging Technologies, IEEE Transactions on [see also Components, Packaging and Manufacturing Technology, Part A: Packaging Technologies, IEEE Transactions*, vol. 26, pp. 616 - 624, 2003.

[22] M. Trivedi and K. Shenai, "Performance of silicon carbide devices in power converters " presented at Proceedings of International Workshop on Integrated Power Packaging, Boston, MA, 2000 July 14 to 15

[23] H. Lendenmann, A. Mukhitdinov, F. Dahlquist, H. Bleichner, M. Irwin, R. Soderholm, and P. Skytt, "4.5 kV 4H-SiC diodes with ideal forward characteristic," *Proceedings of the 13th International Symposium on Power Semiconductor Devices and Ics.*, pp. 31 – 34, 2001 July 4-7.

[24] R. Singh, A.R. Hefner, D. Berning, and J. W. Palmour, "High temperature characteristics of 5 kV, 20 A 4H-SiC PiN rectifiers," *Proceedings of the 13th*

International Symposium on Power Semiconductor Devices and Ics, Osaka, Japan, pp. 45-48, 2001 June 4-7.

[25] P. McCluskey, D. Das, and J. Jordan, "Package of Power Electronics for High Temperature Applications," *CPES Power Electronics Semina*, pp. T2.6 to T2.11, 2000.

[26] http://www.thebulliondesk.com/.

[27] A. Melaiye and W. J. Youngs, "Silver and its application as an antimicrobial agent," *Expert Opinion on Therapeutic Patents*, vol. 15, pp. 125-130, 2005 February.

[28] R. M. German, "Sintering theory and practice " *Wiley and Sons, New York, NY*, 1996.

[29] A. Shimosaka, Y. Ueda, Y. Shirakawa, and J. Hidaka, "Sintering mechanism of two spheres forming a homogeneous solid solubility neck," *KONA, Hosokawa powder technology foundation*, 2003.

[30] P. Barnwell and M. P. O'Neill, "Enabling ceramic circuit technologies for wireless microelectronics packaging," *Wireless Communications Conference, 1997., Proceedings*, pp. 156-161, 1997 August

[31] J. H. Alexander and A. S. Shaikh, "The use of silver and silver plus gold conductors with the ferro low temperature tape," *Electronic Components and Technology Conference, 1993. Proceedings., 43rd*, vol. 1-4, pp. 888 - 892 1993 June.

[32] S. Rane, V. Puri, and D. Amalnerkar, "A study on sintering and microstructure development of fritless silver thick film conductors," *Journal of Materials Science: Materials in Electronics*, vol. 11, pp. 667 - 674, 2000 December.

[33] U. Scheuermann, "Low Temperature Joining Technology - A High Reliability Alternative to Solder Contacts," *Workshop on Metal Ceramic Composites for Functional Application, Vienna*, 1997 June.

[34] H. Schwarzbauer, "Novel Large Area Joining Technique for Improved Power Device Performance," *IEEE Transactions on Industrial Applications*, vol. 27, pp. 93 to 95, 1991.

[35] H. Schwarzhauer, "Method of Securing Electronic Components to a Substrate," *US Patent No. 4 810 672.*, 1998.

[36] S. Klaka and R. Sitting, "Reduction of Thermo-Mechanical Stress by Applying a Low Temperature Joining Technique," *Proceedings of the 6th International Symposium on Power Semiconductor Devices and ICs*, pp. 259-264, 1994 March

[37] J. C. Kim, K. H. Auh, and D. M. Martin, "Multi-level particle packing model of ceramic agglomerates," *Modelling and simulation of matererials of science and. engineering*, vol. 8, pp. 159 to 168, 2000.

[38] P. Bowen and C. Carry, "From powders to sintered pieces: forming, transformations and sintering of nanostructured ceramic oxides," *Powder Technology*, vol. 128, pp. 248– 255, 2002.

[39] M. J. Mayo, "Processing of nanocrystalline ceramics from ultrafine particles," *International materials reviews, 1006*, vol. 41, 1998.

[40] S.W. Wang, L. D. Chen, and T. Hirai, "Densification of Al2O3 powder using spark plasma sintering," *Journal of Materials Research*, vol. 15, 2000 April

[41] J. Freim, J. McKittrick, J. Katz, and K. Sickafus, "Microwave sintering of nanocrystalline -Al2O3 " *Nanostructured Materials*, vol. 4, 1994.

[42] J. R. Groza and R. J. Dowding, "Nanoparticulate materials densification," *Nanostructure Materials*, vol. 7, pp. 749-768, 1996.

[43] J.R.Groza and A. Zavaliangos, "Nanostructured bulk solids by field activated sintering," *Advanced material science*, vol. 5, pp. 24-33, 2003.

[44] G. Xu, I. Lloyd, Y. Carmel, T. Olorunyolemi, and O. Wilson, "Microwave sintering of ZnO at ultra high heating rate," *Jounal of Materials Reviews*, vol. 16, 2001.

[45] D. K. A. Y.Fang, R. Roy, "Microwave sintering of nanophase MgO, TiO2, and Cu metal powders," *An International Conference on the Science, Technology & Applications of Sintering*, vol. 3, 2003.

[46] Z. Liji, W. Li, X. Xiaoming, and W. Kempe, "An investigation on thermal reliability of underfilled PBGA solder joints " *Electronics Packaging Manufacturing, IEEE Transactions*, vol. 25, pp. 284 - 288, 2002.

[47] S. K. Kang, P. Lauro, D.-Y. Shih, D. W. Henderson, T. B. J. Gosselin, C. S.R., G. C., K. J. Puttlitz, and T.-K. Hwang, "Evaluation of thermal fatigue life and failure mechanisms of Sn-Ag-Cu solder joints with reduced Ag contents," *Electronic Components and Technology, 2004. ECTC '04. Proceedings*, vol. 1, pp. 661 - 667, 2004.

[48] J. A. C. a. G. W. Lehman, "Temperature and finite pulse-time effects in the flash method for measuring thermal diffusivity," *Journal of applied physics*, vol. 34, pp. 1909-1913, 1963.

[49] R. J. J. W.J. Parker, C.P. Butler, G.L. Abbot, "Flash method of determing thermal diffusivity, heat capacity and thermal Conductivity ." *Journal of applied physics*, vol. 32, 1964.

[50] H. J. Lee, "Thermal diffusivity in layered and dispersed composites," *PhD dissertation, Purdue University.*, 1975.

[51] www.matweb.com.

[52] G. Frens and Overbeek, *Kolloid Z. Z. Polymer*, vol. 233, pp. 922 to 925, 1969.

[53] G. Berube, *Ferro electronic material systems*, 2004.

[54] W. T. Anderson, "Semiconductor device reliability in extreme high temperature space environments," *Aerospace Conference, 2001, IEEE Proceedings.*, vol. 5, pp. 2457 - 2462.

[55] R. W. Johnson, J. L. Evans, P. Jacobsen, J. R. Thompson, and M. Christopher, "The changing automotive environment: high-temperature electronics," *Electronics Packaging Manufacturing, IEEE Transactions on [see also Components, Packaging and Manufacturing Technology, Part C: Manufacturing, IEEE Transactions*, vol. 27, pp. 164 - 176 2004 July.

[56] A. N. Hammoud, E. D. Baumann, I. T. Myers, and E. Overton, "High temperature power electronics for space," *Presented at the First International High Temperature Electronics Conference, Albuquerque, NM, 16-20 Jun. 1991; sponsored by Sandia National Labs., AF Wright Research Development Center and New Mexico Univ.* , 1991.

[57] R. R. Reston, H. Y. Lee, C. R. Ito, G. J. Trombley, C. K. Havasy, and B. Johnson, "Enhanced gallium arsenide metal-semiconductor field effect transistors designed for high temperature operation," *Aerospace and Electronics Conference, 1994. NAECON 1994., Proceedings of the IEEE 1994 National*, vol. 2, pp. 1138 - 1142, 1994 May.

[58] R. Singh, S. H. Ryu, D. C. Capell, and J. W. Palmour, "High temperature SiC trench gate p-IGBTs," *IEEE Transactions on Electron Devices,*, vol. 50, pp. 774 to 784, 2003.

[59] W. Wondrak, R. Held, E. Niemann, and U. Schmid, "SiC devices for advanced power and high-temperature applications," *IEEE Transactions on Industrial Electronics*, pp. 307 to 308, 2001.

[60] J. Homberger, A. B. Lostetter, K. J. Olejniczak, T. McNutt, S. M. Lal, and A. Mantooth, "Silicon-carbide (SiC) semiconductor power electronics for extreme high-temperature environments," *Proceedings IEEE Aerospace Conference*, vol. 4, pp. 2538 - 2555, 2004.

[61] X. W. Wang, W. J. Zhu, X. Guo, T. P. Ma, J. B. Tucker, and M.V. Rao, "High temperature (450°C) reliable NMISFET's on p-type 6H-SiC," *IEEE IEDM Technical Digest*, pp. 209 - 212, 1999.

[62] B. Michel and D. Vogel, "Packaging and thermomechanical challenges for high temperature electronics," *High Temperature Electronics, 1999. HITEN 99. The Third European Conference*.

[63] McCluskey, F.P.; Jain, R.; Tiwari, N.; Grzybowski, R.; Benoit, and S. J.; Lin, "Die attach and wirebond systems for high temperature electronics," *High Temperature Electronics, 1999. HITEN 99. The Third European Conference*.

[64] E. Savrun, "Packaging considerations for very high temperature microsystems," *Sensors, 2002. Proceedings of IEEE*, vol. 2, pp. 1139 - 1143.

[65] T. Veneruso, "Applications for High Temperature Electronics in Oil, Gas, and Geothermal," *Proceedings-First International High Temperature Electronics Conference, Albuquerque, NM*, 1991 June.

[66] R. W. Chuang and C. C. Lee, "Silver-indium joints produced at low temperature for high temperature devices," *Components and Packaging Technologies, IEEE Transactions on [see also Components, Packaging and Manufacturing Technology, Part A: Packaging Technologies, IEEE Transactions*, vol. 25, pp. 453 - 458, 2002.

[67] R. Singh and J. Richmond, "SiC Power Schottky Diodes in Power Factor Correction Circuits," *Application notes, Cree*, 2002.

[68] J. M. Hancock, "Meeting future application challenges meeting future application challenges in HV semiconductors," *APEC 2004 conference, Infineon Technologies NA, Inc presentation.*, 2004.

[69] K. Fukuda, "Development of SiC Power MOSFETs with low on-resistance," *The international workshop on recent progress in induction accelerators (RPIA)*, 2002.

[70] E. Sancaktar, P. Rajput, and A. Khanolkar, "Correlation of silver migration to the pull out strength of silver wire embedded in an adhesive matrix," *Polymers and Adhesives in Microelectronics and Photonics, 2004. POLYTRONIC 2004. 4th IEEE International Conference* vol. 12-15, pp. 171 - 181, 2004.

[71] J. Bolger, M. Herberg, and C. Moomey, "Proceedings of 1st International SAMPE electronics conference," pp. 616, 1987.

[72] S. Wen, "Design and Analysis of a dimple array interconnect technique for power electronics packaging," *PhD dissertation, Virginia Tech.*, 2002.

[73] X. Liu, "Processing and reliability assessment of solder joint interconnection for power chips," *PhD dissertation, Virginia Tech.*, 2001.

[74] E. M. Wooldridge, C. E. Powers, J. A. Townsend, W. C. Peters, D. P. Cadogan, and J. K. H. Lin, "Effects of manufacturing and development on thin film for the NGST sunshade," *American Institute of Aeronautics and Astronautics*, 2000.

[75] D. M. Kowalski and D. J. Caruso, "Digital printing of metallic digital printing of metallic conductors in support of the burgeoning plastic electronics.," *Cabot Corporation*, 2004

[76] http://www.sei.co.jp/sn/2004/326/6t.html.

[77] http://www.xerox.com/innovation/poe2.shtml.

[78] http://www.foodproductiondaily.com/news/news-ng.asp?id=58399-xink-launches-flexographic.

[79] R. K. Iler, "Multilayers of colloidal particles," *Journal of colloid interface science* vol. 21, pp. 569-594 1966.

[80] G. Decher, " Fuzzy nanoassemblies: toward layered polymeric multicomposites " *Science*, vol. 277, pp. 1232-1237, 1997 August.

[81] A. Delcorte, P. Bertrand, E. Wischerhoff, and A. Laschewsky, "Adsorption of Polyelectrolyte Multilayers on polymer Surfaces," *Langmuir*, vol. 13, pp. 5125-5136, 1997.

[82] J. Mamedov, F. Ostrander, and N. A. K. Aliev, "Stratified assemblies of magnetite nanoparticles and montmorillonite prepared by the layer-by-layer assembly," *Langmuir*, vol. 16, pp. 3941-3949, 2000.

[83] Y. Lvov, K. Ariga, M. Onda, I. Ichinose, and T. Kunitake, "Layer-by-Layer Nanoarchitectonics," *Langmuir*, vol. 13, pp. 6195 to 6210 1997.